

Evaluating the role of inflammasome activation in
models of pathological ocular angiogenesis

Ryan Daniel Makin
Modesto, California

Bachelor of Science, Physiology & Neuroscience
University of California San Diego, 2016

A Dissertation presented to the Graduate Faculty of the University of Virginia in
Candidacy for the
Degree of Doctor of Philosophy

Department of Pathology

University of Virginia
May 2025

Abstract

Pathological angiogenesis in the eye remains at the center of a myriad blinding diseases, including neovascular age-related macular degeneration (nvAMD). Elucidating the mechanisms by which these invasive neovessels proliferate into normally avascular regions is of critical importance. The past two decades of research have identified the inflammasome, a component of the innate immune system responsible for sensing foreign and endogenous danger signals, as a potential mediator of aberrant angiogenesis. However, several previous conflicting reports on the role of inflammasome in this context have only brought to light a clear gap in knowledge.

Here, we expanded the experimental laser-induced choroidal neovascularization (CNV) model, considered to be the field standard, to include subretinal administration of disease-relevant inflammasome agonists. In doing so, we observed increased CNV volume in wild type mice but not mice lacking inflammasome constituents, an effect that was mediated by key components of the NLRP3 inflammasome pathway. Additional studies identified the role of interleukin-1 β (IL-1 β) in promoting chemotaxis and macrophage ingress to the lesion site.

Coincident with our work in expanding the CNV model, we also developed a first-of-its-kind experimental model to assess how physical activity affects the development of CNV lesions in exercise-trained mice. Interestingly, exercise-trained mice exhibited a significant reduction in CNV volume and F4/80 immunopositivity that was independent of sex and distance traveled. Fluorescent *in situ* hybridization signals against mRNA of

several pro-angiogenic and pro-chemotactic factors were also reduced in the exercise-trained cohort, suggesting that physical activity may be a low-cost, non-invasive alternative therapy for nvAMD.

Finally, we discovered that the commercially available and widely used RF/6A cell line, described as ‘chorioretinal endothelial’ cells, exhibits no characteristics of endothelial cells through anatomical, transcriptional, and functional assays. This study underscores the importance of verifying not only the identity of cells used but also the validity of experimental models used in the laboratory.

Collectively, the work here not only reconciles previously disparate observations of the role of inflammasomes in modulating aberrant ocular angiogenesis but also improves the investigational repertoire for those who wish to expand their experimental techniques in identifying potential causes and treatments for pathological angiogenesis.

Acknowledgments

I truly consider myself a product of every person I have had the privilege of calling a friend, a family member, a colleague, or a confidant, each of whom has left an indelible mark on my heart. This is precisely what has made this section extremely emotional and difficult to write and why I saved it for last (no, that's not a teardrop on my keyboard. Why do you ask?)

I first want to thank my mentor, Dr. Bradley Gelfand, and the Center for Advanced Vision Science Director, Dr. Jayakrishna Ambati, for taking a chance on a transplant from San Diego with no real background in cellular and molecular biology techniques. I'll never forget meeting Brad and Dr. Ambati for the first time in person to discuss my job as a lab tech (my interview was on Skype (Zoom wasn't a thing yet (how little we knew back then))). My response to their questions of 'Have you ever worked with DNA? RNA? Protein?' was 'No... No... No...' I thought for sure they picked me for the job by mistake, but they assured me I would be a good fit. Nine years (as of August 2025) later, I find myself on the precipice of being the second graduate student from CAVS, which is truly an honor. Having Brad as a mentor has really been a cornerstone of my graduate experience. From entertaining my 'out there' proposals, to reassuring me that I am right where I belong, to the in depth rehashing of our yearly Spotify Wrappeds, I consider myself lucky to have such an understanding and encouraging mentor.

To my committee, Dr. Jim Mandell, Dr. Janet Cross, Dr. Norbert Leitinger, and Dr. Jayakrishna Ambati, thank you immensely for the involved and informative discussions we have had over the years. In the beginning I know I was very much like a lost puppy,

eager to jump at any and every opportunity to address a new question or line of inquiry, but I am so grateful for your guidance in steering me onto the best path forward.

To this end, I would also not be who I am as a scientist without the Center for Advanced Vision Science and all the postdocs, lab techs, undergrads, and everyone in between. I've seen a lot of personnel change over the past near decade, and everyone has truly made working here such an incredible experience. As a young 21-year-old finding himself on the opposite side of the country in 2016, I would be remiss not to give a shoutout to Gary Pattison, Katie Fox, and Darrell Robinson, our previous lab and mouse colony managers, who really made me feel at home starting from my first day in the Center. I also want to thank Dr. Ivana Apicella, Dr. Daipayan Banerjee, and Dr. Roshni Dholkawala for being my unofficial mentors, for seeing my potential, and for encouraging me to continue to do the science when all I wanted was to give up. Your perseverance and your faith in me is something I will always cherish.

To my lab mates, Dr. Dionne Argyle, Dr. Madhuri Rudraraju, and (soon-to-be Dr.) Joey Olivieri, thank you for putting up with my sass and my mood swings. You have all helped me become a better person and a better scientist, and I have loved all our work together, whether it be through troubleshooting microscopes or foster dams eating their young (sorry Madhuri, I still have no idea why *Nlrp3*^{-/-} pups taste so good).

To my lab techs and undergrads, Hannah Hall, Charles Preston, Anna Steenson, Marcella Mercer, and countless others I know I'm forgetting, I want you to know that showing up and being privileged to teach you and grow with you has been a tremendous

triumph of mine. Being afforded the privilege of loving what you do every day is rare, yet I was somehow blessed to have found that.

To my BIMS besties (and adjacent), Juliana, Samy, Holly, Josh, Andrea, Sean, Sarah, and so many others I am forgetting at the moment; you have truly shown me the meaning of friendship. I am not the easiest person to be friends with, yet here you all still remain, ever loyal and by my side. My graduate experience would not have been as memorable or enjoyable without you, and I sincerely owe you my gratitude forever for keeping my sanity in check when it inevitably got out of control.

To my San Diego friends, Jared, Jacqueline, Chris, Travis, Sabrina, and the Hunties, Olivia, Corinne, Kaitlyn, Morgan, Ali, Chris, Wyatt; moving across the country and leaving you was probably one of the hardest things I have had to do, but I am so fortunate that I've never felt your unwavering support of me fade. Thank you for being a constant in my life.

To my Modesto friends, Kirsten, Hector, Tatiana, Joseph, Ezequiel, and Jason; I am so proud of everything we have accomplished in the 15+ years I have known you. Never for a second have any of you made me doubt my decision to just jump and go for it, and I am so thankful for our continued support of each other.

To Amaris, I thank you so much for being my best friend and the best cat co-parent to my son, Fernando, and for being a solid rock in my tumultuous life. I could not have been blessed with a better person to share a home with for five years. You are not my previous roommate, because we didn't share a room, or even a house. We shared a home together, and having you there made it feel just like that.

To Olivia, my other half, my twin flame; I wouldn't be writing this right now had you not burst into my room at the Nightingale apartment at 7 AM and screamed "I got into UVA Law!! Want to move to Charlottesville with me??" to which I responded "Sure, why not?" You have kept me in check and shown me the meaning of unconditional love. We have been around the world together (literally) and we've shared love and loss alike. I can't imagine my life without you by my side.

To my dad, Dan, my aunts Brandi and Stacie, and my grandparents Mark and Marcia; thank you for your consistent support, love, and general joie de vivre you have instilled in me, from Twain Harte Christmases to cruises and beyond. I could write a dissertation of the movie quotes we have entire conversations in (this one has exhausted me so I won't), but I am forever grateful for you truly showing me how important unconditional love and perseverance is.

To my mom, Amy, my late aunt Lisa, and my grandparents, Jim and Glenda; I would not be the person I am today without your love and support. You have loved me even when I didn't love myself, and for that I am forever grateful. You have supported my every decision in life, from moving to southern California for college to moving to Virginia to take a few years off school and re-evaluate my life. Well, here we are, and I finally made it!

Table of Contents

Abstract	ii
Acknowledgments	iv
Table of Contents	viii
List of Figures	x
List of Abbreviations	xii
Chapter 1: Introduction	1
1.1 Retinal physiology	1
1.1.1 <i>Photoreceptors</i>	1
1.1.2 <i>Retinal pigmented epithelium</i>	2
1.1.3 <i>Choroid</i>	2
1.2 Age-related macular degeneration	5
1.3 Models of pathological ocular angiogenesis	7
1.3.1 <i>Experimental laser-induced choroidal neovascularization</i>	7
1.3.2 <i>Murine models of spontaneous CNV</i>	10
1.4 Macrophage modulation of pathological angiogenesis	11
1.4.1 <i>Inflammasome activation in macrophages</i>	12
1.5 Current theories of inflammasome involvement in pathological angiogenesis	12
1.5.1 <i>Conflicting reports on inflammasome in CNV</i>	13
1.5.2 <i>Inflammasome in spontaneous CNV</i>	14
1.6 Dissertation goals and significance	15
Chapter 2: Inflammasome agonism aggravates choroidal neovascularization	17
2.1 Abstract	17
2.2 Introduction	18
2.3 Materials and Methods	20
2.3.1 <i>Mice</i>	20
2.3.2 <i>Laser-induced CNV and subretinal injection</i>	20
2.3.3 <i>RPE/choroid flatmount preparation and CNV volume quantification</i>	21
2.3.4 <i>F4/80 immunofluorescence and quantification</i>	22
2.3.5 <i>Immunofluorescence</i>	22
2.3.6 <i>Fluorescent in situ hybridization</i>	23
2.3.7 <i>Transwell migration assays</i>	23
2.3.8 <i>Statistics</i>	24
2.4 Results	25
2.4.1 <i>Inflammasome agonists exacerbate experimental CNV</i>	25
2.4.2 <i>The angiostimulatory activity of Alu RNA depends on inflammasome</i>	28
2.4.3 <i>Inflammasome in myeloid cells is critical for Alu RNA-induced CNV exacerbation</i>	33
2.4.4 <i>Inflammasome-dependent macrophage migration drives CNV exacerbation</i> ..	37

2.4.5 <i>Inflammasome-induced macrophage migration is mediated by interleukin-1 beta (IL-1β)</i>	40
2.5 Discussion	45
Chapter 3: Voluntary exercise suppresses choroidal neovascularization in mice.....	47
3.1 Abstract	47
3.2 Introduction	48
3.3 Materials and Methods	50
3.3.1 <i>Mice</i>	50
3.3.2 <i>Voluntary running</i>	50
3.3.3 <i>Laser photocoagulation-induced choroidal neovascularization</i>	51
3.3.4 <i>CNV volume and F4/80 labeling</i>	51
3.3.5 <i>Fluorescent in situ hybridization</i>	51
3.4 Results.....	53
3.4.1 <i>Effect of voluntary exercise on CNV in mice</i>	53
3.4.2 <i>Dose effect of wheel running on CNV</i>	56
3.4.3 <i>Effect of post-injury voluntary exercise on CNV in mice</i>	58
3.4.4 <i>Reduced F4/80+ cells and cytokine transcription in CNV in exercise-trained mice</i>	60
3.5 Discussion	62
Chapter 4: RF/6A chorioretinal cells do not display key endothelial phenotypes.....	65
4.1 Abstract	65
4.2 Introduction	66
4.3 Materials and Methods	68
4.3.1 <i>Cells and reagents</i>	68
4.3.2 <i>RNA isolation, library construction, and sequencing</i>	70
4.3.3 <i>Real-time quantitative PCR analysis</i>	71
4.3.4 <i>Western blotting</i>	72
4.3.5 <i>Immunofluorescent cell labeling</i>	73
4.3.6 <i>Immunohistochemistry</i>	73
4.3.7 <i>Acetylated LDL-uptake</i>	74
4.3.8 <i>Shear stress stimulation and nuclear alignment analysis</i>	74
4.4 Results.....	75
4.4.1 <i>Transcriptomic Profiling of RF/6A cells</i>	75
4.4.2 <i>Weibel-Palade Bodies in RF/6A Cells</i>	79
4.4.3 <i>Functional Endothelial Cell Assays in RF/6A Cells</i>	82
4.5 Discussion	85
Chapter 5: Conclusion.....	88
5.1 Summary of results.....	88
5.2 Future directions	89
References.....	91

List of Figures

Figure 1.1: Histology of human retina.....	4
Figure 1.2: The retina in health and disease	6
Figure 1.3: Schematic of experimental laser-induced CNV	9
Figure 2.1: Inflammasome agonism immediately following laser injury increases CNV volume.....	27
Figure 2.2: Intact NLRP3 inflammasome components are required for inflammasome agonism-dependent CNV exacerbation.....	31
Figure 2.3: <i>Alu</i> RNA does not induce RPE degeneration in <i>Aim2</i>^{-/-} mice.....	32
Figure 2.4: Inflammasome activation in myelomonocytic cells is crucial to laser CNV	34
Figure 2.5: Caspase-1 p20/GFAP immunostaining does not colocalize in CNV lesions	35
Figure 2.6: Representative immunoblot of pro-caspase-1 abundance in BMDM whole cell lysate.	36
Figure 2.7: Inflammasome activation promotes chemotaxis in peripheral BMDM..	39
Figure 2.8: IL-1β neutralization reduces <i>Alu</i> RNA-induced chemotaxis, macrophage accumulation, and laser CNV exacerbation.....	41
Figure 2.9: Combined administration of high-dose Vegfa nAb and IL-1β nAb does not further reduce CNV volume.	42
Figure 2.10: Representative phase-contrast images of choroid vessel sprouts.	44
Figure 3.1: Exercise trained mice develop less CNV than sedentary mice, independent of sex	55
Figure 3.2: CNV volume is not dependent on distance traveled	57
Figure 3.3: Post-injury exercise does not affect CNV development.....	59
Figure 3.4: Voluntary exercised-trained mice and macrophage infiltration in CNV	61
Figure 4.1: RF/6A cells do not express key endothelial transcripts or proteins	78
Figure 4.2: RF/6A cells do not exhibit the endothelial structural protein von Willebrand factor	81

Figure 4.3: RF/6A do not exhibit functional activities normally seen by endothelial cells.....84

List of Abbreviations

<i>Adgre1</i>	adhesion G protein-coupled receptor E1
AMD	age-related macular degeneration
ANOVA	analysis of variance
ASC	apoptosis-associated speck-like protein containing a caspase activation and recruitment domain
ATCC	American Type Culture Collection
AZT	azidothymidine
BCA	bicinchoninic acid
BMDM	bone marrow-derived macrophage
BRB	blood-retina barrier
BSA	bovine serum albumin
CDH5	cadherin 5
cDNA	complementary DNA
CI	confidence interval
CNV	choroidal neovascularization
DAMP	damage-associated molecular patterns
DAPI	4',6-diamidino-2-phenylindole
DME	diabetic macular edema
DMSO	dimethyl sulfoxide
DR	diabetic retinopathy
FITC	fluorescein isothiocyanate
FPKM	fragments per kilobase of transcript per million mapped reads

GA	geographic atrophy
GFAP	glial fibrillary acidic protein
HIF	hypoxia-inducible factor
HREC	primary human microvascular retinal endothelial cell
HUVEC	human umbilical vein endothelial cell
IL-18	interleukin-18
IL-1 β	interleukin-1 β
mREC	primary mouse microvascular retinal endothelial cell
M Φ	macrophage
nAb	neutralizing antibody
NLRP3	NLR family, pyrin domain-containing 3
nvAMD	neovascular age-related macular degeneration
OIR	oxygen-induced retinopathy
PBS-T	phosphate-buffered saline with Tween-20
PECAM1	platelet endothelial cell adhesion molecule-1
PFA	paraformaldehyde
POS	photoreceptor outer segment
qPCR	quantitative real-time PCR
RBP	retinol binding protein
RIPA	radio-immunoprecipitation assay
ROP	retinopathy of prematurity
RPE	retinal pigmented epithelium
SINE	short-interspersed nuclear element

TNF- α	tumor necrosis factor- α
VEGFA	vascular endothelial growth factor
VWF	vonWillebrand factor
WPB	Weibel-Palade body
ZO-1	zonula occludens-1

Chapter 1: Introduction

Pathological angiogenesis, the abnormal growth of blood vessels in tissue that is normally avascular, is a hallmark characteristic of many diseases with seemingly disparate etiology, including cancers¹, rheumatoid arthritis², and diseases of the eye, such as neovascular age-related macular degeneration (nvAMD). Recent research efforts have focused on the elucidation of a potential central mediator of pathological angiogenesis and have identified the dysfunctional activation of the inflammasome, a multimeric complex of the innate immune system, as a targetable candidate. However, the precise role of inflammasome activation in different vascular beds of the eye has yet to be known. The focus of this chapter is to provide a broad overview of the anatomy and physiology of the eye, describe the vasculature in both physiologic and pathologic states, examine models of studying pathological ocular angiogenesis in a laboratory setting, and compare current theories of inflammasome involvement in pathological angiogenesis.

1.1 Retinal physiology

The mammalian retina can be stratified into three major layers — the photoreceptors, the retinal pigmented epithelium, and the choroid — each of which play a role in the maintenance of visual homeostasis, both individually and cooperatively.

1.1.1 Photoreceptors

Photoreceptors are specialized, light-sensing neurons in the posterior region of the eye that are responsible for phototransduction and visual sensation. Whereas rods are predominantly found in the periphery of the retina, cones are almost exclusively positioned in the fovea, the central portion of the retina³. The photoreceptor outer segments (POS)

contain ordered stacks of disks that greatly increase the surface area of available photopigments. Photons entering the retina convert 11-cis-retinal to all-trans-retinal, but photoreceptors lack the necessary enzymatic machinery to restore baseline levels of 11-cis-retinal; thus, they must rely on another cell type—the retinal pigmented epithelium—to accomplish this.

1.1.2 Retinal pigmented epithelium

The retinal pigmented epithelium (RPE) cells are highly polarized, terminally differentiated epithelial cells that form a single layer between the neurosensory retina and the underlying choroidal vasculature (**Figure 1.1**). Utilizing proteins such as zonula occludens-1 (ZO-1), occludin, and claudin, RPE cells form tight junctions that effectively establish the outer blood-retina barrier⁴.

The apical side of each RPE contacts approximately 30 photoreceptors and is responsible for the phagocytosis of the POS through a tightly orchestrated process that involves recognition of accumulated phosphatidylserine on the POS by the RPE, as well as engagement of MerTK, Gas6, and $\alpha V\beta 5$ integrin⁴⁻⁶. Phagocytosis of the POS is just one key process by which the RPE function in visual homeostasis. Light-inactive all-trans-retinal is transported out of the photoreceptors by ATP-binding cassette, sub-family A, member 4 and diffuses into the RPE, where the isomerohydrolase RPE65 converts all-trans-retinal back to 11-cis-retinal, reestablishing the visual cycle⁷.

1.1.3 Choroid

The outer retina is avascular, as depicted in **Figure 1.1**, due to the outer blood-retina barrier. The basement membrane of choroidal endothelial cells and the basolateral

membrane of the retinal pigmented epithelial cells form the outer and inner layer of Bruch's membrane, respectively, a pentalaminar structure composed of extracellular collagenous and fibrous matrices⁸. Maintenance of the structural integrity of Bruch's membrane is of utmost importance in the preservation of high visual acuity; weakening of Bruch's membrane allows nascent and immature blood vessels to invade the normally avascular space, resulting in distortion (and ultimately death) of photoreceptors.

The capillary network of the choroid, the choriocapillaris, is unique in that these capillaries are highly fenestrated and thus are permeable to macromolecules such as albumin, glucose, and retinol binding protein (RBP), the carrier protein for retinol (vitamin A). Permeability of these three major macromolecules each contribute a specific function in maintaining visual homeostasis.

Diffusion of albumin into the extracellular space contributes to the high oncotic pressure of the extravascular stroma, facilitating the movement of fluid from the retina to the choroid for drainage⁹, while glucose permeability establishes a high extraretinal concentration gradient, enabling glucose influx into the retina for the metabolically demanding photoreceptors¹⁰. Finally, RBP permeability is critical for trafficking all-trans-retinol to the retina, preserving the balance of retinol metabolites used in the visual cycle¹¹.

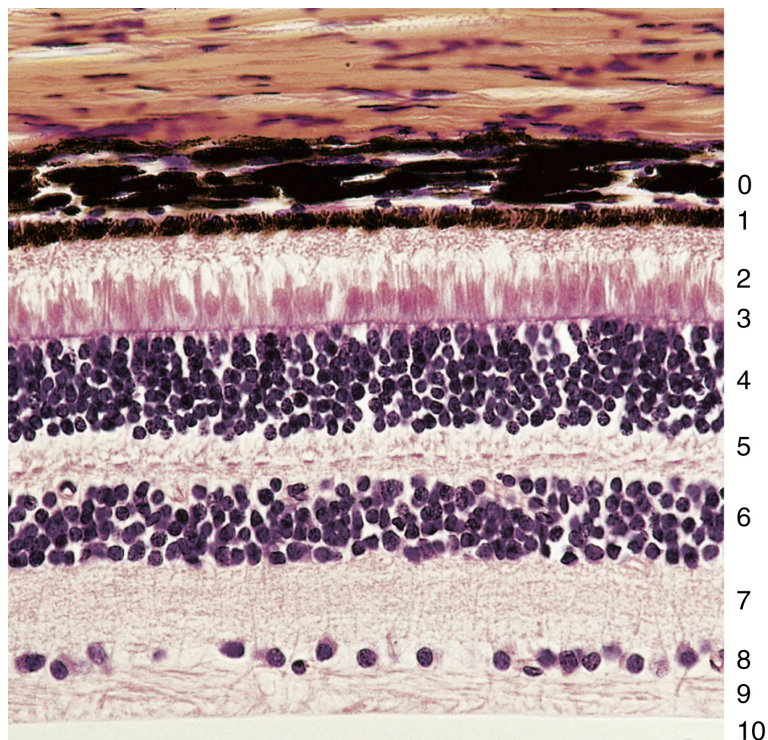


Figure 1.1: Histology of human retina

(0) Choroid, (1) Retinal pigmented epithelium, (2) lamina of rods and cones, (3) external limiting membrane, (4) outer nuclear layer, (5) outer plexiform layer, (6) inner nuclear layer, (7) inner plexiform layer, (8) ganglion cell layer, (9) optic nerve fiber layer, (10) inner limiting membrane. Adapted from Gartner L. Chapter 22: Special Senses. In: Gartner LP, eds. Textbook of Histology. 5th edition. Elsevier; 2021: 545-576.

1.2 Age-related macular degeneration

Age-related macular degeneration (AMD) is a blinding disease that accounts for most blindness in industrialized countries, characterized by progressive dysfunction of the RPE that ultimately results in loss of visual acuity. The earliest stage of AMD, named ‘early AMD,’ is typified by the presence of lipoproteinaceous deposits called ‘drusen’ that accumulate in the sub-RPE space between Bruch’s membrane and the RPE. In early AMD, drusen are medium-sized ($>63\ \mu\text{m}$ and $\leq 125\ \mu\text{m}$) with no other presenting pigmentary abnormalities¹². Disease staging is increased to ‘intermediate’ AMD when observable drusen measure greater than $125\ \mu\text{m}$, either with or without concomitant pigmentary abnormalities¹². Late-stage AMD pathology is further classified into either ‘geographic atrophy’ (GA) or ‘neovascular AMD’ (nvAMD), which can occur in two separate eyes or even either subsequently or concurrently within the same eye^{13,14}. GA is typified by large swaths of hypopigmentation and RPE cell death, whereas nvAMD is characterized by immature, leaky vessels of choroidal origin that invade into the normally avascular outer retina and cause physical distortion of the photoreceptors (**Figure 1.2**). Although GA is the more prevalent form of late-stage AMD, the majority of patients who experience severe vision loss exhibit CNV which, if left untreated, most often causes legal blindness^{15–17}.

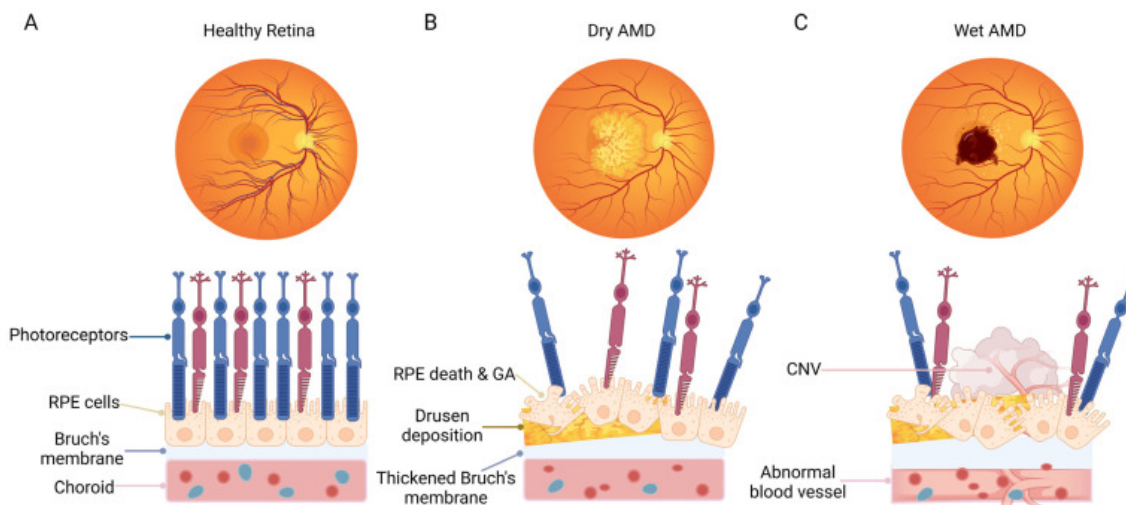


Figure 1.2: The retina in health and disease

(A) Healthy retina. The RPE are tightly packed with no thickening of Bruch's membrane. (B) Representation of dry AMD. Drusen deposits are located within the sub-RPE space and thickening of Bruch's membrane is observed. (C) Representation of nvAMD. Neovessels from the choroid have traversed Bruch's membrane and retinal hemorrhaging is observed. Figure taken from ¹⁸.

1.3 Models of pathological ocular angiogenesis

Animal models of ocular diseases are critical to elucidating molecular mechanisms of, and developing therapeutics for, pathological angiogenesis. This section aims to provide a general background on the methods of studying pathological angiogenesis in a laboratory setting.

1.3.1 *Experimental laser-induced choroidal neovascularization*

First developed by Ryan in 1979 using rhesus macaques¹⁹, the experimental laser-induced choroidal neovascularization model utilizes a krypton or argon laser to induce a break in Bruch's membrane (**Figure 1.3**). Transitioning away from non-human primates, the Campochiaro group developed a murine model in 1998²⁰ which takes advantage of the relative ease and high-throughput capability in mice and is now considered the field standard in investigating CNV.

In this model, subretinal blood vessels from the choroid invade through the Bruch's membrane rupture into the normally avascular outer retina, effectively recapitulating the disease process observed in patients with nvAMD.²⁰ As in excised human nvAMD lesions, vascular endothelial growth factor (VEGF) is upregulated in CNV lesions isolated from the mouse choroid²¹. This model is highly reproducible and has a neatly delineated time course of progression. Pro-inflammatory and pro-angiogenic macrophages are recruited to the lesion site and are observed one day after laser injury, with the local maximum peaking at three days²². Lesion size peaks around day seven and is assessed by either perfusion with intravenous fluorescein isothiocyanate-conjugated dextran (FITC-dextran) followed by

enucleation, or enucleation and immunolabeling with fluorophore-conjugated lectins and imaging by confocal microscopy.

The experimental laser-induced CNV model has become the standard method for studying choroidal neovascularization in mice owing to its relative ease, reproducibility, and relatively short time frame. However, it is not without disadvantages. Grossniklaus and Green describe laser CNV as a “non-specific response to a specific stimulus”²³, underscoring the reality that this model does not perfectly recapitulate clinical disease. Although it is thought that there must be a defect in Bruch’s membrane for the initiation of CNV, loss of integrity in Bruch’s membrane is observed in several diseases of disparate etiologies, including nvAMD, myopia²⁴, and pseudoxanthoma elasticum²⁵. The shortcomings of the acute nature of this injury model have led to the development of less invasive genetic models of CNV that more closely align with the chronic nature of CNV as it relates to aging, as discussed below.

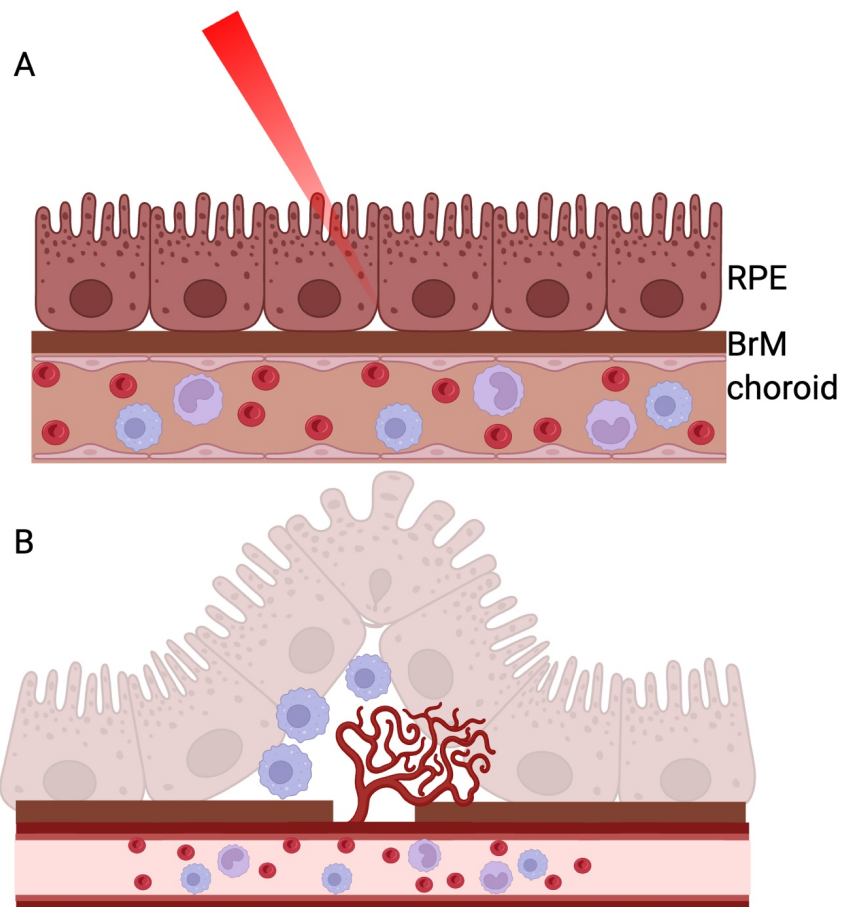


Figure 1.3: Schematic of experimental laser-induced CNV

(A) A laser is focused on the posterior region of the eye to induce a break in Bruch's membrane. (B) Neovessels begin to invade the normally avascular outer retina, reaching a peak volume at seven days post-laser injury. Monocytes are in purple; macrophages are in blue. Adapted from ²⁶.

1.3.2 Murine models of spontaneous CNV

To more thoroughly investigate the onset and progression of CNV with a focus on the chronic nature that is seen in patients, our lab and others have used several age-dependent models of spontaneous CNV in mice.

1.3.2.1 *Dicer1* hypomorph mice

Downregulation of the RNase DICER1 has been implicated in atrophic AMD, most notably that mRNA and protein levels are decreased in donor eyes from patients with the disease²⁷⁻³²; thus, our group previously sought to investigate whether *Dicer1* downregulation in mice could serve as a viable experimental model for retinal pathologies. The *Dicer1*^{d/d} mouse strain contains a gene trap insertion that causes a global 80% reduction in *Dicer1* levels³³, and we observed age-dependent RPE dysfunction¹⁴. Surprisingly, we also observed age-dependent, angiographically active lesions upon fluorescein fundus imaging that were susceptible to anti-VEGF treatment, recapitulating neovascular disease that is present in humans. Spontaneous CNV was also observed in another *Dicer1*-deficient mouse strain, *Dicer1*^{H/H}, as well as the JR5558 strain¹⁴. The spontaneous, age-dependent nature of these neovascular lesions afford the opportunity of studying the progressive nature of CNV maturation, rather than the acute nature of the laser-induced model. However, it is the same dependency on age that limits the throughput of this model.

1.3.2.2 *Vegfa* hyper mice

To elucidate whether increased VEGF in the eye is merely a consequence of disease or a potential cause, the Marneros group utilized the VEGF-A^{lacZKI/WT} mouse strain that has

reduced susceptibility to miRNA-mediated mRNA translation inhibition³⁴⁻³⁶; effectively, these mice have constitutively elevated levels of VEGF-A. Mice with a lacZ insert driven by a RPE-specific promoter did not show any pathology³⁷, whereas the VEGF- A^{lacZKI/WT} mice exhibited loss of RPE barrier function, accumulation of sub-RPE deposits, and extensive spontaneous CNV³⁸. These studies further our experimental capabilities of studying how CNV is initiated and progresses in a more chronic manner, compared to the laser injury model.

1.4 Macrophage modulation of pathological angiogenesis

The integrity of the blood-retina barrier (BRB) establishes in the eye a degree of immune privilege. As reviewed in ³⁹, pigment epithelial-derived immunosuppressive factors, coupled with the structural characteristics of the BRB, prevent the ingress of systemic-derived macrophages. However, these immune cells are known to be potent mediators of angiogenesis through the secretion of both pro-angiogenic factors and extracellular matrix-remodeling metalloproteinases⁴⁰. Through examining postmortem eyes from two patients with diagnosed AMD, Grossniklaus and colleagues found a higher incidence of macrophages in the vascular regions associated with CNV⁴¹. Shortly thereafter, two separate groups reported that ablation of macrophages significantly reduces experimental laser CNV volume^{22,42}. Additionally, a third group observed reduced CNV area in *Ccr2*^{-/-} mice after laser injury despite the demonstrated angiogenic ability of ocular-infiltrating macrophages⁴³, strongly supporting the notion that macrophages are important mediators of the laser CNV response.

1.4.1 Inflammasome activation in macrophages

In addition to their primary role as phagocytes, macrophages also function as integrators of immune stimuli to promote inflammation in other cell types. One mechanism by which this is accomplished is through inflammasomes, multimeric protein complexes whose activation results in the secretion of proinflammatory cytokines and cell death. The basic components of an inflammasome are as follows: 1) a sensor, such as the NLR family pyrin domain containing 3 (NLRP3), that detects damage associated molecular patterns (DAMPs), such as extracellular ATP; 2) an adaptor, most commonly the apoptosis-associated speck-like protein containing a caspase activation and recruitment domain (ASC); and 3) an effector, such as caspase-1, an enzyme that converts inactive pro-peptides into their active form. Inflammasome activation occurs classically through the purinergic receptor P2RX7 that forms pores in the cell membrane in response to increased levels of extracellular ATP⁴⁴. P2X7 pore formation increases potassium permeability in the cell, resulting in potassium efflux. In response to the potassium efflux, NLRP3 recruits ASC and pro-caspase-1, which is in turn autocatalytically cleaved into the p10 and p20 subunits. The now catalytically active caspase-1 binds and cleaves pro-cytokines, such as interleukin-1 beta (IL-1 beta) and interleukin-18 (IL-18), which are secreted and can potentiate the inflammatory response through the recruitment of immune cells⁴⁵.

1.5 Current theories of inflammasome involvement in pathological angiogenesis

While the role of inflammasome activation in the pathogenesis of GA has been largely investigated, its role in aberrant angiogenesis is not well defined. In this section we will discuss the conflicting studies that propose inflammasome activity either inhibits or promotes CNV.

1.5.1 Conflicting reports on inflammasome in CNV

Previous work focusing on the biochemical and immunostimulatory nature of drusen in eyes with GA revealed that accumulation of these extracellular, lipoproteinaceous aggregates resulted in RPE death by necrosis, a known stimulator of NLRP3 inflammasome activation^{46,47}. Doyle and colleagues reported activation of NLRP3 inflammasome in human peripheral blood mononuclear cells (PBMC) by priming with lipopolysaccharide (LPS) and subsequent treatment with drusen isolated from human eyes with GA⁴⁸. In the same study, *Nlrp3*^{-/-} and *Il18*^{-/-} mice were reported to exhibit greater CNV volumes compared to wild-type controls, while mice lacking the interleukin-1 receptor type 1 (*Il1r1*^{-/-}) did not exhibit increased CNV volume. Furthermore, intravitreal administration of IL-18 neutralizing antibodies also significantly increased laser CNV volume. The authors posit that IL-18 is protective in the laser CNV model, further reporting that treatment of an immortalized human RPE cell line (ARPE-19) and immortalized mouse brain endothelial cell line (bEnd.3) with IL-18 reduced the levels of VEGF as detected by ELISA.

In response to this report, a multi-center study spanning five independent laboratories found that even with varying laser powers and protocol parameters, intravitreal administration of recombinant IL-18 did not affect laser CNV size⁴⁹. Furthermore, genetic ablation, siRNA-mediated gene knockdown, or pharmacologic inhibition of the inflammasome constituents *Nlrp3*, *Asc*, and caspase-1 did not affect CNV size relative to WT controls⁴⁹. Because the original study compared eyes treated with IL-18 nAb with eyes that received no injection (rather than the appropriate biological control), the response study included administration of an IgG isotype that was diluted in either PBS

or the diluent of the IL-18 nAb. As expected, IgG in PBS had no effect on CNV volume. Surprisingly, however, IgG diluted in the nAb diluent increased CNV size, an effect that was shown to arise from the known pro-angiogenic molecule glycerol⁵⁰. Thus, the response study concluded that the reported angio-inhibitory effect of IL-18 was due to the glycerol in the diluent formulation.

1.5.2 Inflammasome in spontaneous CNV

As discussed previously, the laser injury model of CNV does not fully recapitulate the disease processes seen in human pathology, a limitation that is addressed by the usage of spontaneous CNV models that reflect the chronic, age-dependent nature of CNV in nvAMD.

Previous work from our group identified enzymatically active caspase-1 in the outer retina of aged *Dicer1^{d/d}* mice that colocalized with regions of CNV¹⁴. To further investigate the role of inflammasome in CNV, we then crossed the *Dicer1^{d/d}* line with mice lacking the inflammasome constituents caspase-1/caspase-11 (*Dicer1^{d/d}* x *Casp1^{-/-};Casp11^{-/-}*) and Myd88 (*Dicer1^{d/d}* x *Myd88^{-/-}*). Whereas almost 80% of eyes from *Dicer1^{d/d}* mice developed neovascularization by 10 months of age, *Dicer1^{d/d}* mice lacking inflammasome constituents were spared¹⁴. In a separate study from the Marneros group utilizing the VEGF-A^{hyper} strain, mice developing CNV as a result of VEGF-A overexpression demonstrated positive NLRP3 immunostaining in the RPE and VEGF-A^{hyper} mice lacking *Nlrp3* developed fewer CNV lesions than VEGF-A^{hyper} mice alone³⁸. Taken together, these two studies demonstrate the critical importance of inflammasome signaling in the development of CNV in two separate models.

1.6 Dissertation goals and significance

Previous research on the involvement of inflammasome activation in age-related macular degeneration has almost been exclusively in the context of non-neovascular AMD. Even so, current literature on the role of inflammasome activation in neovascular AMD, mainly utilizing the laser-induced CNV model, is contradictory, thus necessitating a more refined approach.

The gap in knowledge I sought to address in this work was to reconcile the disparate observations that inflammasome components are not necessary for the laser CNV response but are in fact required for the development of spontaneous CNV lesions in a *Dicer*-deficient mouse model.

The first chapter after this introduction presents our findings that demonstrate a revised laser CNV model in which disease-relevant inflammasome agonists are administered at the time of laser CNV injury. Subretinal administration of these inflammasome agonists increased laser CNV volume in an inflammasome-dependent manner, which we found was specific to myelomonocytic cells. *In vitro* chemotaxis assays revealed the presence of a soluble chemotactic factor, interleukin-1 β , responsible for driving inflammasome-dependent CNV exacerbation, which was abolished with the administration of a neutralizing antibody.

The third chapter focuses on work that was performed concurrently with the above study, in which we developed a first-of-its-kind experimental model to assess how physical exercise affects the development of laser CNV. We found that mice that were allowed to voluntarily exercise on a running wheel prior to laser CNV administration developed

smaller CNV lesions compared to sedentary mice, which correlated with a decrease in macrophage recruitment and chemotactic cytokine mRNA expression.

The fourth chapter presents transcriptomic, anatomical, and functional data that suggests a commonly used cell line in ophthalmology research, the RF/6A line, does not express endothelial characteristics that the source literature claims. Taken together, these three chapters constitute a body of work that is grounded in addressing not only specific questions, such as how inflammasome activation contributes to pathological angiogenesis, but also presents critical analyses of both previously established and recently developed methodologies that improve upon both current and future investigations into pathological angiogenesis.

Chapter 2: Inflammasome agonism aggravates choroidal neovascularization

This chapter is a modified version of the previously published article:

Makin RD, Apicella I, Dholkawala R, Fukuda S, Hirahara S, Hirano Y, Kim Y, Nagasaka A, Nagasaka Y, Narendran S, Pereira S, Varshney A, Wang S-b, Ambati J, Gelfand BD. *Inflammasome agonism aggravates choroidal neovascularization*. *Angiogenesis* (2024).

2.1 Abstract

Inflammasome activation is implicated in diseases of aberrant angiogenesis such as age-related macular degeneration (AMD), though its precise role in choroidal neovascularization (CNV), a characteristic pathology of advanced AMD, is ill-defined. Reports on inhibition of inflammasome constituents on CNV are variable and the precise role of inflammasome in mediating pathological angiogenesis is unclear. Historically, subretinal injection of inflammasome agonists alone has been used to investigate retinal pigmented epithelium (RPE) degeneration, while the laser photocoagulation model has been used to study pathological angiogenesis in a model of CNV. Here, we report that the simultaneous introduction of any of several disease-relevant inflammasome agonists (Alu or B2 RNA, Alu cDNA, or oligomerized amyloid β (1–40)) exacerbates laser-induced CNV. These activities were diminished or abrogated by genetic or pharmacological targeting of inflammasome signaling constituents including P2rx7, Nlrp3, caspase-1, caspase-11, and Myd88, as well as in myeloid-specific caspase-1 knockout mice. Alu RNA treatment induced inflammasome activation in macrophages within the CNV lesion, and increased accumulation of macrophages in an inflammasome-dependent manner. Finally, IL-1 β neutralization prevented inflammasome agonist-induced chemotaxis, macrophage trafficking, and angiogenesis. Collectively, these observations support a model wherein inflammasome stimulation promotes and exacerbates CNV and may be a therapeutic target for diseases of angiogenesis such as neovascular AMD.

2.2 Introduction

Inflammasome activation is implicated in the pathogenesis of a variety of complex diseases, including retinal diseases such as age-related macular degeneration (AMD) and diabetic retinopathy. In the context of AMD, evidence supports that inflammasome activation promotes atrophic retinal degeneration in cell and animal models and geographic atrophy¹, the advanced form of dry AMD.

Conversely, neovascular AMD is characterized by aberrant growth of blood vessels into the outer retina, which is normally avascular. These pathological neovessels typically emerge from the underlying choroid or inner retina. Mice lacking inflammasome constituents are protected against spontaneous choroidal neovascularization (CNV) in mouse models driven by an excess of VEGFA or DICER1 deficiency^{14,51}. Conversely, the role of inflammasome in laser photocoagulation-induced CNV, the benchmark model of choroidal angiogenesis which is driven by a thermal injury burn to the pigmented epithelium that results in an acute angiogenic and wound healing response, lacks consensus. Initial reports suggested that *Nlrp3*^{-/-} mice exhibit elevated laser-induced CNV⁴⁸, though this finding was challenged by a multinational consortium which found that genetic or pharmacologic inhibition of core inflammasome constituents or effectors does not increase experimental CNV⁴⁹. Still others have reported that pharmacologic inhibition of caspase-1 suppresses CNV⁵¹.

It is conceivable that laser photocoagulation, an artificial injury stimulus, does not consistently stimulate or rely on inflammasome to induce angiogenesis, which may contribute to the heterogeneous findings of inflammasome involvement in

genetic/spontaneous and injury/acute models of CNV. Therefore, we sought to investigate the role of inflammasome activation in CNV by introducing a new model in which subretinal administration of disease-relevant inflammasome stimulators is performed with laser-induced CNV. Using this novel model, we report that while inflammasome constituents are dispensable for the laser CNV response, the addition of inflammasome stimulators exacerbates pathologic choroidal angiogenesis, and that in the presence of inflammasome agonists, genetic or pharmacologic intervention of inflammasome signaling significantly improves CNV outcomes in mice.

2.3 Materials and Methods

2.3.1 Mice

All experiments involving animals were approved by the University of Virginia Animal Care and Use Committee and in accordance with the Association for Research in Vision and Ophthalmology Statement for the Use of Animals in Ophthalmic and Visual Research.

Mice were maintained on a constant 12:12-h light–dark cycle. Water and food were provided ad libitum. Mice were euthanized with CO₂ gas under constant gas flow. C57BL/6J wild-type, *P2rx7^{-/-}*, *Casp1^{-/-}/11^{-/-}*, *LysM-Cre*, and *Aim2^{-/-}* mice were obtained from The Jackson Laboratory. *Casp1^{-/-}/11^{-/-};Casp11^{Tg}* mice, described elsewhere⁵², were a generous gift from V. M. Dixit (Genentech, South San Francisco, California). *Myd88^{-/-}* mice were generously provided by S. Akira via T. Hawn and D. T. Golenbock. *Casp1^{ff}* mice were a generous gift from Dr. Richard Flavell (Yale University). *Nlrp3^{-/-}* mice have been previously described⁵³. For all procedures, anesthesia was achieved by intraperitoneal injection of 100 mg/kg ketamine hydrochloride (Ft. Dodge Animal Health, Overland Park, Kansas, US) and 10 mg/kg xylazine (Phoenix Scientific, San Marcos, California, US), and pupils were dilated with topical 1% tropicamide and 2.5% phenylephrine (Alcon Laboratories, Elkridge, Maryland, US).

2.3.2 Laser-induced CNV and subretinal injection

A schematic of the laser-induced CNV and injection procedure is depicted in **Fig 1a**. Experimental CNV was induced by performing a single laser photocoagulation burn with an OcuLight GL laser system (532 nm, 180 mW, 100 ms, 75 μ m; Iridex Corporation,

Mountain View, CA, USA) bilaterally in 6- to 8-week-old mice. Immediately following laser CNV, subretinal injection of experimental compounds was performed as described previously⁵⁴. Briefly, a 5 μ l microsyringe was filled with 1-2 μ l of reagent and attached to a custom 37G needle. The needle was then introduced at a 60° angle until it touched the retina and a retinotomy was induced to access the subretinal space. The reagent was then slowly dispensed into the subretinal space such that the resulting detachment encompassed the area previously treated with the laser. The following reagents were used for subretinal injection: PBS (VWR, Radnor, PA, US; 97063-660); *in vitro* transcribed *Alu*, B1, and B2 RNAs as previously described⁵⁵; plasmid-encoded *Alu* RNA and empty plasmid control with NeuroPORTER Transfection Reagent (AMSBIO, Cambridge, MA, US; AMS.T400150) as previously described⁵⁶; amyloid- β as previously described⁵⁷. For intravitreal injections the following reagents were administered immediately following laser thermal injury and subretinal injections: azidothymidine (AZT), 0.5 nmol (Selleck Chemicals, Houston, TX, US; S2579); 2-ethyl-AZT, 0.5 nmol (previously described in⁵⁷); Z-WEHD-FMK (R&D, Minneapolis, MN, US; FMK002) or control peptide Z-FA-FMK (R&D; FMKC01); IL-1 β neutralizing antibody, 500 ng (R&D, MAB4012) or isotype IgG, 500 ng (Thermo, 14-4888-81); MyD88 inhibitory peptide or control peptide (Novus, Centennial, CO, US; NBP2-29328-1mg).

2.3.3 RPE/choroid flatmount preparation and CNV volume quantification

RPE flatmounts were obtained as previously described⁵⁴. At the indicated timepoint, eyes were enucleated and fixed in 4% paraformaldehyde/PBS for 1 hour at room temperature. After removal of the cornea, lens, and neurosensory retina, flatmounts were dehydrated and rehydrated through a methanol series, washed in 1x PBS, and incubated in

blocking buffer (1% BSA in PBST) for 1 hour at 4 °C. Flatmounts were then incubated with 0.7% FITC-isolectin B4 overnight at 4 °C. Flatmounts were then washed in 1x PBST and mounted on glass slides with Vectashield antifade mounting medium (Vector Biolabs, Newark, CA, US; H-1000-10). CNV volumes were quantified as previously described⁵⁸.

2.3.4 F4/80 immunofluorescence and quantification

For F4/80 immunofluorescence on flatmounts, eyes were processed as described above. Eyes were then incubated in rat anti-mouse F4/80:RPE (Bio-Rad, Hercules, CA, US; MCA497PE, clone Cl:A3-1) overnight at 4 °C. Washing and imaging was also performed as described above. Macrophage numbers were manually quantified by a masked grader using the FIJI plugin Cell Counter (<https://imagej.net/ij/plugins/cell-counter.html>) who was blinded to the experimental conditions.

2.3.5 Immunofluorescence

Fresh, unfixed eyes were embedded in optimal cutting temperature medium (Tissue-Tek OCT Compound, VWR; 25608-930) and frozen in liquid nitrogen-cooled isopentane. Immunofluorescent analysis was performed by blocking 4% PFA-fixed sections with donkey block (2% normal donkey serum; 1% BSA; 0.1% Triton X-100; 0.05% Tween-20; 0.05% NaN₃ in PBS) for 1 hour at 37 °C followed by overnight incubation at 4 °C with the following antibodies: PE anti-mouse/human CD11b 1:50, clone M1/70 (BioLegend, San Diego, CA, US; 101207); anti-cleaved caspase-1 (Asp296) 1:100, clone E2G2I (Cell Signaling Technology, Danvers, MA, US; 89332). Anti-cleaved caspase-1 antibodies were detected with Alexa Fluor 647-conjugated donkey anti-rabbit

secondary antibody (Thermo, A-31573) at a concentration of 1:1000 in donkey block. Equivalent amount of rabbit IgG was used for isotype control.

2.3.6 *Fluorescent in situ hybridization*

Fresh-frozen cryosections prepared as above were probed with the RNAscope Multiplex Fluorescent Reagent Kit v2 (ACDBio, Newark, CA) according to manufacturer's instructions using the following probes: Mm-Il1b (# 316891); Mm-Adgre1-C2 (# 460651-C2); Mm-P2ry12-C3 (# 317601-C3). Probes were detected with the following fluorophores diluted 1:1000 in RNAscope TSA buffer: Opal 520 (Akoya Biosciences, Marlborough, MA, # FP1487001KT); Opal 570 (Akoya, # FP1488001KT); Opal 650 (Akoya, # FP1496001KT). Imaging was performed on a Nikon A1R confocal microscope.

2.3.7 *Transwell migration assays*

The chemotactic ability of WT BMDM was assessed using 8.0 μm permeable polycarbonate inserts (Celltreat, Pepperell, MA; 230633). Four hours before addition of chemotactic agent, 600 μL 2% BMDM media was added to the bottom well of a 24-well plate and 60,000 cells in 100 μL 2% BMDM media were seeded into the insert. After four hours, media from the bottom well was aspirated and replaced with the chemoattractant under study and incubated at 37 °C/5% CO₂ for twelve hours. The following chemoattractants were used: recombinant mouse VEGF₁₆₄ protein, 50 ng/mL (R&D; 493-MV-005); conditioned media from *Alu* RNA-transfected WT and *Casp1*^{-/-} BMDM, diluted to 10% in RPMI (ThermoFisher; 12440061). Inserts were then rinsed three times in 1x PBS, unigrated cells on the apical side of the transwell scraped with a cotton-tipped

applicator, and fixed in 4% PFA/PBS for one hour. After rinsing three times in 1x PBS, membranes were excised with a scalpel and mounted on glass slides in ProLong Gold Antifade with DAPI (ThermoFisher, P36935). For each membrane, five fields of view at 20X were imaged with a Nikon Eclipse Ti2 inverted widefield fluorescence microscope and quantified in FIJI (<http://fiji.sc/>).

2.3.8 Statistics

Using empirical data on the variability of PBS-injected laser CNV lesions (**Fig 1c**), power analysis determined that a minimum of N=5 eyes are needed to detect a 50% change in CNV volume with 80% power. Experiments were designed to exceed this to account for technical complications. Statistical analyses were performed using GraphPad Prism (GraphPad Software, Version 9.1.2, San Diego, CA, US). Unless otherwise stated, results are shown as mean \pm standard error of mean. *P* values of less than 0.05 were deemed statistically significant by either two-tailed Mann Whitney U test, two-tailed Kruskal-Wallis test, or one- or two-way ANOVA with multiple comparisons corrections, as stated in the figure legends.

2.4 Results

2.4.1 Inflammasome agonists exacerbate experimental CNV

To test the hypothesis that inflammasome activators promote excess choroidal angiogenesis, we adapted the laser photocoagulation model by applying a single laser burn to wild-type C57BL/6J mice eyes followed immediately by subretinal injection of PBS or *Alu* RNA, which is an AMD-related inflammasome agonist transcribed from short interspersed nuclear element (SINE) retrotransposons^{31,56} (**Figure 2.1A**). Seven days later, *Alu* RNA-treated eyes exhibited a dramatic increase in the volume of the CNV lesion compared to saline-treated eyes (**Figure 2.1B, C**). Similarly, subretinal administration of a plasmid expressing *Alu* RNA (pAlu) with transfection reagent resulted in an increased CNV response compared to the transfection of an empty plasmid (pNull) (**Figure 2.1D**).

Administration of murine SINE B2 RNA, which like *Alu* RNA is an inflammasome agonist^{31,56}, also exacerbated CNV (**Figure 2.1E**). Interestingly, mouse SINE B1 RNA, which is a poorer inflammasome agonist⁵⁵, did not significantly affect CNV (**Figure 2.1E**).

Alu RNA can be reverse transcribed by the LINE-1 reverse transcriptase into a complementary DNA (*Alu* cDNA) which stimulates inflammasome activation, promotes RPE death, and is enriched in the retina of human AMD eyes^{59,60}. Subretinal delivery of synthetic *Alu* cDNA also increased the volume of CNV lesions (**Figure 2.1F**). To assess whether this angiostimulatory property was unique to SINE-derived oligonucleotides, we tested amyloid- β , another inflammasome agonist that accumulates in human AMD⁶¹⁻⁶³, contributes to spontaneous CNV in a mouse model⁶⁴, and promotes inflammasome-dependent RPE death^{57,65}. Subretinal delivery of oligomerized amyloid- β_{1-40} , but not a

control peptide (amyloid- β_{40-1}), likewise aggravated CNV (**Figure 2.1F**). These findings indicate that multiple inflammasome agonists of different compositions can amplify the choroidal angiogenic response in the laser injury model.

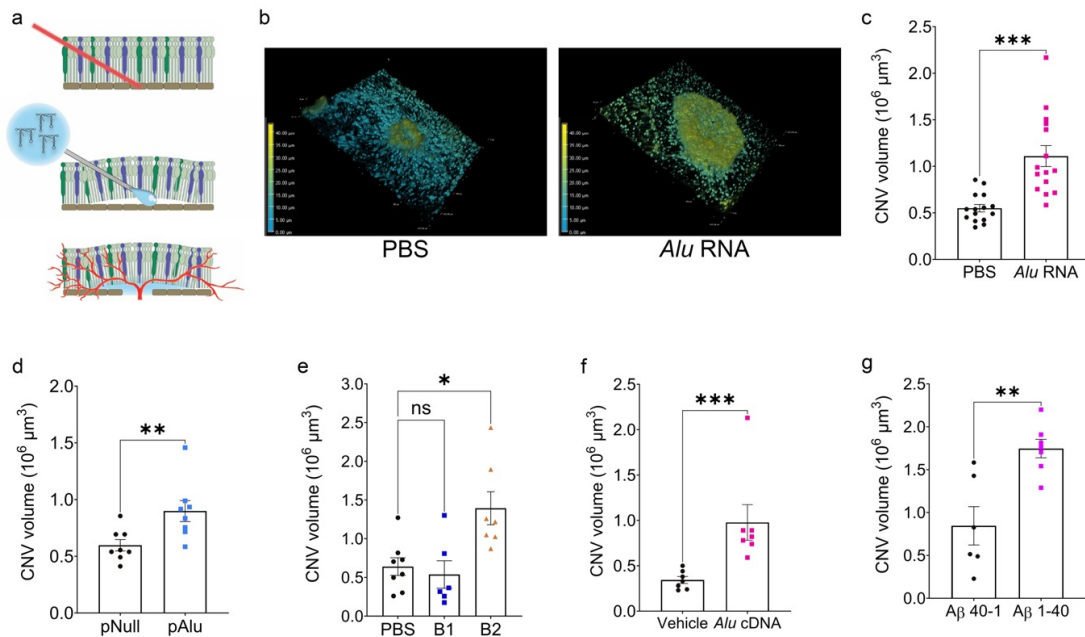


Figure 2.1: Inflammation agonism immediately following laser injury increases CNV volume

(a) Schematic demonstrating the combined laser CNV and subretinal injection (SRI) model. First, a laser burn is applied to rupture Bruch's membrane. Subretinal injection is performed immediately following laser injury at the same site, and neovascularization begins to form around day 3. (b) Representative depth-coded 3D projections of laser CNV with SRI of PBS (left) or *Alu* RNA (right). Dimensions: $633.25 \mu\text{m} \times 633.25 \mu\text{m} \times 46 \mu\text{m}$ (c) CNV volumes quantified 7 days after combined laser injury and SRI of *Alu* RNA ($P=0.0001$, Mann-Whitney test. $N = 15$ per group). (d) CNV volumes quantified 7 days after combined laser injury and in vivo transfection of plasmid-encoded *Alu* via SRI ($P<0.01$, Mann-Whitney test. $N = 8$ per group). (e) CNV volumes quantified 7 days after combined laser injury and SRI of PBS, B1 ($P>0.99$ vs. PBS), or B2 RNA ($P=0.03$ vs. PBS, Kruskal-Wallis test. $N = 6$ (B1), $N = 7$ (B2)). (f) CNV volumes quantified 7 days after combined laser injury and SRI of *Alu* cDNA ($P=0.01$, Mann-Whitney test. $N = 7$ (vehicle), $N = 7$ (*Alu* cDNA)). (g) CNV volumes quantified 7 days after combined laser injury and SRI of A β ($P<0.01$, Mann-Whitney test. $N = 6$ (A β_{40-1}), $N = 7$ (A β_{1-40})).

2.4.2 The angiostimulatory activity of *Alu* RNA depends on inflammasome

As inflammasome agonists may have pleiotropic effects aside from inflammasome activation, we next sought to determine whether this angiostimulatory effect was indeed dependent on inflammasome activity. To test this, we administered *Alu* RNA immediately following laser injury in mice lacking constituents of the inflammasome pathway, or in wild-type mice treated with pharmacologic inflammasome inhibitors.

The ATP receptor P2X7 is an upstream driver of inflammasome activation and is required for *Alu* RNA-induced RPE degeneration³². In *P2rx7^{-/-}* mice, *Alu* RNA did not exacerbate laser-induced CNV (**Figure 2.2A**). Nucleoside reverse transcriptase inhibitors (NRTIs) prevent P2X7-dependent inflammasome activation and RPE degeneration^{57,58,66,67}. Administering the NRTI zidovudine (AZT) into the vitreous of wild-type mice immediately following thermal laser burn and subretinal *Alu* RNA injection also abrogated the angiostimulatory response (**Figure 2.2B**). In addition to targeting P2X7, NRTIs also inhibit reverse transcriptases. A 2-ethoxylated-modified derivative of AZT that does not inhibit reverse transcriptase but retains anti-inflammatory activities⁶⁷ also blunted *Alu* RNA-induced CNV (**Figure 2.2B**), further supporting that the angiostimulatory activity of *Alu* RNA depends on P2X7.

Downstream of P2X7 activation, *Alu* RNA stimulates inflammasome assembly consisting of NLRP3, ASC, and the protease caspase-1³¹. As in *P2rx7^{-/-}* mice, CNV lesions in mice lacking NLRP3 (*Nlrp3^{-/-}*) were also unaffected by *Alu* RNA (**Figure 2.2C**). Conversely, mice lacking AIM2 (*Aim2^{-/-}*), an alternative inflammasome receptor that does

not mediate *Alu* RNA-induced RPE death (**Figure 2.3**), were susceptible to *Alu* RNA-induced exacerbation of CNV (**Figure 2.2D**).

We next investigated the contribution of caspase-1, the inflammasome effector protease. Mice lacking both caspase-1 and the non-canonical inflammasome effector caspase-11 (*Casp1^{-/-};Casp11^{-/-}*) are resistant to *Alu* RNA-induced RPE degeneration³¹. Similarly, *Casp1^{-/-}/Casp11^{-/-}* mice were resistant to the angiostimulatory activity of *Alu* RNA in CNV (**Figure 2.2E**). In double knockout mice in which caspase-11 expression is rescued by a transgene (*Casp1^{-/-}; Casp11^{-/-};Tg⁺*), *Alu* RNA treatment did not affect CNV (**Figure 2.2E**), supporting that caspase-1 is essential for *Alu* RNA stimulated CNV. Furthermore, administration of Z-WEHD-FMK, a cell-permeable irreversible inhibitor of caspase-1, into the vitreous humor of wild-type mice also abrogated the angiostimulatory effect of *Alu* RNA on laser CNV (**Figure 2.2F**). RPE degeneration by *Alu* RNA also depends on the activity of caspase-11⁶⁸. Mice lacking just caspase-11 (*Casp11^{-/-}*) were partially protected against *Alu* RNA-induced CNV exacerbation (**Figure 2.2E**), indicative of some contribution of non-canonical inflammasome activation to this process.

Inflammasome activation results in maturation of the effector cytokines IL-1 β and IL-18, whose signal transduction requires the adaptor MyD88⁶⁹. Mice lacking MyD88 (*Myd88^{-/-}*) are protected against *Alu* RNA-induced RPE degeneration³¹. In *Myd88^{-/-}* mice, administration of *Alu* RNA did not affect CNV volume (**Figure 2.2G**). Additionally, whereas *Alu* RNA induced excess CNV in eyes receiving a cell-permeable control inhibitor via intravitreal injection, administration of a MYD88 homodimerization peptide inhibitor⁷⁰ diminished the effect of *Alu* RNA on laser CNV (**Figure 2.2F**).

Collectively, these findings suggest that in the presence of an inflammasome agonist, inflammasome signaling amplifies pathological choroidal angiogenesis.

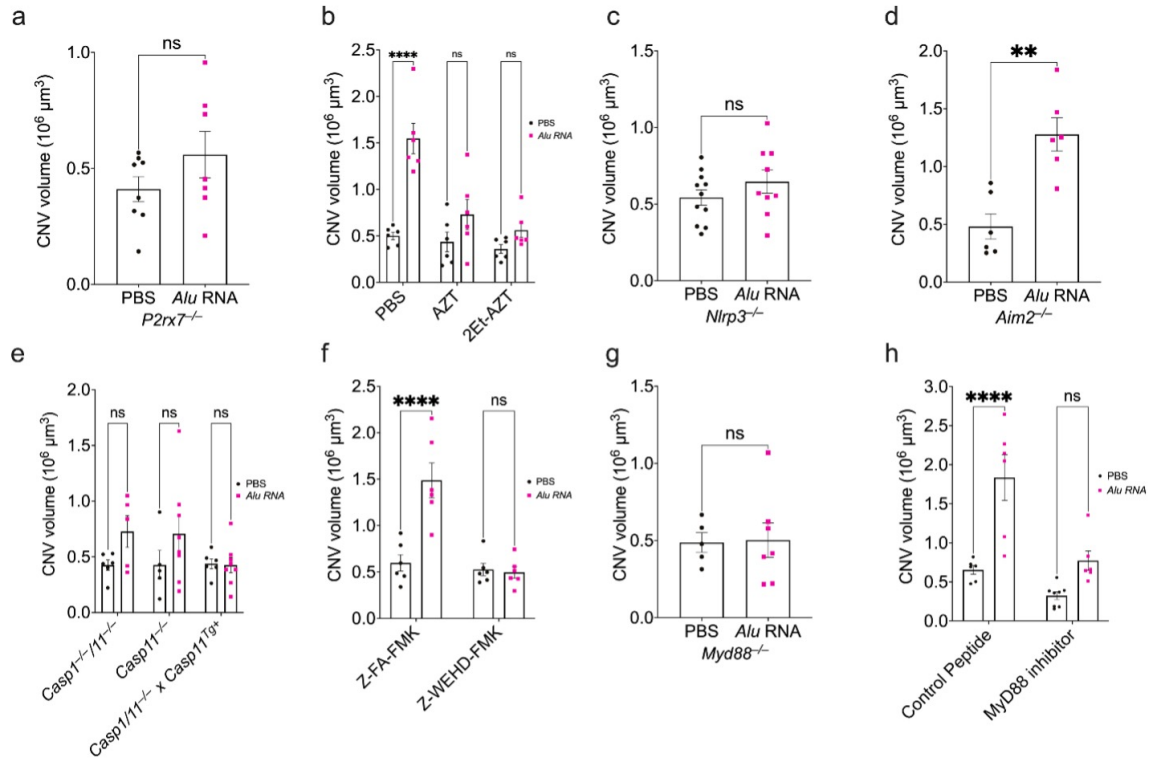


Figure 2.2: Intact NLRP3 inflammasome components are required for inflammasome agonism-dependent CNV exacerbation

(A) CNV volumes quantified 7 days after combined laser injury and SRI of *Alu* RNA in *P2rx7*^{-/-} mice ($P > 0.99$, Mann-Whitney test. $N = 7-8$). (B) CNV volumes quantified 7 days after combined laser injury, SRI of *Alu* RNA, and intravitreal pretreatment with PBS ($P < 0.01$), AZT ($P = 0.20$), or K8 ($P = 0.50$) (two-way ANOVA. $N = 6$ per group). (C) Quantification of CNV volume 7 days post *Alu* RNA SRI in *Nlrp3*^{-/-} mice ($P = 0.412$, Mann-Whitney test. $N = 11$ (PBS), $N = 9$ (*Alu* RNA)). (D) CNV volumes quantification 7 days after laser injury and SRI of *Alu* RNA in *Aim2*^{-/-} mice ($P < 0.01$, Mann-Whitney test. $N = 6$ per group). (E) CNV volumes quantified after combined laser injury and SRI of *Alu* RNA in *Casp1/11*^{-/-} ($P = 0.25$), *Casp11*^{-/-} ($P = 0.25$), and *Casp1/11*^{-/-} x *Casp11*^{Tg+} ($P > 0.99$) (two-way ANOVA, $N \geq 5$ per group). (F) CNV volume quantification 7 days after combined laser injury, intravitreal administration of either control peptide Z-FA-FMK ($P < 0.01$) or caspase-1 inhibitor Z-WEHD-FMK ($P = 0.98$), and *Alu* RNA SRI (two-way ANOVA, $N = 6$ per group). (G) CNV volumes quantified after 7 days post-laser injury and *Alu* RNA SRI in *Myd88*^{-/-} mice ($P = 0.79$, Mann-Whitney U test, $N \geq 5$ per group). (H) CNV volumes quantified 7 days after combined laser injury, intravitreal administration of a peptide MyD88 inhibitor ($P = 0.08$) or control peptide ($P < 0.01$), and *Alu* RNA SRI ($P = 0.08$, two-way ANOVA, $N \geq 6$ per group)

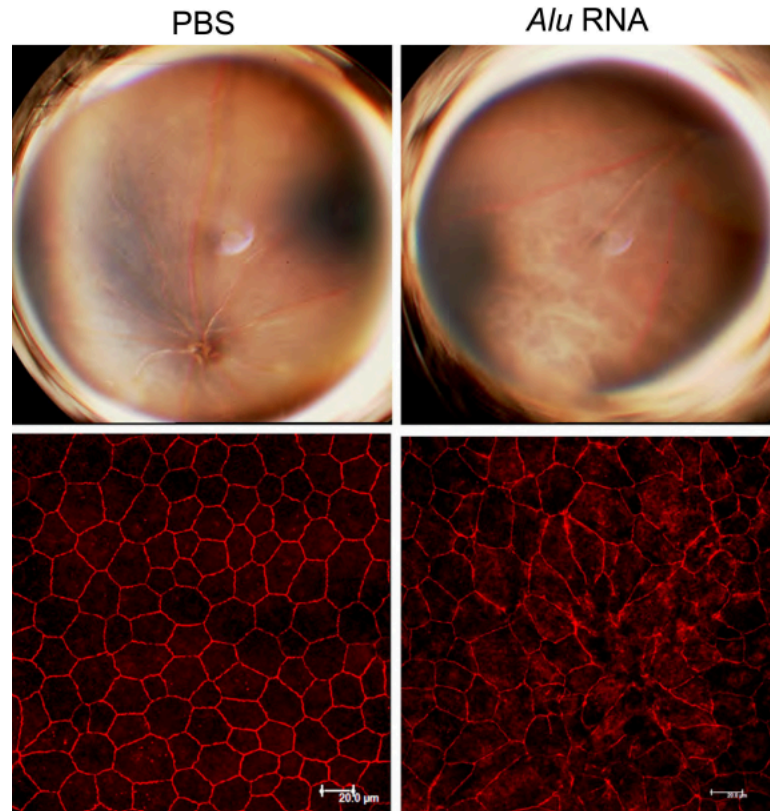


Figure 2.3: *Alu* RNA does not induce RPE degeneration in *Aim2*^{-/-} mice. Fundus images (top) and RPE flatmounts of immunolabeled ZO-1 (bottom) of *Aim2* mice subretinally injected with PBS (left) or *Alu* RNA (right). Scale bars: 20 μm.

2.4.3 Inflammasome in myeloid cells is critical for *Alu* RNA-induced CNV exacerbation

Laser CNV is a multicellular process involving multiple resident and recruited cells. Among these, circulating macrophages and neutrophils are recruited to CNV lesions and drive their growth^{71,72}. In *Alu* RNA-treated CNV lesions, immunofluorescent labeling revealed robust inflammasome activation via positive immunolabeling of the p20 subunit of caspase-1, which in part co-localized with CD11b⁺ macrophages (MΦ) (**Figure 2.4A**). In addition, we observed substantial co-labeling of p20 and GFAP in Müller glia overlying the CNV lesion, though this p20/GFAP pattern was not as specific to the *Alu* RNA-treated CNV lesion as the p20/CD11b⁺ (**Figure 2.5**). Therefore, we chose to assess whether inflammasome-dependent CNV expansion depends on inflammasome activation in myeloid cells, we generated myelomonocytic cell-specific caspase-1 knockout mice (*LysM-Cre; Casp1^{loxP/loxP}*). We confirmed caspase-1 protein ablation by western blotting (**Figure 2.6**). *Alu* RNA-stimulated CNV was abrogated in *LysM-Cre; Casp1^{loxP/loxP}*, but not in *LysM-Cre*-expressing control mice (*LysM-Cre; Casp1^{+/+}*) (**Figure 2.4B**), strongly suggesting inflammasome activation in myelomonocytic cells is responsible for *Alu*-RNA induced CNV aggravation.

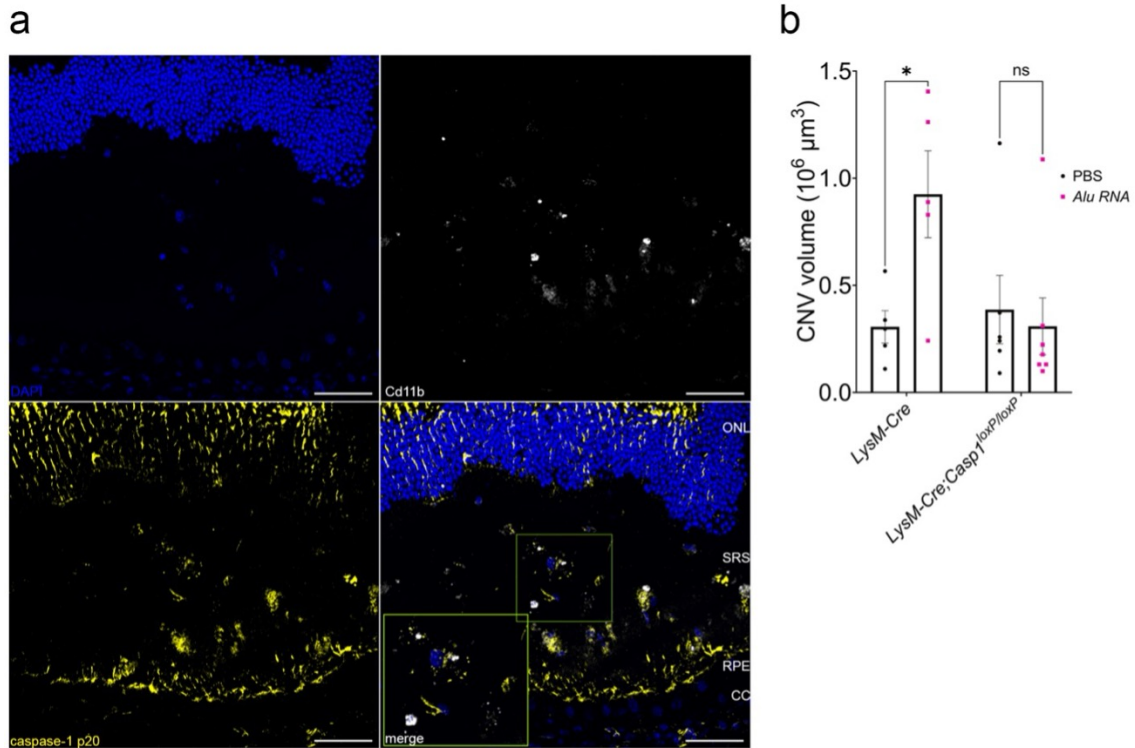


Figure 2.4: Inflammasome activation in myelomonocytic cells is crucial to laser CNV

(a) Representative immunofluorescence images of cross-section of mouse retinae treated with *Alu* RNA. Slides were stained with indicated antibodies. Scale bars: 50 μm . CC: choriocapillaris; RPE: retinal pigmented epithelium; SRS: subretinal space; ONL: outer nuclear layer (b) CNV volume quantification 7 days post laser injury and *Alu* RNA SRI in *LysM-Cre* (P=0.03, N=5) and *Casp1^{loxP} x LysM-Cre* (P=0.91, N=6) mice (two-way ANOVA).

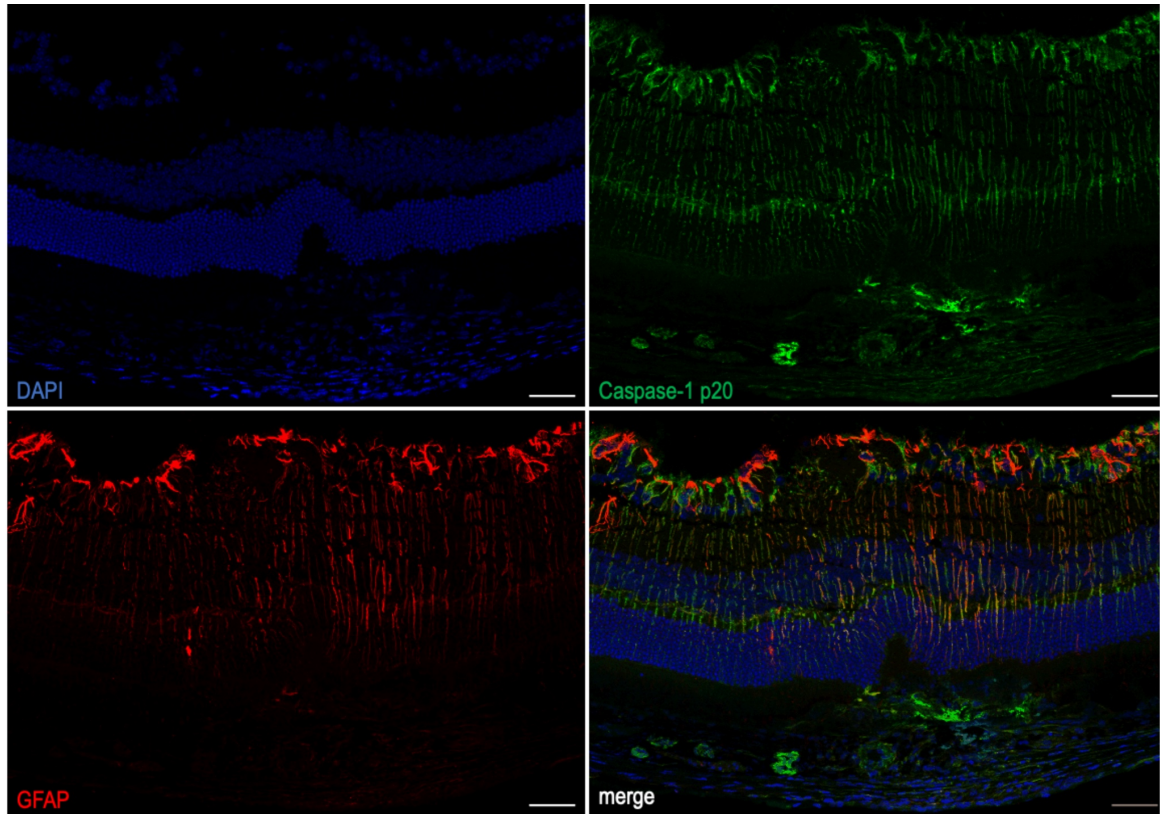


Figure 2.5: Caspase-1 p20/GFAP immunostaining does not colocalize in CNV lesions
Representative fluorescent micrographs of WT cryosections labeled with anti-caspase-1 p20 and anti-GFAP antibodies. Scale bar: 50 μ m.

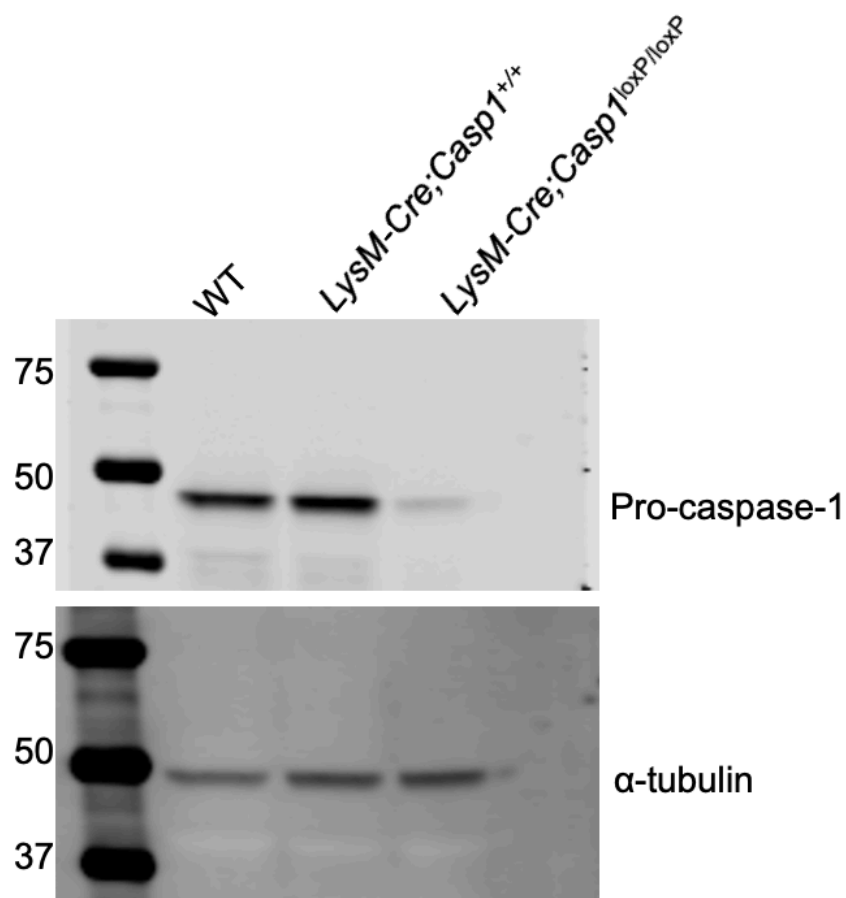


Figure 2.6: Representative immunoblot of pro-caspase-1 abundance in BMDM whole cell lysate.

Protein was isolated from WT, *LysM-Cre;Casp1^{+/+}*, and *LysM-Cre;Casp1^{loxP/loxP}* mice. Membranes were probed with an anti- α -tubulin antibody as a loading control.

2.4.4 Inflammasome-dependent macrophage migration drives CNV exacerbation

Based on the observation that inflammasome activation in myelomonocytic cells is required for inflammasome-induced CNV aggravation, we sought to assess whether inflammasome agonists and constituents affect macrophage recruitment in CNV. We quantified M ϕ migration *in vivo* by measuring the number of F4/80⁺ cells in *Alu* RNA-treated CNV lesions of WT and *Nlrp3*^{-/-} mice. In the absence of an inflammasome agonist, CNV lesions from mice lacking Nlrp3 had similar F4/80⁺ immunolabeling cell count after laser injury compared to wild-type mice (**Figure 2.7A**). Treatment with *Alu* RNA induced a greater number of CNV-associated F4/80⁺ cells in WT but not in *Nlrp3*^{-/-} mice. Taken together, these findings suggest that inflammasome activation may mediate CNV exacerbation through the recruitment of immune cells.

To assess the contribution of inflammasome in macrophage recruitment, a Boyden chamber assay was used in which WT M ϕ were allowed to migrate towards a chemoattractant agent through a permeable support. As anticipated, a VEGF gradient stimulated robust M ϕ migration (**Figure 2.7B**). Neither DMSO nor Ac-YVAD-cmk, a cell-permeable caspase-1 inhibitor, impaired VEGF-induced chemotaxis, confirming that inflammasome inhibition did not affect the VEGF-induced chemotactic response (**Figure 2.7B**). Next, we assessed whether inflammasome activation stimulates production of chemotactic signals. Conditioned media from *Alu* RNA-transfected wild-type M ϕ stimulated chemotaxis to a similar degree as VEGF. However, conditioned media from *Casp1*^{-/-}; *Casp11*^{-/-} M ϕ exhibited no detectable chemotactic activity following *Alu* RNA transfection (**Figure 2.7C**). Similarly, conditioned media from WT M ϕ pretreated with the caspase-1 inhibitor Ac-YVAD-cmk no longer exhibited *Alu* RNA-induced chemotactic

activity (**Figure 2.7D**). These findings indicate that inflammasome activation stimulates the production of soluble chemotactic factors.

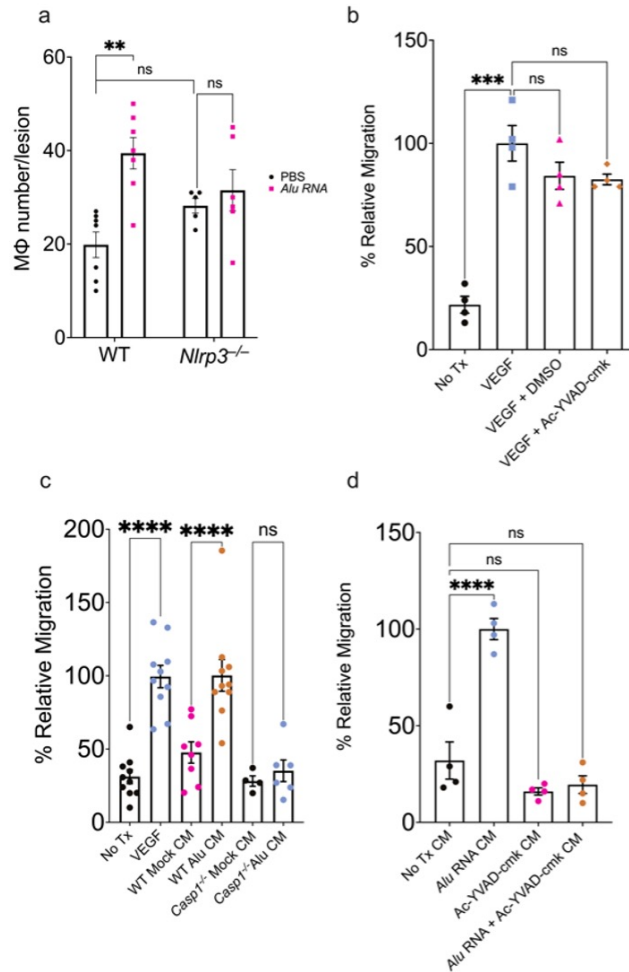


Figure 2.7: Inflammation promotes chemotaxis in peripheral BMDM

(a) Macrophage number quantification after 3 days post laser injury and *Alu* RNA SRI in WT ($P=0.03$, $N=7$) and *Nlrp3*^{-/-} ($P=0.85$, $N=7$, two-way ANOVA). (b) Relative migration of WT BMDM toward the following chemoattractants: VEGF, VEGF + DMSO, VEGF + Ac-YVAD-cmk ($P<0.001$ compared to untreated cells, $N=4$, ordinary one-way ANOVA with Tukey's multiple comparisons test). (c) Relative migration quantification of *Alu* RNA-transfected WT BMDM conditioned media ($P<0.01$, $N\geq 8$) and *Alu* RNA-transfected *Casp1*^{-/-} BMDM ($P=0.97$, $N\geq 4$, ordinary one-way ANOVA with Tukey's multiple comparisons test). (d) Relative migration of WT BMDM with the following conditioned media as chemoattractant: *Alu* RNA-transfected WT BMDM ($P<0.01$); untransfected WT BMDM pretreated with Ac-YVAD-cmk ($P=0.24$); Ac-YVAD-cmk pretreated, *Alu* RNA-transfected WT BMDM ($P=0.43$, $N=4$, ordinary one-way ANOVA with Tukey's multiple comparisons test).

2.4.5 Inflammasome-induced macrophage migration is mediated by interleukin-1 beta (IL-1 β)

We sought to identify the inflammasome-dependent chemotactic factor responsible for macrophage migration. We focused on IL-1 β as transfection of *Alu* RNA in WT M ϕ induces its robust secretion⁵⁵ and it possesses chemotactic activity⁷³. Conditioned media from *Alu* RNA-transfected WT BMDM incubated with an IL-1 β neutralizing antibody (nAb) significantly inhibited WT BMDM chemotaxis (**Figure 2.8A**). Consistent with a putative role in CNV, we detected robust *Il1b* mRNA expression that colocalized with *Adgre1* mRNA (encoding the M ϕ marker F4/80) in CNV lesions of *Alu* RNA-treated eyes (**Figure 2.8B**). Intravitreal administration of an IL-1 β nAb reduced M ϕ accumulation (**Figure 2.8C**) and day three CNV volume (**Figure 2.8D**) in *Alu* RNA-treated eyes. We sought to determine whether combined administration of nAbs targeting Vegfa and IL-1 β reduced CNV volumes in an additive manner. Intravitreal administration of nAbs against either Vegfa or IL-1 β reduced day seven CNV volumes (**Figure 2.9**). Combined administration of low dose Vegfa nAb (1 ng) and IL-1 β nAb reduced CNV volume to a greater extent than low dose Vegfa nAb alone; interestingly, combined administration of high dose Vegfa nAb (5 ng) and IL-1 β nAb had no further reductive effect compared to high dose Vegfa nAb alone (**Figure 2.9**). These findings suggest that while the effects of Vegfa and IL-1 β inhibition appear to overlap, combining these two treatments may result in some increased therapeutic effect under specific conditions.

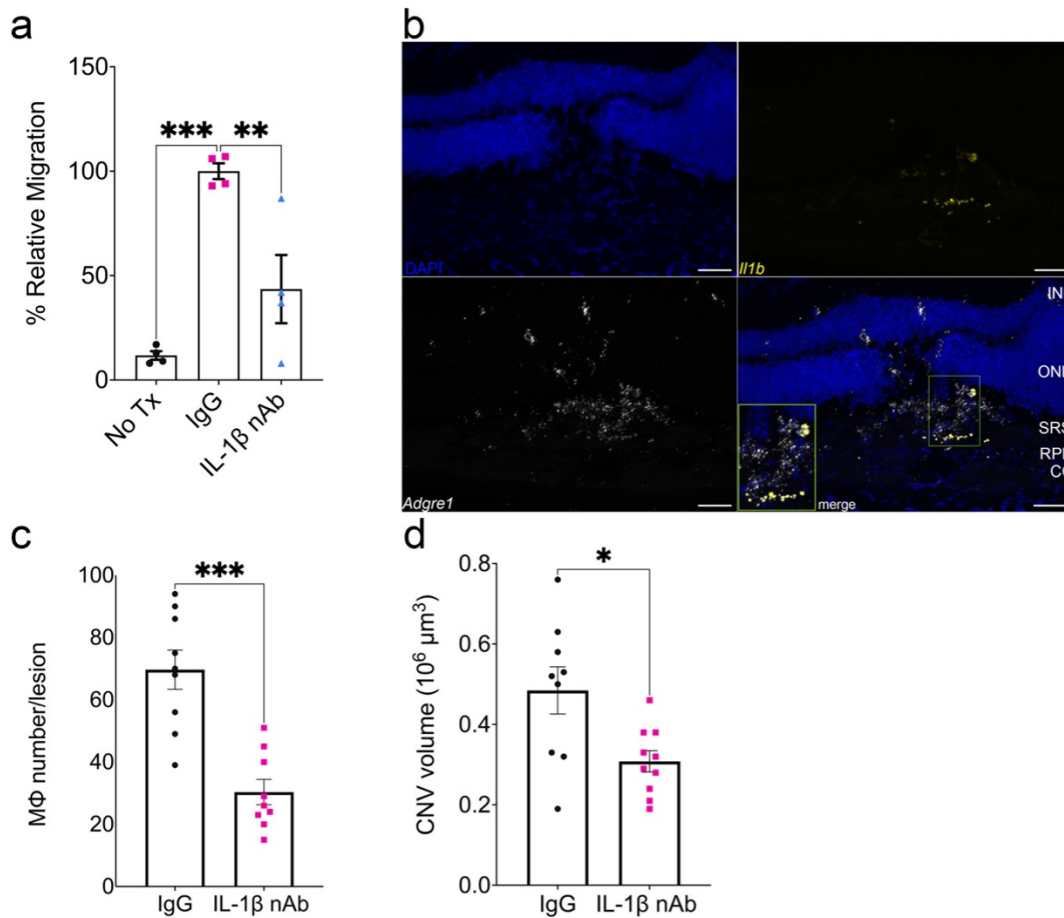


Figure 2.8: IL-1 β neutralization reduces Alu RNA-induced chemotaxis, macrophage accumulation, and laser CNV exacerbation.

(a) Relative migration of Alu RNA-transfected WT BMDM conditioned media pretreated with either IgG ($P < 0.01$) or IL-1 β neutralizing antibody ($P < 0.01$, $N = 4$, ordinary one-way ANOVA with Tukey's multiple comparisons test). (b) Representative images of Alu RNA-treated laser CNV lesions hybridized with probes against *Il1b* and *Adgre1*. Scale bar: 50 μm . CC: choriocapillaris; RPE: retinal pigmented epithelium; SRS: subretinal space; ONL: outer nuclear layer; INL: inner nuclear layer (c) Macrophage number and (d) CNV volume quantification after 3 days post laser injury and Alu RNA subretinal injection with either 500 ng IgG1 or IL-1 β neutralizing antibody ($P < 0.001$, $N = 8-10$)

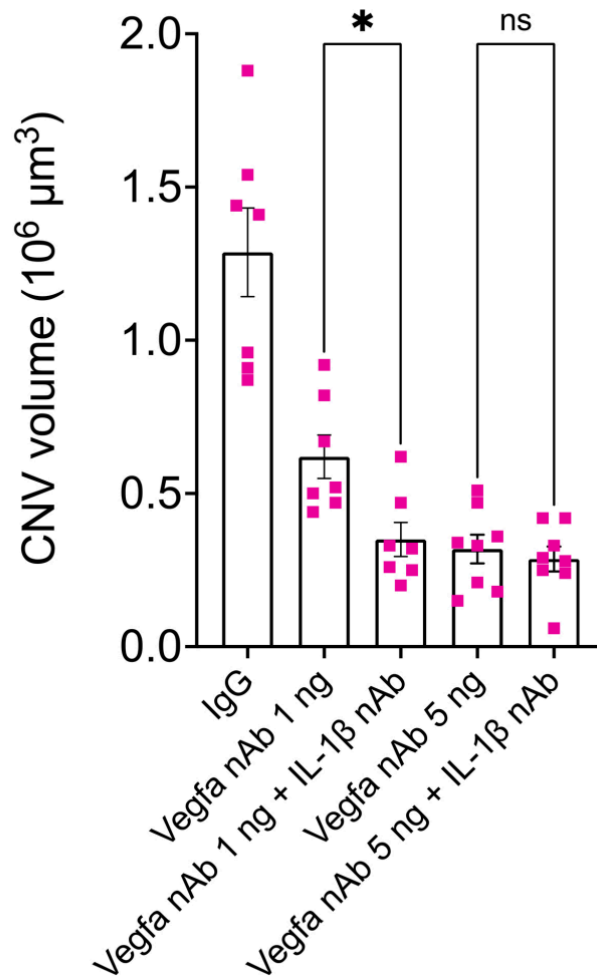


Figure 2.9: Combined administration of high-dose Vegfa nAb and IL-1β nAb does not further reduce CNV volume.

CNV volumes quantified 7 days post-laser injury, *Alu* RNA subretinal injection, and intravitreal administration of Vegfa neutralizing antibody with or without IL-1β neutralizing antibody.

M ϕ inflammasome activation and IL-1 β production could conceivably promote angiogenesis in two non-mutually exclusive ways. First, inflammasome agonists enhance M ϕ ingressation (**Figure 2.7A**), which may be sufficient to drive increased angiogenesis. In addition, an inflammasome agonist could enhance the angiogenic potential of ingressed M ϕ . To test these concepts, an ex vivo choroidal sprouting assay was used as previously described^{74,75}. Three days after seeding choroid pieces from WT mice in growth factor-reduced Matrigel, an equal number of mock- or *Alu* RNA-transfected BMDM were added to each developing sprout and sprout size was quantified on day six. Consistent with previous reports⁷⁵, adding BMDM led to enhanced choroidal sprouting (**Figure 2.10**). However, *Alu* RNA-transfected BMDM did not further exacerbate sprout growth compared to mock-transfected BMDM (**Figure 2.10**). We interpret this finding to mean that inflammasome activation does not enhance the intrinsic angiogenic potential of BMDM but rather exacerbates angiogenesis by increasing the extent of M ϕ ingressation.

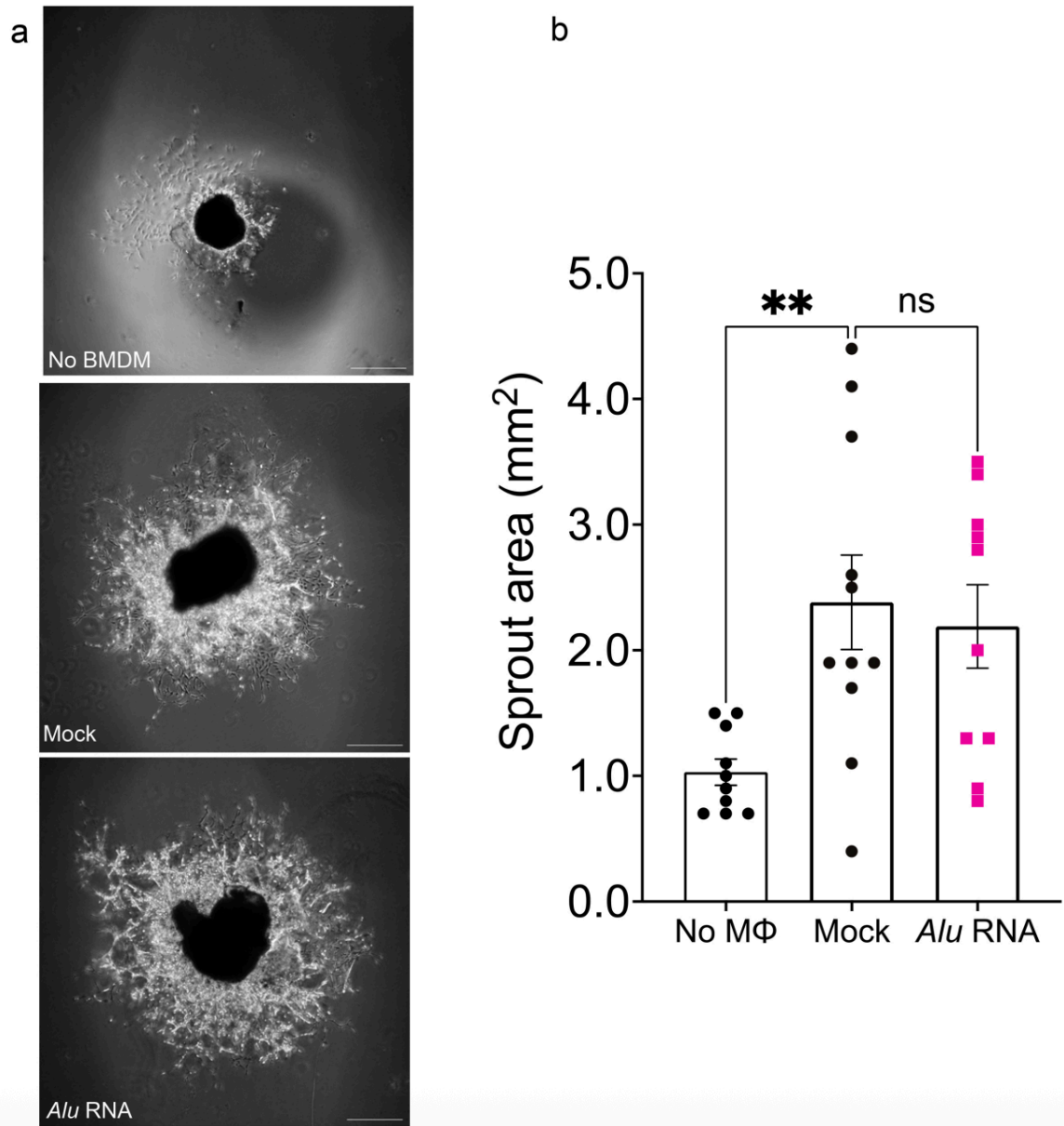


Figure 2.10: Representative phase-contrast images of choroid vessel sprouts. Sprouts were seeded with either no BMDM (top), mock-transfected (middle) or *Alu* RNA-transfected (bottom) BMDM. (b) Quantification of choroid sprouts from (a). N=10-11. Scale bar: 500 μ m.

2.5 Discussion

We report a new method by which to interrogate the consequences of inflammasome activation in pathological neovascularization using experimental laser CNV. Immediately following laser thermal injury, subretinal administration of several inflammasome agonists exacerbated CNV volume in WT mice. This effect was abrogated by genetic deletion and pharmacological inhibition of the inflammasome activator P2X7, constituents of the NLRP3 inflammasome, and the adaptor MyD88. To assess the role of macrophage inflammasome in CNV, myeloid-specific caspase-1 knockouts underwent *Alu* RNA subretinal injection post-laser injury and demonstrated significantly less lesion volume and F4/80+ macrophage recruitment. We also observed inflammasome activation that colocalized to F4/80+ macrophages within the lesion site in retinal cryosections. To assess the role of inflammasome-mediated cytokine production in macrophage chemotaxis, conditioned media from *Alu* RNA-transfected WT and *caspase-1/11*^{-/-} BMDM was used as the chemoattractant in a transwell migration assay. Conditioned media from transfected WT, but not caspase-1 deleted, BMDM induced chemotaxis in WT BMDM, suggesting a soluble factor arising from inflammasome activation to be the mediator of chemotaxis.

The downstream effects of inflammasome activation in mediating angiogenesis are context specific. Whereas the work presented here as well as previous work from our group⁷⁶ and others⁷⁷ suggest a pro-angiogenic role of inflammasome activation, NLRP3 inflammasome activation has been reported to possess anti-angiogenic properties in models of hindlimb ischemia^{78,79} and ocular herpes simplex virus 1 infection⁸⁰. Inflammasome

activation in macrophages was critical to the *Alu* RNA-exacerbated laser CNV phenotype, possibly due to the synergistic role of VEGF and IL-1 β in promoting angiogenesis⁷³.

The findings presented here suggest an experimental approach to help bridge the disparate observations that, while inhibition of inflammasome constituents does not affect experimental laser CNV development, they significantly contribute to the development of CNV in several spontaneous mouse models. By simultaneously inducing CNV and administering inflammasome agonists, it is possible to assess how inflammasome activation directly contributes to CNV development. This model however is not without limitations, as the experimental laser CNV method is an injury-based approach to studying pathological ocular neovascularization. The extent to which findings apply to other ocular neovascular settings, such as CNV in human AMD or in pathologic myopia requires more investigation. Still, these findings along with previous reports on the role of inflammasome in spontaneous CNV^{51,76} support the idea that inflammasome activation promotes pathological angiogenesis.

This study also adds pathological angiogenesis to the catalog of retinal pathologies in which inflammasome is implicated, which previously included RPE cell death, retinal degeneration, and neurovascular dysfunction in diabetes^{31,81,82}. By implicating inflammasome directly in pathological angiogenesis, our findings support further investigation into inflammasome as a therapeutic target for pathological angiogenesis in retinal diseases such as AMD, diabetic retinopathy, and retinopathy of prematurity, as well as in other contexts of pathological angiogenesis such as cornea and solid tumors

Chapter 3: Voluntary exercise suppresses choroidal neovascularization in mice

This chapter is a modified version of the previously published article:

Makin RD*, Argyle DA*, Hirahara S, Nagasaka Y, Zhang M, Yan Z, Kerur N, Ambati J, Gelfand BD. *Voluntary exercise suppresses choroidal neovascularization in mice*. Invest Ophthalmol Vis Sci. 2020;61(5):52. <https://doi.org/10.1167/iovs.61.5.52>

3.1 Abstract

Purpose: To determine the effect of voluntary exercise on choroidal neovascularization (CNV) in mice.

Methods: Age- and sex-matched wild-type C57BL/6J mice were housed in cages equipped with or without running wheels. After four weeks of voluntary running or sedentariness, mice were subjected to laser injury to induce CNV. Following surgical recovery, mice were placed back in cages with or without exercise wheels for 7 days. CNV lesion volumes were measured by confocal microscopy. The effect of wheel running only in the 7 days following injury was also evaluated. Macrophage abundance and cytokine expression were quantified.

Results: In the first study, exercise-trained mice exhibited a 45% reduction in CNV volume compared to sedentary mice. In the replication study, a 32% reduction in CNV volume in exercise-trained mice was observed (P=0.029). Combining these two studies, voluntary exercise was found to reduce CNV by 41% (P=0.0005). Exercise-trained male and female mice had similar CNV volumes (P=0.76). The daily running distance did not correlate with CNV lesion size. Exercise only after the laser injury without a preconditioning period did not reduce CNV size (P=0.41). CNV lesions of exercise-trained mice also exhibited significantly lower F4/80+ macrophage staining and *Vegfa* and *Ccl2* mRNA expression.

Conclusions: These findings provide the first experimental evidence that voluntary exercise improves CNV outcomes.

3.2 Introduction

Pathological neovascularization underlies dozens of vision-threatening diseases including age-related macular degeneration (AMD), corneal neovascularization, glaucoma, diabetic retinopathy, and retinopathy of prematurity. Although intraocular anti-VEGFA therapies are a clinical success, they are not a panacea. For example, 12-25% of neovascular AMD patients, representing hundreds of thousands of individuals in the U.S.⁸³, have 20/200 vision or worse despite treatment⁸⁴⁻⁸⁶. Prolonged exposure to anti-VEGFA is accompanied by loss of initial visual acuity gains⁸⁷⁻⁹⁰, and a significant portion of anti-VEGFA-exposed eyes develop untreatable central retinal atrophy^{86,91}. Moreover, between 2013 and 2015, 3.75 million doses of FDA approved anti-VEGFA drugs were administered in the U.S., costing patients, taxpayers, insurers, and providers approximately \$7.5B⁸⁴. Thus, there is a compelling need for new, inexpensive anti-angiogenic strategies that can target the molecular drivers of neovascularization.

Physical activity is a non-invasive, patient-controlled, and inexpensive intervention that improves numerous health outcomes both in healthy people and in those suffering from diverse clinical conditions (systematically reviewed in ^{92,93}). In contrast to prevalent conditions such as diabetes⁹⁴, cardiovascular disease^{95,96}, and neurocognitive disease⁹⁷, the relationship between exercise and AMD is far less established. Numerous epidemiological studies have attempted to characterize this impact, with the majority reporting a positive influence of physical activity on AMD and related outcomes (e.g. large macular drusen)⁹⁸⁻¹¹⁴. A recent systematic meta-analysis of nine studies on exercise and AMD in White subjects found that physical activity was associated with modest reduction in early AMD (odds ratio 0.92; 95% confidence interval (CI), 0.86-0.98) and a dramatic reduction in late

AMD (odds ratio 0.59; CI, 0.49-0.72)¹¹⁵. Together, these findings suggest that physical activity may represent a significant modifiable risk factor for AMD.

Here, we sought to examine the effects of voluntary wheel running, a physiological model of endurance exercise in mice, on laser photocoagulation-induced CNV in a rigorous and controlled experimental setting.

3.3 Materials and Methods

3.3.1 Mice

All animal protocols were approved by the Institutional Animal Care and Use Committee of the University of Virginia. Animal studies adhered to the ARVO Statement for the Use of Animals in Ophthalmic and Vision Research. Male and female C57BL/6J mice were housed in temperature-controlled (21°C) cages in a pathogen-free room with a 12:12-h light-dark cycle and free access to water and normal chow.

3.3.2 Voluntary running

Voluntary wheel running has been widely used to induce physiological adaptations including muscle fiber transformation, angiogenesis, mitochondrial biogenesis, and mitophagy with significantly improved physiological and metabolic functions and protection against chronic diseases^{116–122}. A voluntary regimen allows mice to exercise during their normal active dark cycle^{123–125}, which would be disrupted by forced exercise regimens, such as treadmill running and swimming-. Forced exercise is reported to cause acute and chronic stress responses that can manifest systemically^{126–129} and may confound results. Finally, perhaps because of these issues, direct comparison of voluntary and forced exercises has found voluntary exercise superior in improving other pathological phenotypes^{130–132}. Voluntary running was conducted as established previously¹²². Briefly, mice in the exercise group were housed individually in cages equipped with running wheels and sedentary mice were housed in cages not equipped with running wheels. Daily running was recorded via a computerized monitoring system, as described in previous studies^{116,118}.

3.3.3 Laser photocoagulation-induced choroidal neovascularization

Laser photocoagulation (532 nm, 180 mW, 100 ms, 75 μ m) (OcuLight GL; IRIDEX Corp., Mountain View, CA, USA) was performed bilaterally (4 spots per eye) on day 0 to induce CNV as previously described¹³³. Irrespective of the exercise protocol, mice were 3 months old at the time of laser injury.

3.3.4 CNV volume and F4/80 labeling

Following laser injury, mice were euthanized, eyes were enucleated and fixed with 4% paraformaldehyde for 30 minutes at 4°C. Eyecups were incubated with 0.7% FITC-isolectin B4 (Vector Laboratories, Burlingame, CA, USA), and R-phycoerythrin-conjugated anti-F4/80 (Bio-Rad, Hercules, CA, USA) and the flat mounts of RPE-choroid-sclera were mounted in antifade medium (Immu-Mount Vectashield Mounting Medium; Vector Laboratories). CNV volume was visualized using a scanning laser confocal microscope (Nikon AR1, Nikon Instruments). Volumes were quantified using Image J software (<http://imagej.nih.gov/ij/>; provided in the public domain by the National Institutes of Health, Bethesda, MD, USA) as previously reported¹³³. F4/80 labeling was quantified by densitometry of the F4/80 signal in the maximum z-projection of the CNV lesion.

3.3.5 Fluorescent in situ hybridization

Enucleated mouse eyes were embedded in optimal cutting temperature (OCT) medium (Sakura Finetek USA, Torrance, CA) and snap frozen in liquid nitrogen-supercooled isopentane. 7 μ m-thick sections were hybridized with RNAscope probes for Ccl2 (ID: 311791), Il6 (ID: 315891), and Vegfa (ID: 412261) according to manufacturer's instructions (ACDBio, Newark, CA). Sections were mounted in Invitrogen™ ProLong™

Gold Antifade Mountant with DAPI (Thermo Scientific, Waltham, MA) and imaged on a Nikon A1R inverted confocal microscope (Nikon Instruments Inc., Melville, NY). Quantification of absolute transcripts was performed in ImageJ. The integrated density of an individual punctum was measured as the first peak in the intensity histogram of each 8-bit greyscale image, thresholded to reduce background. Then, the following equation was used to calculate the total number of transcripts:

$$\frac{\Sigma \textit{integrated density}}{\textit{average intensity of single dot}} \times \textit{area of image} \times \textit{section thickness}.$$

3.4 Results

3.4.1 *Effect of voluntary exercise on CNV in mice*

The first study design is depicted in **Figure 3.1A**. Age- and sex-matched wild-type C57BL/6J mice were singly housed in cages equipped with or without running wheels (N=3 male sedentary, N=3 female sedentary, N=3 male exercise, N=3 female exercise). After four weeks of voluntary running, mice were anesthetized and subjected to laser injury to induce CNV. Following surgical recovery, mice were placed back in cages with or without exercise wheels for seven days, at which time animals were euthanized and CNV lesions were analyzed. Seven days after injury was selected as an endpoint because the lesion is sufficiently large to measure accurately and the lesion is actively expanding, with a peak volume occurring at 14 days¹³⁴, allowing us to quantify pathology in a state that is both established and expanding.

In total, N=40 CNV lesions from sedentary and N=48 lesions from exercise-trained mice were included for analysis in Study 1. One mouse in the sedentary group was excluded because the procedure failed, possibly due to its poor health. We observed a 45% reduction in CNV volume in exercise-trained mice compared to sedentary mice (P=0.017 by two-tailed Mann-Whitney U test, **Figure 3.1B**). Exercise-trained male and female mice had similar CNV volumes (P=0.99, **Figure 3.1C**). We did not find a significant difference in body weights of exercise or sedentary mice (25.1 ± 0.8 g vs. 25.5 ± 1.1 g, P=0.76). We conducted a replication study of similar design, with the exception that sedentary mice were not individually housed, as CNV volumes from individually housed mice were not significantly different from group-housed mice as established in prior studies. In the replication study, an additional N=25 CNV lesions from sedentary mice and N=19 CNV

lesions from exercise-trained mice were analyzed. In this second study, we again observed a reduction in CNV volumes in exercise-trained compared to sedentary mice ($P=0.029$, **Figure 3.1D**). Combining these two studies, voluntary exercise was found to reduce CNV by 41% ($P=0.0005$, **Figure 3.1E**).

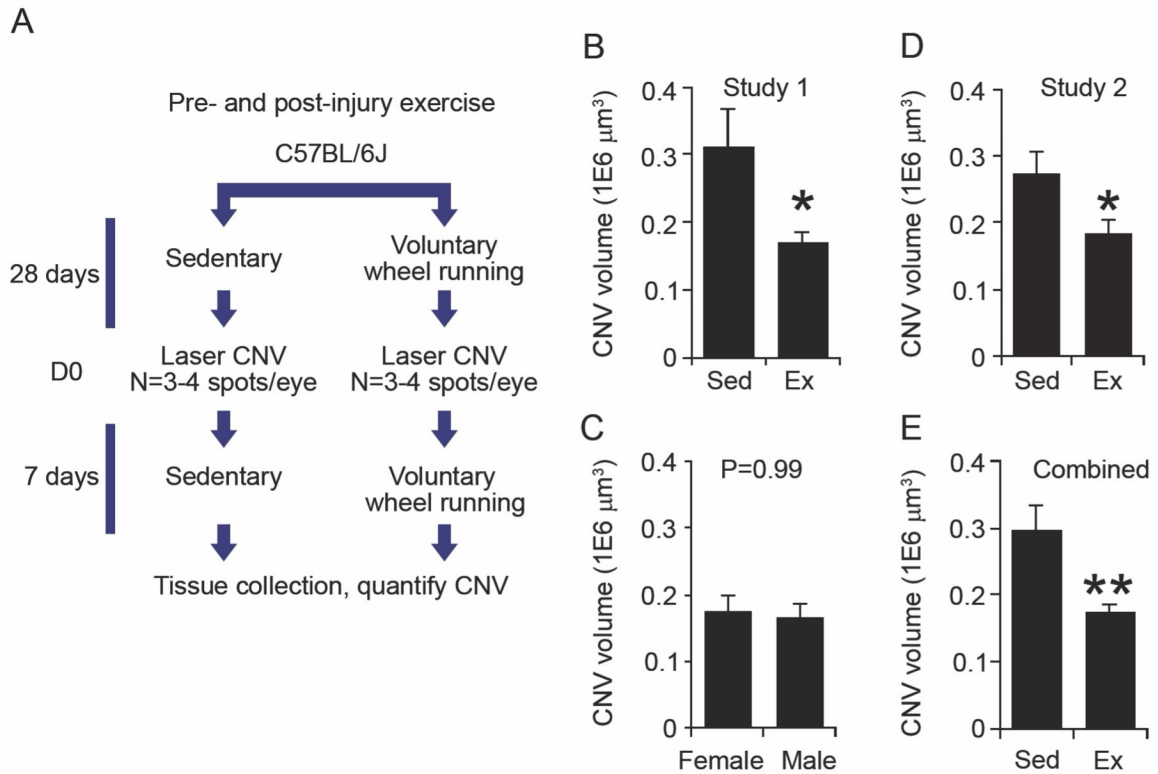


Figure 3.1: Exercise trained mice develop less CNV than sedentary mice, independent of sex

(A) Study design for Studies 1 and 2: C57BL/6J mice were housed with (voluntary wheel running) or without (sedentary) an exercise wheel for 28 days. After laser photocoagulation on day 29, mice were returned to their respective cages for seven days. (B) CNV volume in sedentary and exercise-trained mice in Study 1. (C) CNV volume in exercise-trained male and female mice ($P=0.99$, Mann-Whitney U test). (D) CNV volume in sedentary and exercise-trained mice in Study 2. (E) CNV volumes from Studies 1 and 2 combined. $N=65$ sedentary, $N=67$ exercise. * $P<0.05$, ** $P<0.01$.

3.4.2 Dose effect of wheel running on CNV

Throughout both studies, mice with exercise wheels traveled an average of 8.2 km/day, comparable to C57BL/6J in previous studies^{135,136}. Quantifying the relationship between running activity and CNV volume in individual mice, the average daily distance traveled did not correlate strongly with CNV volume ($R=-0.11$, $P=0.80$, **Figure 3.2A**). Daily distance traveled was significantly greater in mice prior to laser photocoagulation surgery ($P=0.03$ by two-tailed paired Student's t-test). Neither the daily distance traveled prior to nor after surgery significantly correlated with CNV volume(**Figure 3.2B, C**), though there was a slight negative relationship between post-surgery run distance and CNV volume that did not reach statistical significance ($R=-0.21$, $P=0.64$, **Figure 3.2C**).

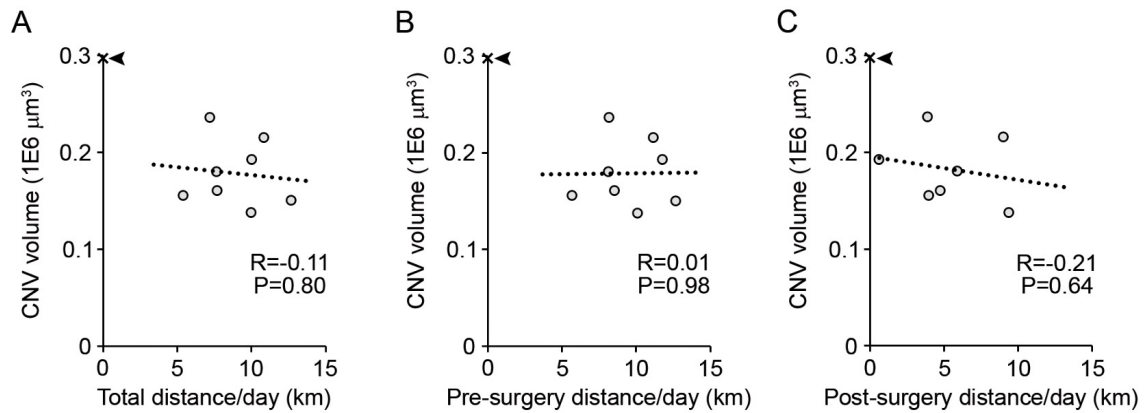


Figure 3.2: CNV volume is not dependent on distance traveled

(A) The average CNV volume of each mouse plotted against its average distance traveled throughout the duration of the experiment. Arrow on y-axis denotes the average CNV volume in sedentary mice. (B) The average CNV volume of each mouse plotted against its average distance traveled prior to laser photocoagulation surgery. (C) The average CNV volume of each mouse plotted against its average distance traveled after laser photocoagulation surgery.

3.4.3 *Effect of post-injury voluntary exercise on CNV in mice*

We sought to determine whether exercise undertaken concurrent with pathology, without pre-injury preconditioning, was sufficient to improve CNV outcomes. To isolate the effects of post-injury exercise, a second study design was conducted as depicted in **Figure 3.3A**. Here, mice were allowed a brief three-day acclimation period with the exercise wheel, followed by laser injury to induce CNV, and then permitted to exercise throughout the recovery period with or without exercise wheels. Once again, a replication study of similar design was performed. In the first of two independent post-injury exercise trials (Study 3), a total of N=44 CNV lesions from sedentary and N=45 lesions from post-injury exercise-trained mice were included for analysis. We observed a 21% reduction in CNV volume in exercise-trained mice compared to sedentary mice, though this effect did not achieve statistical significance (P=1.0 by two-tailed Mann-Whitney U test, **Figure 3.3B**). In a replication study of similar design (Study 4), an additional N=54 CNV lesions from sedentary mice and N=23 CNV lesions from exercise-trained mice were analyzed. In this second study, we again observed a non-significant reduction in CNV volumes in exercise-trained compared to sedentary mice (8% reduction, P=0.32, **Figure 3.3C**). Combining these two studies, post-injury exercise did not significantly reduce CNV (P=0.41, **Figure 3.3D**).

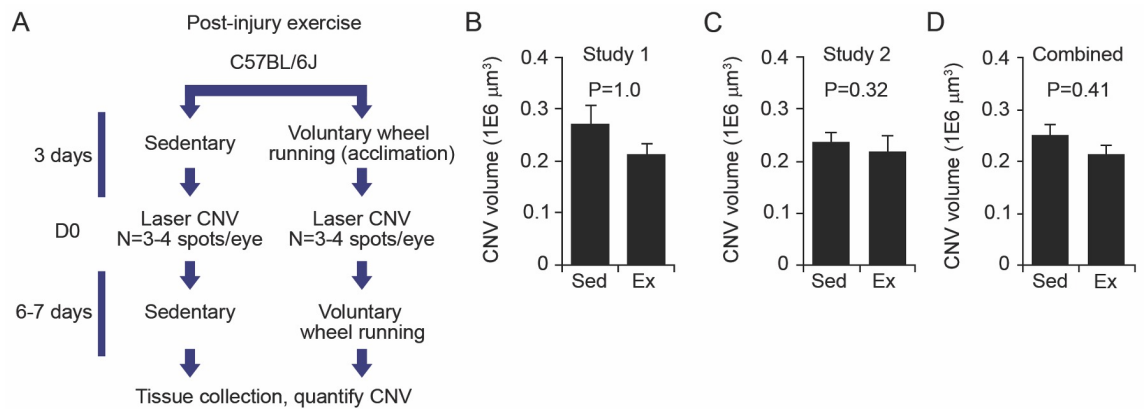


Figure 3.3: Post-injury exercise does not affect CNV development

(A) Study design for Studies 3 and 4: C57BL/6J mice were housed with or without an exercise wheel for 3 days to acclimate. Then, mice were subjected to laser photocoagulation surgery and returned to their respective cages for seven (Study 3) or six days (Study 4). (B) CNV volume in sedentary and post-injury, exercise-trained mice in Study 3. N=44 sedentary, N=45 post-injury, exercise-trained, P=1.0 by Mann-Whitney U test. (C) CNV volume in sedentary and post-injury, exercise-trained mice in Study 4. N=54 sedentary, N=23 post-injury, exercise-trained. P=0.32 by Mann-Whitney U test. (D) CNV volumes from Studies 3 and 4 combined. P=0.41 by Mann-Whitney U test.

3.4.4 Reduced F4/80+ cells and cytokine transcription in CNV in exercise-trained mice

Immune cells, including macrophages (M ϕ), are prevalent in human CNV¹³⁷⁻¹⁴⁰ and critically contribute to experimental CNV^{42,141,142}. We quantified the effect of exercise training on immune cell infiltration in CNV seven days after injury by measuring F4/80 immunolabeling in RPE/CNV whole mounts. In mice undergoing pre- and post-injury exercise, we observed a dramatic 72% reduction in F4/80 positive staining in the CNV lesions of exercise-trained mice compared with sedentary mice (P=0.037, **Figure 3.4A**). Additionally, we utilized *in situ* hybridization to quantify the absolute number of transcripts of angiogenic cytokines in CNV lesions of exercise-trained and sedentary mice. In exercise trained eyes, we observed a 38% reduction in *Vegfa* mRNA (P=0.012 by two tailed t-test) and 71% reduction in *Ccl2* mRNA (P=0.021) in CNV lesions of exercise-trained eyes compared to lesions from sedentary mice (**Figure 3.4B**). We also observed a 32% reduction in *Il6* mRNA in lesions of exercise-trained eyes, though this was not statistically significant (P=0.18).

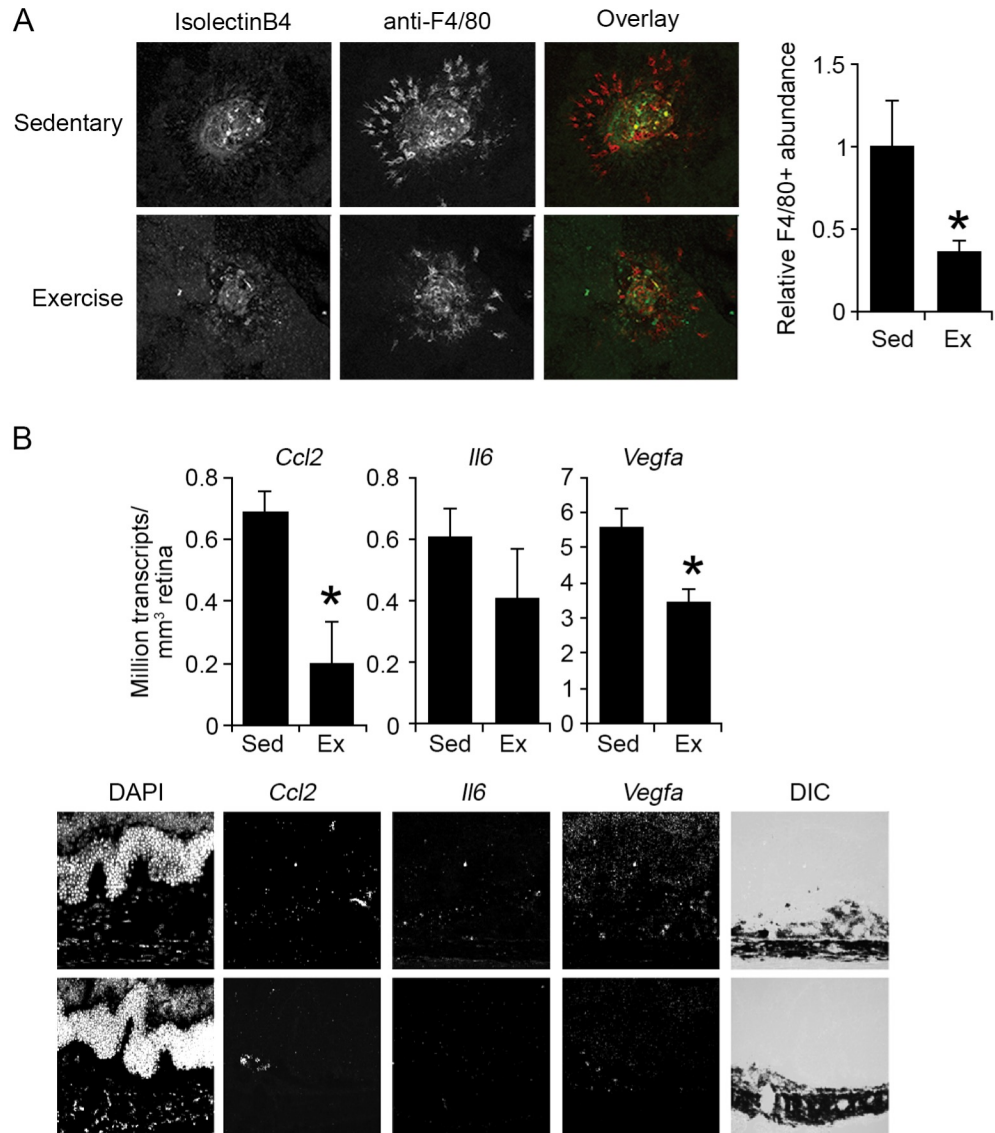


Figure 3.4: Voluntary exercised-trained mice and macrophage infiltration in CNV
(A) Fluorescent micrographs of choroid-RPE sclera flat mounts from sedentary (top) and exercise-trained (bottom) mice seven days after laser injury. Isolectin-B4 depicted in green in overlay and F4/80 depicted in red in overlay. Quantification of F4/80+ staining depicted at right. N=14 lesions from sedentary and N=15 from exercise-trained mice (following the protocol in Figure 1A). **(B)** Representative images (top) and quantification (bottom) of *in situ* hybridization of mRNA in retina of sedentary and exercise-trained mice (following the protocol in Figure 1A) seven days after laser injury. N=3 lesions per condition. *P<0.05 by two-tailed student's t-test.

3.5 Discussion

This study provides the first experimental evidence on the influence of physical activity on CNV, supporting the findings of epidemiologic studies reporting beneficial effects of exercise on AMD-related pathologies. The dose effect of exercise was modest and did not achieve statistical significance. We interpret these findings to mean that the amount of exercise undertaken in this experimental design exceeded the threshold to achieve the maximal effect. Limiting exercise training to the CNV lesion growth period did not significantly reduce lesion size. We interpret this finding to mean that exercise preconditioning prior to the initiation of CNV is necessary to achieve a salutary effect.

In contrast to CNV, prior studies in mice report that exercise promotes angiogenesis and vascularity in skeletal muscle¹¹², brain¹³⁸, and subcutaneous adipose tissue¹³⁹. It appears that the mechanisms by which exercise affects blood vessel homeostasis in these tissues may differ from CNV. We observed that lesions of exercise-trained mice exhibited reduced F4/80+ labeling and cytokine expression, suggesting that exercise may impart immunomodulatory effects. Indeed, exercise has been shown to ameliorate macrophage mobilization in a murine aging model¹⁴³ and in high-fat diet-induced inflammation^{144–146}. Whether reduced immune cell recruitment is a driver of the beneficial effects of voluntary exercise on CNV is an important avenue of future study, as is identifying molecular intermediates of this effect.

Voluntary exercise induces a variety of systemic changes that may modulate CNV size, including food consumption and plasma cholesterol. Interestingly, short-term voluntary exercise is reported to induce an anorexic effect in mice, with reduced food

consumption^{145,147} while prolonged voluntary wheel running increases food consumption^{148,149}. Voluntary exercise is reported to lower plasma triglycerides in humans¹⁵⁰ and triglycerides and cholesterol turnover in mice¹⁵¹.

Prior studies have found that voluntary exercise does not affect fasting blood glucose levels in normal, non-diabetic mice^{152,153}. We found no significant difference in body weights of exercise and sedentary mice. Therefore, we find it unlikely that blood glucose or body weight per se are responsible for the effect of exercise on CNV we observed. The extent to which these exercise-modifiable biomarkers correlate with CNV lesion size is an important avenue of future study.

Apart from our findings in CNV, exercise has also been reported to prevent retinal degeneration in normal aged mice^{154,155}, in light-induced retinal degeneration¹⁵⁶, and in a light injury model of retinitis pigmentosa¹⁵⁷. Thus, the beneficial effects of exercise on the retina may extend beyond suppressing pathological angiogenesis.

A recent study found that Korean men, but not women, self-reporting five or more sessions of vigorous exercise per week were significantly more likely to develop neovascular AMD (hazard ratio, 1.54; CI, 1.15-2.06)¹⁵⁸. However, limitations in the methodology of this study include survival bias of the low physical activity cohort ('left truncation'), and potential disproportionate underreporting of neovascular AMD in the non-active group¹⁵⁹. Other studies have also reported marginal positive associations between physical activity and risk of developing AMD^{160,161}. It should also be noted that the definitions of "adequate", "moderate", "strenuous" and "vigorous" physical activity are non-uniform between studies. In general, it is challenging to draw conclusions from

epidemiologic studies of this nature due to the potential unreliability of questionnaire-based data¹⁶² and the confounding effects that vision loss may have on the amount and type of exercise an individual undertakes¹⁶³. Thus, the continued study of exercise on AMD-relevant phenotypes in experimental models may provide clarity as to the nature of the effect and mechanistic drivers of physical activity in this condition.

Physical activity may be a low-cost, effective, and non-invasive treatment option in the prevention with several eye diseases, including AMD. Identifying the molecular mediators that couple physical activity and CNV is an important avenue of research to understand the relationship between this complex modifiable risk factor and retinal disease. This study presents an experimental platform from which such investigations may be undertaken in future studies. The translational relevance of this study must be considered in the context of the limitations of mouse voluntary wheel running as a model for human exercise and laser photocoagulation as a model of CNV in human patients. Ultimately, the extent to which exercise proves beneficial for humans suffering with or at risk of developing CNV must be tested in the context of controlled, prospective clinical trials.

Chapter 4: RF/6A chorioretinal cells do not display key endothelial phenotypes

This chapter is a modified version of the previously published article:

Makin RD, Apicella I, Nagasaka Y, Kaneko H, Turner SD, Kerur N, Ambati J, Gelfand BD. *RF/6A chorioretinal endothelial cells do not display key endothelial phenotypes*. Invest Ophthalmol Vis Sci. 2018;59:5795-5802.

4.1 Abstract

Purpose: The misuse of inauthentic cell lines is widely recognized as a major threat to the integrity of biomedical science. Whereas the majority of efforts to address this have focused on DNA profiling, we sought to anatomically, transcriptionally, and functionally authenticate the RF/6A chorioretinal cell line, which is widely used as an endothelial cell line to model retinal and choroidal angiogenesis.

Methods: Multiple vials of RF/6A cells obtained from different commercial distributors were studied to validate their genetic, transcriptomic, anatomic, and functional fidelity to bona fide endothelial cells.

Results: Transcriptomic profiles of RF/6A cells obtained either de novo or from a public data repository did not correspond to endothelial gene expression signatures. Expression of established endothelial markers were very low or undetectable in RF/6A compared to primary human endothelial cells. Importantly, RF/6A cells also did not display functional characteristics of endothelial cells such as uptake of acetylated LDL, expression of E-selectin in response to TNF- α exposure, alignment in the direction of shear stress, and AKT and ERK1/2 phosphorylation following VEGFA stimulation.

Conclusions: Multiple independent sources of RF/6A do not exhibit key endothelial cell phenotypes. Therefore, these cells appear unsuitable as surrogates for choroidal or retinal endothelial cells. Further, cell line authentication methods should extend beyond genomic profiling to include anatomic, transcriptional, and functional assessments.

4.2 Introduction

The vessels of the choroid and retina nourish the outer and inner retina respectively. Dysfunction, aberrant growth, and involution of the endothelial cells lining these vessels are of critical importance to diverse ophthalmic conditions, including the most common causes of untreatable blindness, namely choroidal neovascularization in neovascular age-related macular degeneration (AMD)³⁹, choroidal involution in atrophic AMD¹⁶⁴, and retinal vessel proliferation in proliferative diabetic retinopathy and leakage in diabetic macular edema (DME)¹⁶⁵. Collectively, chorioretinal vascular instability affects the vision of over 56 million people worldwide^{166,167}. As evidence of the broad recognition of their role in human vision diseases, numerous cell-based models have been adopted to further understanding of the physiology and pathophysiology of choroidal and retinal endothelial cells.

RF/6A cells, described in the literature as “chorioretinal endothelial cells”, are among the most prevalent *in vitro* choroidal and retinal endothelial cell model employed in the literature. Originally isolated in 1968 from a crude choroid-retina preparation of a rhesus macaque fetus in mid-gestation, these spontaneously transformed cells were established as endothelial cells by virtue of their cobblestone morphology, positivity for VWF, and presence of Weibel-Palade bodies (WPB), an endothelial-specific organelle¹⁶⁸. The investigators that established this cell line reported that after over 500 passages, VWF expression was reduced or absent, but that these cells retained WPB and morphological characteristics of endothelial cells. Since that time, RF/6A have been widely adopted to model angiogenesis, cell differentiation, and responses to various drug and environmental treatments in the choroid and retina.

Despite their widespread use, a rigorous and contemporary characterization of the endothelial cell properties of RF/6A cells has not been reported. Here, we report that commercially distributed RF/6A cells lack essentially all classic endothelial cell markers and numerous functional behaviors. These findings assume broad importance for the research community that utilizes RF/6A cells to model the vascular biology and pathology of the choroid and retina.

4.3 Materials and Methods

4.3.1 Cells and reagents

All cells were maintained in a sterile humidified incubator at 37°C in 5% atmospheric CO₂. We used RF/6A purchased on four separate occasions (

Table 4.1). RF/6A-1 and -3 were cultivated in Dulbecco's Modified Eagle Media, as in¹⁶⁹. RF/6A-2 were cultivated in Eagle's Modified Essential Media, as recommended by ATCC. RF/6A-4 were cultivated in RPMI 1640 as recommended by RIKEN BRC. All basal media formulations were supplemented with 10% heat-inactivated fetal bovine serum and 100 U/mL penicillin and 100 U/mL streptomycin. Human umbilical vein endothelial cells (HUVEC) and primary mouse microvascular retinal endothelial cells (mREC, isolated from C57BL/6) were purchased from Lonza and Cell Biologics, respectively, and grown on gelatin coated plastic dishes in Vascular Cell Basal Medium supplemented with the Endothelial Cell Growth Kit-VEGF (EGM, ATCC). Primary human microvascular retinal endothelial cells (HREC) were purchased from Cell Systems, grown on plastic dishes coated with Attachment Factor in Complete Classic Medium Kit with Serum as recommended by the manufacturer. Primary cells were used at or below passage 7. Cells were stimulated with recombinant human TNF- α (Peprotech), and recombinant human VEGFA-165 (R&D Systems).

Table 4.1: Details of RF/6A cells used in this study

	Purchased From	Purchase Date	Lot#	Deposit Year	Passage at Deposition
-1	ATCC	August 2017	700791	2016	34
-2	ATCC	April 2018	700791	2016	34
-3	ATCC	May 2015	60281248	2011	33
-4	RIKEN BRC	April 2018	3	1999	9

4.3.2 RNA isolation, library construction, and sequencing

Total RNA was isolated from RF/6A using the RNeasy Micro Kit (Thermo Fisher) according to the manufacturer's specifications. RNA quality was confirmed by Agilent Bioanalyzer (Agilent Technologies). Library construction and sequencing (50 bp single-end) were performed by BGI on a BGISEQ-500 sequencing platform. Raw sequencing data is available in the Gene Expression Omnibus at accession GSE113674. Reads were assessed for quality using FastQC (https://www.bioinformatics.babraham.ac.uk/projects/fastq_screen/). Transcript abundance was quantified using Salmon¹⁷⁰ followed by importing and summarizing transcript abundances to the gene level as previously described¹⁷¹. The DESeq2 Bioconductor package¹⁷² in the R statistical computing environment¹⁷³ was used for normalizing count data, performing exploratory data analysis including principal components analysis clustering, estimating dispersion, and fitting a negative binomial model for each gene to assess genes for differential expression. After obtaining a list of differentially expressed genes, log fold changes, and p-values, the Benjamini-Hochberg False Discovery Rate procedure was used to correct p-values for multiple testing.

4.3.3 Real-time quantitative PCR analysis

For HUVEC, HREC, RF/6A-1, -2, and -3, total RNA was collected using the RNeasy Micro kit (Qiagen) and DNase treated and reverse transcribed using QuantiTect (Qiagen). For RF/6A-4, RNA was isolated using RNeasy Mini kit (Qiagen), and reverse transcribed using ReverTra Ace qPCR RT Master Mix with gDNA Remover (TOYOBO). Diluted cDNA was amplified by quantitative real-time PCR (qPCR) (Applied Biosystems) with Power SYBR Green Master Mix (Thermo Fisher). The qPCR cycling conditions were 50°C for 2 minutes, 95°C for 10 minutes, followed by 40 cycles of a two-step amplification program (95°C for 15 seconds and 58°C for 1 minute). Relative expression of target genes was determined by the $2^{-\Delta\Delta C_t}$ method. cDNA from unstimulated HUVEC was used to calculate PCR efficiency for CDH5 and VWF primers, and cDNA from TNF- α -stimulated HUVEC and RF/6A were used to calculate PCR efficiency of E-selectin and d primer sets. Oligonucleotide primers sequences are described in Table 4.2

Table 4.2: qPCR primer sequences used in this study

Species	Target	Forward (5'→3')	Reverse (3'→5')
<i>Hs & Mm</i>	PECAM1	GCCTGCAGTCTTCACTCTCA	TCTTCCCATTTTGCACCGTC
<i>Hs & Mm</i>	PECAM1	TGCAGTCTTCACTCTCAGGA	CCATTTTGCACCGTCCAGTC
<i>Hs & Mm</i>	CDH5	CTCATCAGCCTTGGGATAGC	GGGAGCCAGAGGAAGTCTTT
<i>Hs & Mm</i>	VWF	AGGGAAAATCCTGGATGAGC	GCCTGCTGCAGTAGAAATCG
<i>H. sapiens</i>	SELE	GCTCCCAGTGGAGTCCAACAT	TTCCCAGATGCACCTGTTT
<i>M. mulatta</i>	SELE	CCCAGTGGAGTCCAACACTCC	CTCTAGTTCCCAGACGCAC
<i>H. sapiens</i>	B2M	CCAACATCAACATCTTGGTCAG	ACCACAACCATGCCTTACTTTAT
<i>M. mulatta</i>	B2M	TTGAGGTATCTGGGCAGCT	CAAGCTTCGAGTGCAAGAGA

4.3.4 Western blotting

Cells were homogenized in either RIPA buffer (Pierce) supplemented with protease inhibitor mixture (Pierce), or directly in 1x Laemmli buffer (Bio-Rad) supplemented with β -mercaptoethanol (Sigma). Protein concentrations of RIPA lysates were determined using a BCA assay kit (Thermo) with BSA as a standard. Proteins (20-40 μ g) were separated on a run on 4-20% polyacrylamide Tris-glycine gels (Thermo Fisher) and transferred to PVDF membranes. The transferred membranes were blocked for 1 h at room temperature in Odyssey Blocking Buffer (LI-COR) and incubated at 4 °C overnight with primary antibodies against: human and rhesus PECAM1 (1:500; Abcam JC/70A), human and mouse VE-cadherin (1:200, Santa Cruz C-19), phospho-AKT (Ser473) (1:1,000, Cell Signaling, 12694S), phospho-ERK1/2 (Thr202/Tyr204) (1:1,000, Cell Signaling, 4370), α -tubulin (1:5,000, Abcam, ab89984), vinculin (1:1,000, Sigma, V4139), and β -actin (1:1,000, Abcam, ab13822). The signals were visualized with an Odyssey imaging system.

4.3.5 Immunofluorescent cell labeling

Cells plated on gelatin-coated glass slides (Nunc Lab-Tek II Chamber Slide System) were allowed to attach overnight. Cells were fixed for 20 minutes in 4% PFA (Electron Microscopy Sciences), then incubated in blocking solution consisting of 2% normal donkey serum, 1% BSA, 0.1% Triton X-100, 0.05% Tween 20, 0.05% sodium azide in 1X PBS (w/o Ca²⁺/Mg²⁺), pH 7.2 for 30 min, followed by 30 min blocking in Protein Block, Serum-free (Dako) + 0.1% Triton X-100. Sheep anti-Rab27a (Thermo Fisher) or an equivalent concentration of sheep IgG (Thermo Fisher) was diluted 1:40 in donkey serum blocking solution for 1 h at room temperature, followed by Alexa Fluor 488-conjugated donkey anti-sheep IgG (Thermo). Cells were mounted in ProLong Gold Antifade with DAPI (Thermo Fisher) and visualized on an inverted Nikon A1R fluorescent microscope. Identical imaging parameters (objective, light intensity, gain, exposure) were used between slides and samples.

4.3.6 Immunohistochemistry

5 µm paraffin sections from formalin fixed eyes of *Macaca fascicularis* were deparaffinized, hydrated, and subjected to antigen retrieval by trypsin digestion. Sections were incubated overnight at 4 °C with anti-PECAM1 (Abcam, JC/70A) diluted 1:50 in Antibody Diluent (Dako). Antibody staining was visualized using a streptavidin conjugated anti-mouse, VECTASTAIN ABC-AP Kit, and VECTOR Blue Alkaline Phosphatase Substrate Kit (all from Vector Labs).

4.3.7 Acetylated LDL-uptake

After an overnight incubation in serum-free medium, 10 $\mu\text{g/mL}$ DiI Acetylated LDL (Thermo Fisher, L3484) was added to the culture medium for 4-16 h. Live cells were washed in PBS and visualized using a Nikon A1R fluorescent microscope.

4.3.8 Shear stress stimulation and nuclear alignment analysis

Cells were seeded into tissue culture-treated 0.4 mm height flow chambers (Ibidi) and allowed to reach confluence for three days. Cells were stimulated with shear stress (5 dyne/cm^2) for 48 h at 37 $^{\circ}\text{C}$, 5% CO_2 by perfusing complete cell culture media with a peristaltic pump and an inline pulse dampener. Control cells were maintained in static (no flow) conditions. Following stimulation, cells were gently washed in PBS, fixed in 4% PFA, incubated with Acti-stain 488 phalloidin (Cytoskeleton, Inc.). Slides were filled with ProLong Gold Antifade with DAPI (Thermo Fisher) and visualized on an inverted Nikon A1R fluorescent microscope. Binarized nuclear images were analyzed using the ImageJ ellipse function to quantify the orientation of the nuclear long axis relative to the flow direction. A total of 3,500-5,600 nuclei were analyzed per condition.

4.4 Results

4.4.1 Transcriptomic Profiling of RF/6A cells

Using FastQ screening of high-throughput RNA sequencing, we confirmed that RF/6A-1 cells were of *M. mulatta* origin, with >95% of reads mapping to the rhesus macaque genome, of which 22.15% mapped uniquely to the *M. mulatta* genome, compared to human (0.29%), rat, mouse, drosophila, chicken, E. coli, PhiX (all 0%). Next, we sought to determine whether the RF/6A transcriptome was consistent with that of endothelial cells. As a positive control for *bona fide* endothelial cell transcriptomes, we analyzed publicly deposited RNAseq libraries of human umbilical vein endothelial cells (HUVEC) from a separate laboratory and study¹⁷⁴. As additional positive controls, we analyzed two separate publicly deposited RNAseq libraries of human microvascular retinal endothelial cells (HREC)^{175,176}. In addition to our own RNAseq study, we also analyzed transcriptomic libraries of unstimulated RF/6A cells deposited into a public database by a separate laboratory from an independent study¹⁶⁹.

We also evaluated abundance of individual genes that are established as being enriched in endothelial cells (*CDH5*, *ENG*, *ICAM2*, *KDR*, *MCAM*, *PECAMI*, *TEK*, and *VWF*). As assessed by fragments per kilobase of exon model (FPKM) rank, abundance of these transcripts was enriched to a far greater extent in HUVEC¹⁷⁴ (mean 99%ile) and HREC^{175,176} (mean 98%ile and 99%ile respectively) than in the RF/6A-1 cells of our study (39%ile) or in RF/6A from an independent study¹⁶⁹ (44%ile) (**Figure 4.1A**).

To confirm these RNAseq findings, we designed two primer pairs that amplify sequences of *PECAMI* mRNA that share perfect homology between human and rhesus

macaque. *PECAM1* mRNA abundance was 1,988-120,323-fold lower in RF/6A from four sources compared to HUVEC and 11,326-685,439-fold lower compared to HREC (**Figure 4.1B**). We next used an antibody that recognizes PECAM1 of both human and non-human primate origin (Abcam, JC/70A). Western blotting of HUVEC lysates exhibited strong expression of PECAM1 (**Figure 4.1C**). Conversely, no band was detected in RF/6A lysates from any of four sources (**Figure 4.1C**). We confirmed that nonhuman primate endothelium of the choroid and retina express PECAM1 by immunolabeling sections from *Macaca fascicularis* (which shares 100% homology with *M. mulatta*) with the same antibody (**Figure 4.1D**).

We also investigated the expression of vascular endothelial cadherin (VE-cadherin, encoded by the gene *CDH5*), which is robustly expressed in normal human choroidal endothelium¹⁷⁷. In consonance with RNA-seq data, qPCR using a primer pair that recognizes a conserved region of human and macaque *CDH5*, which encodes vascular endothelial cadherin (VE-Cad), resulted in undetectable or and at least 590-fold lower *CDH5* mRNA in RF/6A cells than in HUVEC and 1,424-fold lower than HREC (**Figure 4.1E**). Consistent with the lack of robust *CDH5* mRNA expression, VE-Cad protein was undetectable by immunoblotting in any of four RF/6A cell lines (**Figure 4.1F**). We confirmed that the antibody (Santa Cruz, sc-6458, C-19) was capable of detecting evolutionarily conserved portions of the VE-Cad protein by immunoblotting human and mouse endothelial cells (**Figure 4.1G**). Collectively, we interpret these findings to indicate that RF/6A do not resemble choroidal and retinal endothelial cells with respect to expression of endothelial-specific genes.

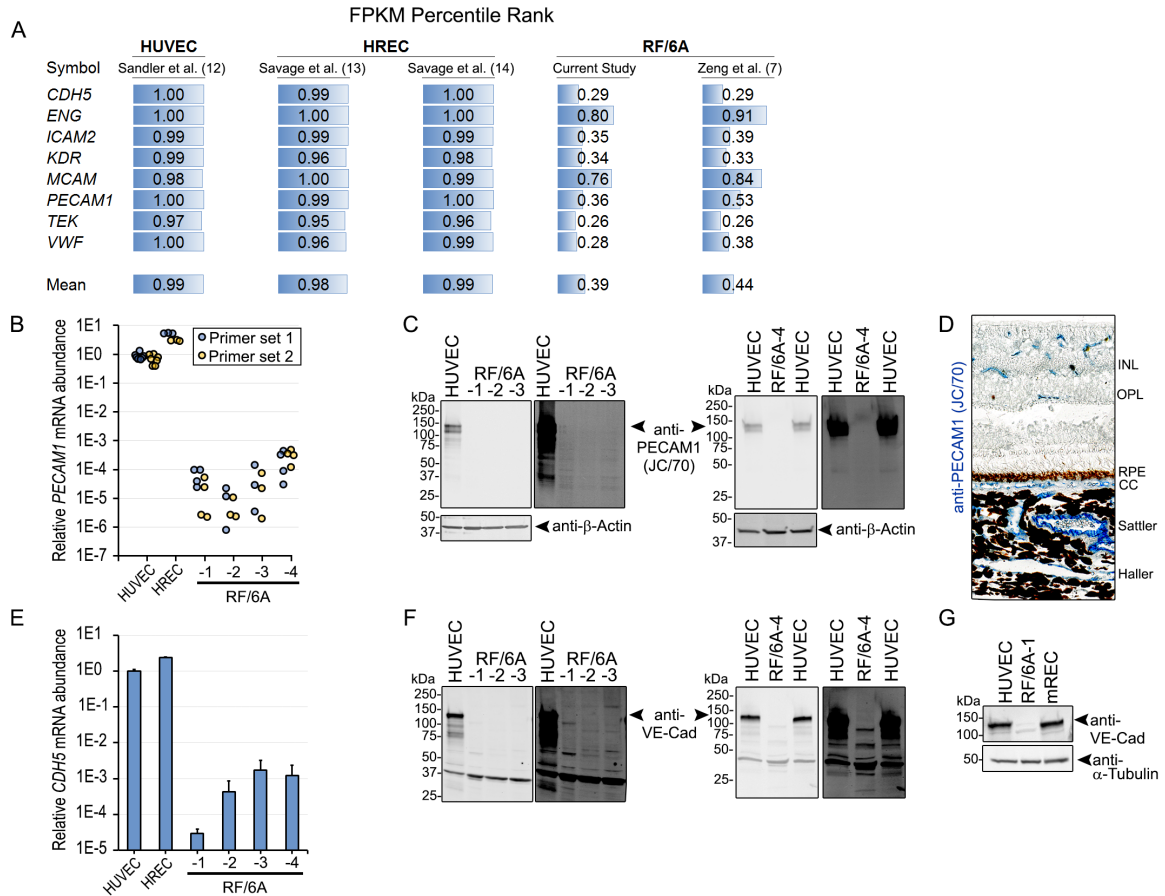


Figure 4.1: RF/6A cells do not express key endothelial transcripts or proteins

(A) Average percentile rank of common endothelial cell-enriched genes. 1.00 refers to genes expressed approaching the 100th percentile compared to all mapped genes in the sample. (B) PECAM1 mRNA abundance by qPCR using two independent primer sets that amplify homologous regions of human and rhesus mRNAs. Normalized to B2M. (C) Immunoblotting for PECAM1 in HUVEC and RF/6A. Low (left) and high (right) exposures shown. (D) Immunohistochemistry of *M. fascicularis* eye with the JC/70A PECAM1 antibody. Reaction product is blue. INL = inner nuclear layer, OPL = outer plexiform layer, RPE = retinal pigmented epithelium, CC = choriocapillaris, Sattler = Sattler's layer, Haller = Haller's layer. (E) Abundance of CDH5 mRNA, which encodes for VE-Cadherin (VE-Cad), by qPCR using primers that amplify a homologous region of human and rhesus mRNAs. Normalized to B2M. (F) Immunoblotting of VE-Cad in HUVEC and RF/6A. Low (left) and high (right) exposures shown. (G) VE-Cad immunoblotting of HUVEC, RF/6A-1, and mREC.

4.4.2 Weibel-Palade Bodies in RF/6A Cells

When first described, the endothelial cell origin of RF/6A was ascribed to the presence of Weibel-Palade bodies (WPB), an endothelial cell-specific regulated secretory organelle that functions in the storage and secretion of von Willebrand factor (VWF), P-selectin¹⁷⁸, tissue plasminogen activator¹⁷⁹, and interleukin-8¹⁸⁰. Ultrastructural analysis of developing¹⁸¹ and pathological¹⁸² choroidal vessels demonstrate WPB present within the choroidal endothelium of humans. In rhesus monkeys, WPB are reported in retinal vessels¹⁸³ and in choroidal vessels in experimental laser-induced choroidal neovascularization¹⁸⁴. Primary and immortalized human choroidal endothelial cells are also reported to be VWF positive^{185,186}. Thus, *bona fide* choroidal and retinal endothelial cells would be expected to contain WPB.

VWF is both necessary and sufficient for formation of WPB. Indeed, the microstructure of WPB is composed of VWF helices and tubules¹⁸⁷. In the original description of these cells¹⁶⁸, RF/6A cells were reported to retain WPB even at later passages despite losing VWF expression. qPCR analysis of *VWF* mRNA confirmed RNA-seq data that expression in RF/6A cells was relatively low (**Figure 4.2A**). In RF/6A-1-3, *VWF* mRNA was 572-7,441-fold lower than HUVEC and 16,257-211,382-fold lower than HREC. Interestingly, *VWF* mRNA was relatively higher in RF/6A-4, but still ~34-fold lower than HUVEC and 971-fold lower than HREC. We next performed transmission electron microscopy to visualize WPB. Whereas WPB were readily detected in HUVEC and mREC, these structures were absent in RF/6A-1 cells (**Figure 4.2B**). As a complementary approach to visualizing WPB, we performed immunofluorescent labeling of the GTPase Rab27a, which localizes to mature WPB¹⁸⁸⁻¹⁹⁰, using an antibody that

recognizes human, mouse, and rat homologs (Thermo Fisher PA5-47907). Small, rod-shaped, Rab27a-positive organelles consistent with WPB were readily observed in HUVEC (**Figure 4.2C**). Conversely, WBP-like structures were undetectable in both RF/6A-1 and -2 cells, where Rab27a staining was diffuse, consistent with staining observed in non-endothelial cells in other studies¹⁸⁸. In RF/6A-3 cells, approximately 25% of cells exhibited Rab27a staining consistent with WPB, suggesting that the complete loss of this endothelial cell-specific characteristic may have occurred relatively recently. Collectively, we interpret these findings to indicate that commercially distributed RF/6A cells do not robustly express VWF and are not identifiable as endothelial cells based on the presence of WPB.

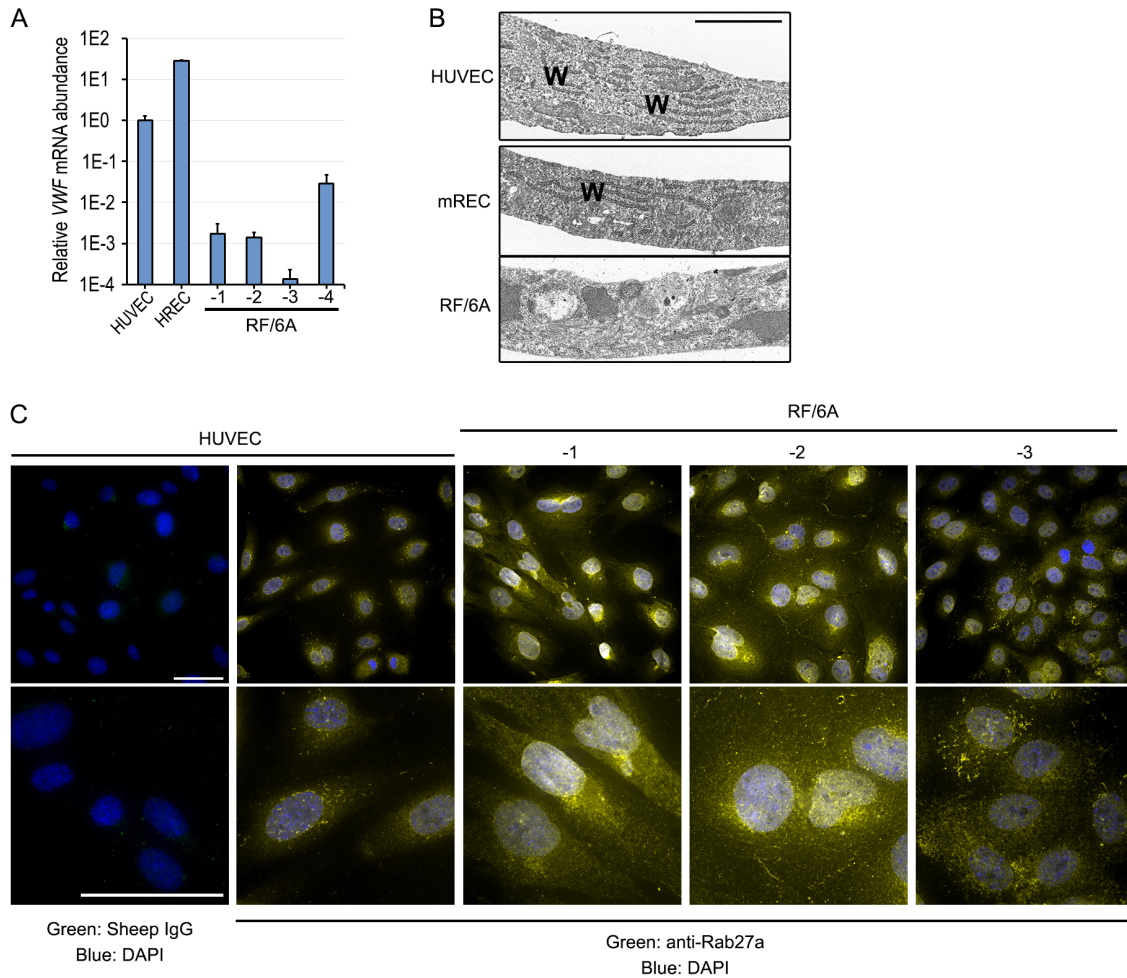


Figure 4.2: RF/6A cells do not exhibit the endothelial structural protein von Willebrand factor

(A) qPCR analysis of *VWF* mRNA in HUVEC, HREC, and RF/6A using primers that amplify homologous regions of human and rhesus mRNAs. (B) Transmission electron micrographs of HUVEC, mREC, and RF/6A-1. Weibel-Palade bodies are long rod-like structures, denoted by “W”. Scale bar = 2 μ m. (C) Low (top) and high (bottom) magnification images of immunofluorescent staining for Rab27a in HUVEC, and RF/6A cells. Note rod-like structures corresponding to WPB in HUVEC, which are absent in RF/6A-1 and -2, and sporadic in RF/6A-3. Scale bar in low magnification = 50 μ m, in high magnification = 10 μ m.

4.4.3 Functional Endothelial Cell Assays in RF/6A Cells

We sought to determine whether RF/6A cells exhibited characteristic endothelial cell behaviors. Recruitment and trafficking of leukocytes to areas of inflammation are critical functions of the endothelium, which is accomplished by expression of a cadre of surface receptors. We analyzed the relative expression of the endothelial-specific protein E-selectin (encoded by *SELE*) both basally and in response to TNF- α stimulation in comparison to HUVEC. Under basal conditions, RF/6A-1, -2, and -3 expressed 507-, 1,697, and 748-fold less *SELE* respectively compared to HUVEC and 336-, 1,125-, and 496-fold less than HREC (**Figure 4.3A**). Following stimulation with recombinant human TNF- α (50 ng/mL, 4 h), which is biologically active in human and non-human primate, *SELE* expression was 7,130-57,994-fold greater in HUVEC and 107-870-fold greater in HREC than in RF/6A cells. TNF- α -stimulation of RF/6A cells resulted in less *SELE* than the levels measured in *unstimulated* HUVEC and HREC. We interpret these findings to mean that RF/6A cells are not a suitable model to study TNF- α -stimulated endothelial inflammation.

Another long established functional behavior of endothelial cells, including an immortalized human choroidal endothelial cell line¹⁸⁶, is uptake and metabolism of acetylated low density lipoprotein (ac-LDL)¹⁹¹. Primary HUVEC and HREC exhibited robust ac-LDL uptake. Conversely, RF/6A-1 and -2 cells failed to accumulate ac-LDL in detectable levels (**Figure 4.3B**). We interpret this finding to mean that RF/6A also lack this characteristic endothelial cell behavior.

Alignment in the direction of blood flow is another widely conserved property of endothelial cells. Like most of the vascular tree, human choroidal endothelium aligns parallel to the direction of shear stress *in situ* (**Figure 4.3C**). Shear stress-induced cell alignment is governed by a mechanosensory complex consisting of PECAM1, VE-cadherin, and VEGF-R2, none of which is robustly expressed in RF/6A (**Figure 4.1B**). Consistent with the lack of mechanosensory constituents, shear stress stimulation did not induce RF/6A-1 alignment in the direction of shear stress. Rather, we observed a modest but statistically significant realignment of cells *perpendicular* to the direction of shear stress (**Figure 4.3D**), a phenotype reported in vascular smooth muscle cells^{192,193}, and fibroblasts^{194,195}. We interpret this finding to mean that RF/6A are not a suitable model to study endothelial-specific responses to fluid shear stress.

Finally, we next sought to clarify the extent to which RF/6A responded to VEGF stimulation by investigating signaling intermediates that are activated by VEGF in endothelial cells. Whereas treatment with recombinant human VEGFA-165, which shares 100% identity with *M. mulatta* VEGFA, induced rapid and robust phosphorylation of AKT and ERK1/2 in HUVEC, RF/6A-1, -2, and -3 cells exhibited delayed and diminished phosphorylation of these signaling constituents (**Figure 4.3E**). The relative biochemical insensitivity of RF/6A cells to VEGF-A is consistent with the relatively low expression of canonical VEGFA receptors (VEGF-R1, R2, NRP1, and NRP2) observed in RF/6A by RNAseq. We interpret these findings to mean that RF/6A cells are not a robust model in which to assess VEGFA stimulation of endothelial cells.

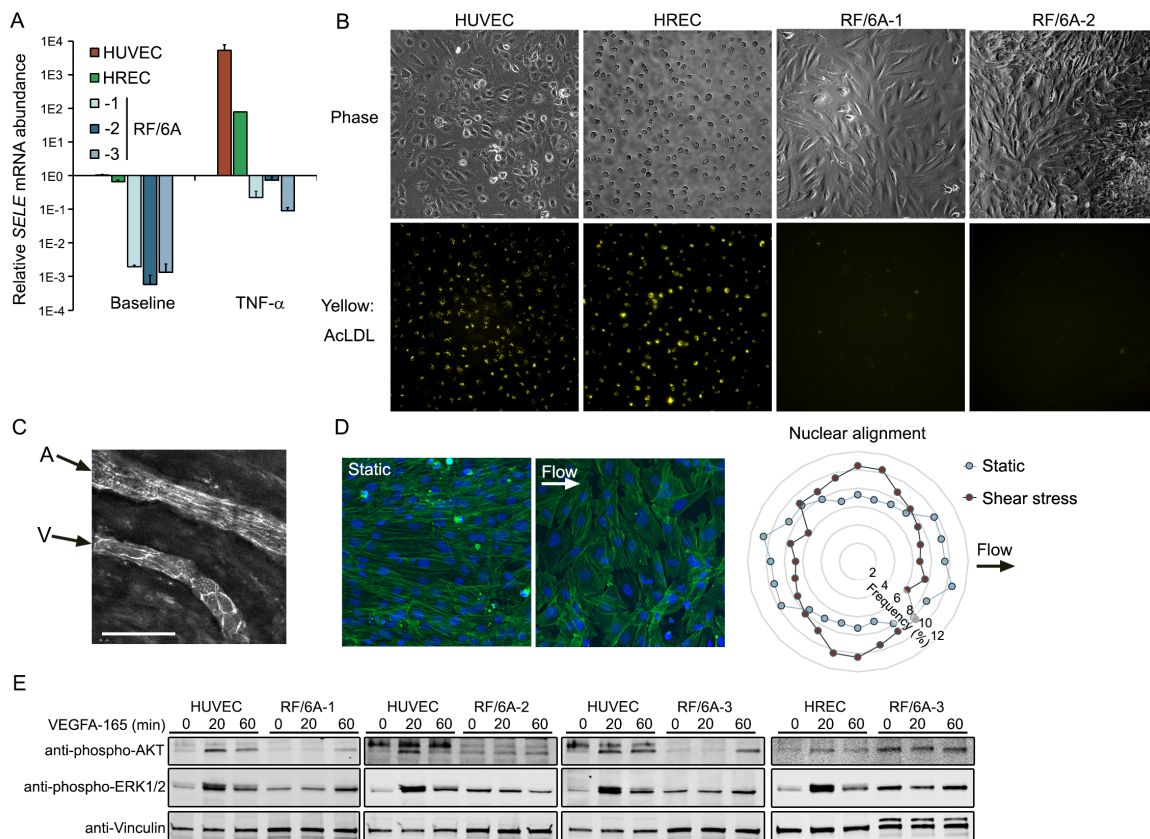


Figure 4.3: RF/6A do not exhibit functional activities normally seen by endothelial cells

(A) qPCR analysis of *SELE* mRNA 4 h after treatment with human TNF- α at 50 ng/mL. *SELE* primers amplify a region conserved between human and macaque. Normalized to *B2M*. (B) Representative phase (top) and DiI (bottom) images of HUVEC, HREC, and RF/6A after treatment with DiI-labeled acetylated LDL. (C) Arteriole/venule pair in Sattler's layer of a normal human eye labeled with PECAM1 to outline cell junctions. Arrows indicate flow direction. (D) Fluorescent micrographs of RF/6A under static (no flow) and shear stress conditions labeled with phalloidin and DAPI. Nuclear orientation was quantified with respect to the flow direction. (E) Immunoblotting of AKT and ERK1/2 phosphorylation in HUVEC, HREC, and RF/6A cells after VEGF-A stimulation for indicated durations.

4.5 Discussion

This study provides the first rigorous analysis of the endothelial cell characteristics of the RF/6A cell line. One metric by which the suitability of an experimental tool can be judged is whether it possesses “face validity”, or similarity to the condition it seeks to model. The RF/6A line does not express an identifiable endothelial cell transcriptome, express established endothelial cell markers or possess morphological characteristics of choroidal and retinal endothelial cells. Given the recognized heterogeneity of endothelial cells throughout the vascular tree (reviewed in¹⁹⁶), it bears mentioning that choroidal and retinal endothelial cells in culture or *in situ* possess each of these traits as demonstrated either in the literature or by the experiments herein. Thus, it is not simply the case that RF/6A cells do not exhibit these features because they reflect unique properties of “chorioretinal” endothelial cells.

A second criterion upon which to judge a model is “target validity”, or the ability to reproduce the effects of targets of inquiry or stimuli in the real system. RF/6A cells do not respond to diverse stimuli - shear stress, TNF- α , or VEGFA - in a manner consistent with endothelial cells. VEGFA-induced effects on choroidal and retinal endothelial cells underlie blinding conditions in millions of individuals. Therefore, it is particularly damning that RF/6A cells lack robust expression of canonical VEGF receptors at levels near that of *bona fide* endothelial cells, and that RF/6A cells are relatively insensitive to this stimulus. Thus, the RF/6A cell line also fails the target validity criteria.

Aside from VWF positivity, no quantitative characterization of this cell line has been published with respect to endothelial gene expression and characteristic behaviors.

Presumably, these features were present in the founding cell(s) and have been lost over successive passages. Although the causes and kinetics of this loss of endothelial characteristics are unclear, one potential cause of loss of VWF reactivity is that VWF antagonizes endothelial proliferation¹⁹⁷. Over time, the RF/6A line may have drifted towards low VWF, rapidly dividing cells. These findings do not exclude the possibility that under certain culturing conditions such as confluency, media composition, and exogenous extracellular matrix, RF/6A may adopt EC characteristics. However, we interpret the data acquired from RF/6A cells from four batches, two suppliers, cultured in three distinct media formulations to suggest that the lack of endothelial characteristics in contemporary commercially available RF/6A is robust.

Numerous studies have employed RF/6A in capillary tube formation assays to assess the angiogenic potential of experimental compounds, drugs, and signaling intermediates. Importantly, capillary tube formation is not an endothelial cell-specific property; multiple non-endothelial cell types exhibit the capacity to form capillary like networks when plated on 3-D basement membrane, including primary human fibroblasts¹⁹⁸, breast¹⁹⁸⁻²⁰⁰, prostate¹⁹⁸, melanoma^{200,201}, glioblastoma^{198,200,202}, and bladder cancer cell lines²⁰³, and macrophages from multiple myeloma patients²⁰⁴. Thus, findings from tube formation assays of RF/6A cells to glean insights into the behavior of actual endothelial cells should be interpreted with caution.

Cell line misidentification and contamination are widely considered major threats to scientific rigor and confidence^{205,206}. In response, publishing and grant administering institutions have established new guidelines and requirements to safeguard against these

errors. Cell line authentication best practices focus on establishing the species and genetic homogeneity of the line. In 1999, Dirks and colleagues used DNA fingerprinting to establish that ECV304, a widely used “endothelial” cell line, was in fact a subclone of T24 bladder carcinoma cells²⁰³. This finding was made in the context of a cell line that was known at the time to deviate from fundamental endothelial cell characteristics, including the absence of expression of PECAM1 and VWF, and inability to stimulate E-selectin expression²⁰⁷. Regrettably, the now 19-year-old revelation that ECV304 line is not endothelial has not eradicated its use in the literature as a model of endothelium in 2018.

Unlike ECV304/T24 cells, the RF/6A line would likely pass muster if the best practices recommended of cell line providers (ATCC), journal editors, and the NIH were followed – the species of origin was uniquely identified as being of rhesus macaque origin, free from human or mouse cell line contaminants. The present findings in RF/6A cells suggest that confirming the genetic identity of a cell line is a necessary but not a sufficient step towards establishing the identity and utility of a cellular model. We strongly encourage investigators to quantify the validity of cell lines by transcriptional profiling and in relevant functional assays.

The use of better-characterized choroidal and retinal endothelial cells should supplant the use of RF/6A cells in the future. We caution laboratories against the use of RF/6A cells as an experimental model of endothelial cells.

Chapter 5: Conclusion

5.1 Summary of results

Throughout this dissertation, we have focused on thematically related aspects of various models for studying pathological angiogenesis in the eye. In light of previous and contradictory reports, we first reconciled the demonstrated role of inflammasome constituents in spontaneous CNV with the observations that laser CNV is not affected by inflammasome constituent inhibition. By adapting the laser CNV model to include inflammasome agonists, we now know the consequences of inflammasome activation in this model, as well as highlighting the critical role of macrophage-derived IL-1 β .

Considering the high fiscal and social burden wrought by monthly visits to the ophthalmologist for intravitreal injections, we sought to investigate whether exercise, a non-invasive and low-cost intervention, could have potential therapeutic implications for nvAMD. By developing a novel training regime, we demonstrated that voluntary exercise before laser CNV administration in mice was sufficient to reduce vessel growth and inflammatory cell ingressions.

Our studies on the anatomical, transcriptional, and functional characteristics of the RF/6A cell line, which at the time of manuscript publication was one of the most used cell lines in labs studying chorioretinal diseases, highlights the need for more cautionary profiling of widely used cell lines and thorough evaluation of the models utilized in one's field.

Taken together, the work presented here resolves previously outstanding contradictions in the field, provides both new and improved methods for investigating

choroidal neovascularization, and advances our understanding of the precise role of inflammasome activation in the pathogenesis of CNV.

5.2 Future directions

The studies presented here are by no means all inclusive. To determine the precise mechanism by which subretinally injected inflammasome agonists effect a proangiogenic phenotype, we must consider which cell types are most likely to be affected first *in situ*. While we now know that inflammasome activation and macrophage-derived IL-1 β does indeed lead to laser CNV exacerbation, further work is needed to define both the intramolecular and intercellular effects of inflammasome activation as it pertains to laser CNV.

One proposed method by which to address this is to subretinally inject inflammasome agonists into mice lacking Nlrp3 specifically in RPE or myelomonocytic cells, or both. This would add to the results we observed in our 2024 Angiogenesis manuscript, where we performed subretinal injection of *Alu* RNA in mice lacking caspase-1 in myelomonocytic cells. If mice lacking Nlrp3 in RPE *and* myelomonocytic cells exhibit a greater reduction in CNV volume compared to *Nlrp3*^{-/-} in RPE *or* myelomonocytic cells, this suggests a potential paracrine relationship in which these cells potentiate each other's response to inflammasome activation.

As previously mentioned, the precise cells that are directly responsible for the *Alu* RNA-induced inflammasome agonism is not clearly delineated. The findings presented here suggest that inflammasome activation in myelomonocytic cells is crucial to the exacerbation of laser CNV in the presence of an inflammasome agonist, but we must

consider other pertinent cell types. Future experiments should address the potential role of inflammasome activation in RPE and microglia in mediating inflammasome-driven CNV exacerbation. For example, **Figure 2.7** demonstrates how conditioned media from *Alu* RNA-transfected BMDM stimulates chemotaxis in WT BMDM in an IL-1 β -dependent manner. Additional studies utilizing conditioned media from *Alu* RNA-transfected RPE would improve on the overall model of inflammasome-mediated chemotaxis and CNV exacerbation. Likewise, subretinal administration of inflammasome agonists in microglia-specific inflammasome knockout mice, utilizing *Cx3cr1-Cre* or *P2ry12-Cre*, would provide further insight into the cell-specific role of the CNV exacerbation we observe.

Regarding our exercise studies, previous research has shown that superoxide dismutase 3 (SOD3) is upregulated in exercised individuals within the context of type 2 diabetes mellitus²⁰⁸. In this study, extracellular vesicle-associated SOD3 through exercise training was shown to improve angiogenic potential and wound healing. Albeit this may seem to be contradictory to our observations that exercise *decreases* laser CNV responses, the effect of SOD3 on angiogenesis and wound healing could potentially be varied throughout different vascular beds. Therefore, it is plausible that exercise might increase angiogenesis in one organ system and inhibit it in another; to this end, an interesting approach would be to transfuse blood from exercised mice into sedentary mice which are then subjected to the laser CNV protocol to determine if the angioinhibitory effect of exercise is recapitulated in the sedentary mice. This would allow us to determine if the angioinhibitory agents are secreted into the blood and therefore systemically derived; if there is no inhibition in response to laser CNV, this result would suggest exercise has some eye-specific, local effect that results in reduces angiogenesis.

References

1. Liu, Z.-L., Chen, H.-H., Zheng, L.-L., Sun, L.-P. & Shi, L. Angiogenic signaling pathways and anti-angiogenic therapy for cancer. *Signal Transduct. Target. Ther.* **8**, 198 (2023).
2. Maruotti, N., Cantatore, F. P., Crivellato, E., Vacca, A. & Ribatti, D. Angiogenesis in rheumatoid arthritis. *Histol. Histopathol.* **21**, 557–566 (2006).
3. Purves, D. *et al.* Anatomical Distribution of Rods and Cones. in *Neuroscience. 2nd edition* (Sinauer Associates, 2001).
4. Yang, S., Zhou, J. & Li, D. Functions and Diseases of the Retinal Pigment Epithelium. *Front. Pharmacol.* **12**, 727870 (2021).
5. Kwon, W. & Freeman, S. A. Phagocytosis by the Retinal Pigment Epithelium: Recognition, Resolution, Recycling. *Front. Immunol.* **11**, (2020).
6. Rothlin, C. V., Carrera-Silva, E. A., Bosurgi, L. & Ghosh, S. TAM Receptor Signaling in Immune Homeostasis. *Annu. Rev. Immunol.* **33**, 355–391 (2015).
7. Molday, R. S., Beharry, S., Ahn, J. & Zhong, M. Binding of N-retinylidene-PE to ABCA4 and a model for its transport across membranes. *Adv. Exp. Med. Biol.* **572**, 465–470 (2006).
8. Edwards, M. & Luty, G. A. Bruch's Membrane and the Choroid in Age-Related Macular Degeneration. in *Age-related Macular Degeneration: From Clinic to Genes*

- and Back to Patient Management* (eds. Chew, E. Y. & Swaroop, A.) 89–119 (Springer International Publishing, Cham, 2021). doi:10.1007/978-3-030-66014-7_4.
9. Nickla, D. L. & Wallman, J. THE MULTIFUNCTIONAL CHOROID. *Prog. Retin. Eye Res.* **29**, 144 (2009).
 10. Bill, A., Sperber, G. & Ujiie, K. Physiology of the choroidal vascular bed. *Int. Ophthalmol.* **6**, 101–107 (1983).
 11. Noy, N. Retinoid-binding proteins : mediators of retinoid action. (2000).
 12. García-Layana, A., Cabrera-López, F., García-Arumí, J., Arias-Barquet, L. & Ruiz-Moreno, J. M. Early and intermediate age-related macular degeneration: update and clinical review. *Clin. Interv. Aging* **12**, 1579–1587 (2017).
 13. Sunness, J. S., Gonzalez-Baron, J., Bressler, N. M., Hawkins, B. & Applegate, C. A. The development of choroidal neovascularization in eyes with the geographic atrophy form of age-related macular degeneration. *Ophthalmology* **106**, 910–919 (1999).
 14. Wright, C. B. *et al.* Chronic Dicer1 deficiency promotes atrophic and neovascular outer retinal pathologies in mice. *Proc. Natl. Acad. Sci. U. S. A.* **117**, 2579–2587 (2020).
 15. Booij, J. C., Baas, D. C., Beisekeeva, J., Gorgels, T. G. M. F. & Bergen, A. a. B. The dynamic nature of Bruch's membrane. *Prog. Retin. Eye Res.* **29**, 1–18 (2010).
 16. Campochiaro, P. A., Soloway, P., Ryan, S. J. & Miller, J. W. The pathogenesis of choroidal neovascularization in patients with age-related macular degeneration. *Mol. Vis.* **5**, 34 (1999).

17. de Jong, P. T. V. M. Age-related macular degeneration. *N. Engl. J. Med.* **355**, 1474–1485 (2006).
18. Qu, S., Lin, H., Pfeiffer, N. & Grus, F. H. Age-Related Macular Degeneration and Mitochondria-Associated Autoantibodies: A Review of the Specific Pathogenesis and Therapeutic Strategies. *Int. J. Mol. Sci.* **25**, 1624 (2024).
19. Ryan, S. J. The development of an experimental model of subretinal neovascularization in disciform macular degeneration. *Trans. Am. Ophthalmol. Soc.* **77**, 707–745 (1979).
20. Tobe, T. *et al.* Targeted disruption of the FGF2 gene does not prevent choroidal neovascularization in a murine model. *Am. J. Pathol.* **153**, 1641–1646 (1998).
21. Kwak, N., Okamoto, N., Wood, J. M. & Campochiaro, P. A. VEGF is major stimulator in model of choroidal neovascularization. *Invest. Ophthalmol. Vis. Sci.* **41**, 3158–3164 (2000).
22. Sakurai, E., Anand, A., Ambati, B. K., van Rooijen, N. & Ambati, J. Macrophage depletion inhibits experimental choroidal neovascularization. *Invest. Ophthalmol. Vis. Sci.* **44**, 3578–3585 (2003).
23. Grossniklaus, H. E. & Green, W. R. Choroidal neovascularization. *Am. J. Ophthalmol.* **137**, 496–503 (2004).
24. Chan, W.-M. *et al.* Choroidal neovascularisation in pathological myopia: an update in management. *Br. J. Ophthalmol.* **89**, 1522–1528 (2005).

25. Nika, M. & Besirli, C. G. Choroidal neovascularization and angioid streaks in pseudoxanthoma elasticum. *Int. J. Ophthalmol.* **4**, 449–451 (2011).
26. Makin, R. D. *et al.* Inflammasome activation aggravates choroidal neovascularization. *Angiogenesis* (2024) doi:10.1007/s10456-024-09949-1.
27. Dridi, S. *et al.* ERK1/2 activation is a therapeutic target in age-related macular degeneration. *Proc. Natl. Acad. Sci.* **109**, 13781–13786 (2012).
28. Gelfand, B. D. *et al.* Iron Toxicity in the Retina Requires Alu RNA and the NLRP3 Inflammasome. *Cell Rep.* **11**, 1686–1693 (2015).
29. Kaneko, H. *et al.* DICER1 deficit induces Alu RNA toxicity in age-related macular degeneration. *Nature* **471**, 325–330 (2011).
30. Kim, Y. *et al.* DICER1/Alu RNA dysmetabolism induces Caspase-8-mediated cell death in age-related macular degeneration. *Proc. Natl. Acad. Sci. U. S. A.* **111**, 16082–16087 (2014).
31. Tarallo, V. *et al.* DICER1 loss and Alu RNA induce age-related macular degeneration via the NLRP3 inflammasome and MyD88. *Cell* **149**, 847–859 (2012).
32. Kerur, N. *et al.* TLR-independent and P2X7-dependent signaling mediate Alu RNA-induced NLRP3 inflammasome activation in geographic atrophy. *Invest. Ophthalmol. Vis. Sci.* **54**, 7395–7401 (2013).

33. Otsuka, M. *et al.* Hypersusceptibility to vesicular stomatitis virus infection in Dicer1-deficient mice is due to impaired miR24 and miR93 expression. *Immunity* **27**, 123–134 (2007).
34. Cervi, D. *et al.* Enhanced natural-killer cell and erythropoietic activities in VEGF-A-overexpressing mice delay F-MuLV-induced erythroleukemia. *Blood* **109**, 2139–2146 (2007).
35. Miquerol, L., Gertsenstein, M., Harpal, K., Rossant, J. & Nagy, A. Multiple developmental roles of VEGF suggested by a LacZ-tagged allele. *Dev. Biol.* **212**, 307–322 (1999).
36. Jafarifar, F., Yao, P., Eswarappa, S. M. & Fox, P. L. Repression of VEGFA by CA-rich element-binding microRNAs is modulated by hnRNP L. *EMBO J.* **30**, 1324–1334 (2011).
37. Wilkie, A. L., Jordan, S. A. & Jackson, I. J. Neural crest progenitors of the melanocyte lineage: coat colour patterns revisited. *Dev. Camb. Engl.* **129**, 3349–3357 (2002).
38. Marneros, A. G. NLRP3 inflammasome blockade inhibits VEGF-A-induced age-related macular degeneration. *Cell Rep.* **4**, 945–958 (2013).
39. Ambati, J., Atkinson, J. P. & Gelfand, B. D. Immunology of age-related macular degeneration. *Nat. Rev. Immunol.* **13**, 438–451 (2013).
40. Kvant, A. *et al.* Matrix metalloproteinase (MMP) expression in experimental choroidal neovascularization. *Curr. Eye Res.* **21**, 684–690 (2000).

41. Grossniklaus, H. E. *et al.* Correlation of histologic 2-dimensional reconstruction and confocal scanning laser microscopic imaging of choroidal neovascularization in eyes with age-related maculopathy. *Arch. Ophthalmol. Chic. Ill 1960* **118**, 625–629 (2000).
42. Espinosa-Heidmann, D. G. *et al.* Macrophage depletion diminishes lesion size and severity in experimental choroidal neovascularization. *Invest. Ophthalmol. Vis. Sci.* **44**, 3586–3592 (2003).
43. Tsutsumi, C. *et al.* The critical role of ocular-infiltrating macrophages in the development of choroidal neovascularization. *J. Leukoc. Biol.* **74**, 25–32 (2003).
44. Sluyter, R. The P2X7 Receptor. *Adv. Exp. Med. Biol.* **1051**, 17–53 (2017).
45. Latz, E., Xiao, T. S. & Stutz, A. Activation and regulation of the inflammasomes. *Nat. Rev. Immunol.* **13**, 397–411 (2013).
46. Gao, H. & Hollyfield, J. G. Aging of the human retina. Differential loss of neurons and retinal pigment epithelial cells. *Invest. Ophthalmol. Vis. Sci.* **33**, 1–17 (1992).
47. Iyer, S. S. *et al.* Necrotic cells trigger a sterile inflammatory response through the Nlrp3 inflammasome. *Proc. Natl. Acad. Sci. U. S. A.* **106**, 20388–20393 (2009).
48. Doyle, S. L. *et al.* NLRP3 has a protective role in age-related macular degeneration through the induction of IL-18 by drusen components. *Nat. Med.* **18**, 791–798 (2012).
49. Hirano, Y. *et al.* IL-18 is not therapeutic for neovascular age-related macular degeneration. *Nat. Med.* **20**, 1372–1375 (2014).

50. Dobson, D. E. *et al.* 1-Butyryl-glycerol: a novel angiogenesis factor secreted by differentiating adipocytes. *Cell* **61**, 223–230 (1990).
51. Marneros, A. G. NLRP3 inflammasome blockade inhibits VEGF-A-induced age-related macular degeneration. *Cell Rep.* **4**, 945–958 (2013).
52. Kayagaki, N. *et al.* Non-canonical inflammasome activation targets caspase-11. *Nature* **479**, 117–121 (2011).
53. Kanneganti, T.-D. *et al.* Bacterial RNA and small antiviral compounds activate caspase-1 through cryopyrin/Nalp3. *Nature* **440**, 233–236 (2006).
54. Huang, P. *et al.* Subretinal injection in mice to study retinal physiology and disease. *Nat. Protoc.* **17**, 1468–1485 (2022).
55. Wang, S.-B. *et al.* DDX17 is an essential mediator of sterile NLRC4 inflammasome activation by retrotransposon RNAs. *Sci. Immunol.* **6**, eabi4493 (2021).
56. Kaneko, H. *et al.* DICER1 deficit induces Alu RNA toxicity in age-related macular degeneration. *Nature* **471**, 325–330 (2011).
57. Narendran, S. *et al.* Nucleoside reverse transcriptase inhibitors and Kamuvudines inhibit amyloid- β induced retinal pigmented epithelium degeneration. *Signal Transduct. Target. Ther.* **6**, 149 (2021).
58. Narendran, S. *et al.* A Clinical Metabolite of Azidothymidine Inhibits Experimental Choroidal Neovascularization and Retinal Pigmented Epithelium Degeneration. *Invest. Ophthalmol. Vis. Sci.* **61**, 4 (2020).

59. Fukuda, S. *et al.* Cytoplasmic synthesis of endogenous Alu complementary DNA via reverse transcription and implications in age-related macular degeneration. *Proc. Natl. Acad. Sci. U. S. A.* **118**, (2021).
60. Fukuda, S. *et al.* Alu complementary DNA is enriched in atrophic macular degeneration and triggers retinal pigmented epithelium toxicity via cytosolic innate immunity. *Sci. Adv.* **7**, eabj3658 (2022).
61. Luibl, V. *et al.* Drusen deposits associated with aging and age-related macular degeneration contain nonfibrillar amyloid oligomers. *J. Clin. Invest.* **116**, 378–385 (2006).
62. Isas, J. M. *et al.* Soluble and Mature Amyloid Fibrils in Drusen Deposits. *Invest. Ophthalmol. Vis. Sci.* **51**, 1304–1310 (2010).
63. Ohno-Matsui, K. Parallel findings in age-related macular degeneration and Alzheimer's disease. *Prog. Retin. Eye Res.* **30**, 217–238 (2011).
64. Malek, G. *et al.* Apolipoprotein E allele-dependent pathogenesis: A model for age-related retinal degeneration. *Proc. Natl. Acad. Sci.* **102**, 11900–11905 (2005).
65. Ding, J.-D. *et al.* Anti-amyloid therapy protects against retinal pigmented epithelium damage and vision loss in a model of age-related macular degeneration. *Proc. Natl. Acad. Sci. U. S. A.* **108**, E279-87 (2011).
66. Fowler, B. J. *et al.* Nucleoside reverse transcriptase inhibitors possess intrinsic anti-inflammatory activity. *Science* **346**, 1000–1003 (2014).

67. JAYAKRISHNA, A. & BENJAMIN, F. COMPOSITIONS AND METHODS FOR TREATING RETINAL DEGRADATION. (2021).
68. Kerur, N. *et al.* cGAS drives noncanonical-inflammasome activation in age-related macular degeneration. *Nat. Med.* **24**, 50–61 (2018).
69. Adachi, O. *et al.* Targeted disruption of the MyD88 gene results in loss of IL-1- and IL-18-mediated function. *Immunity* **9**, 143–150 (1998).
70. Loiarro, M. *et al.* Peptide-mediated interference of TIR domain dimerization in MyD88 inhibits interleukin-1-dependent activation of NF- κ B. *J. Biol. Chem.* **280**, 15809–15814 (2005).
71. Sakurai, E., Anand, A., Ambati, B. K., Van Rooijen, N. & Ambati, J. Macrophage depletion inhibits experimental choroidal neovascularization. *Invest. Ophthalmol. Vis. Sci.* (2003) doi:10.1167/iovs.03-0097.
72. Espinosa-Heidmann, D. G. *et al.* Bone Marrow Transplantation Transfers Age-Related Susceptibility to Neovascular Remodeling in Murine Laser-Induced Choroidal Neovascularization. *Invest. Ophthalmol. Vis. Sci.* **54**, 7439–7449 (2013).
73. Carmi, Y. *et al.* The role of macrophage-derived IL-1 in induction and maintenance of angiogenesis. *J. Immunol. Baltim. Md 1950* **183**, 4705–4714 (2009).
74. Shao, Z. *et al.* Choroid Sprouting Assay: An Ex Vivo Model of Microvascular Angiogenesis. *PLoS ONE* **8**, e69552 (2013).

75. Droho, S., Cuda, C. M., Perlman, H. & Lavine, J. A. Monocyte-Derived Macrophages Are Necessary for Beta-Adrenergic Receptor-Driven Choroidal Neovascularization Inhibition. *Invest. Ophthalmol. Vis. Sci.* **60**, 5059–5069 (2019).
76. Wright, C. B. *et al.* Chronic Dicer1 deficiency promotes atrophic and neovascular outer retinal pathologies in mice. *Proc. Natl. Acad. Sci. U. S. A.* (2020) doi:10.1073/pnas.1909761117.
77. Malsy, J., Alvarado, A. C., Lamontagne, J. O., Strittmatter, K. & Marneros, A. G. Distinct effects of complement and of NLRP3- and non-NLRP3 inflammasomes for choroidal neovascularization. *eLife* **9**, e60194 (2020).
78. Vogel, S. *et al.* TLR4-dependent upregulation of the platelet NLRP3 inflammasome promotes platelet aggregation in a murine model of hindlimb ischemia. *Biochem. Biophys. Res. Commun.* **508**, 614–619 (2019).
79. Ma, Y. *et al.* Heme Oxygenase-1 in Macrophages Impairs the Perfusion Recovery After Hindlimb Ischemia by Suppressing Autolysosome-Dependent Degradation of NLRP3. *Arterioscler. Thromb. Vasc. Biol.* **41**, 1710–1723 (2021).
80. Gimenez, F. *et al.* The inflammasome NLRP3 plays a protective role against a viral immunopathological lesion. *J. Leukoc. Biol.* **99**, 647–657 (2016).
81. Loukovaara, S. *et al.* NLRP3 inflammasome activation is associated with proliferative diabetic retinopathy. *Acta Ophthalmol. (Copenh.)* **95**, 803–808 (2017).

82. Ambati, J. *et al.* Repurposing anti-inflammasome NRTIs for improving insulin sensitivity and reducing type 2 diabetes development. *Nat. Commun.* **11**, 4737 (2020).
83. Friedman, D. S. *et al.* Prevalence of age-related macular degeneration in the United States. *Arch. Ophthalmol. Chic. Ill 1960* **122**, 564–572 (2004).
84. Rosenfeld, P. J. *et al.* Estimating Medicare and Patient Savings From the Use of Bevacizumab for the Treatment of Exudative Age-related Macular Degeneration. *Am. J. Ophthalmol.* **191**, 135–139 (2018).
85. Chakravarthy, U. *et al.* Alternative treatments to inhibit VEGF in age-related choroidal neovascularisation: 2-year findings of the IVAN randomised controlled trial. *Lancet Lond. Engl.* **382**, 1258–1267 (2013).
86. Rofagha, S. *et al.* Seven-year outcomes in ranibizumab-treated patients in ANCHOR, MARINA, and HORIZON: a multicenter cohort study (SEVEN-UP). *Ophthalmology* **120**, 2292–2299 (2013).
87. Singer, M. A. *et al.* HORIZON: an open-label extension trial of ranibizumab for choroidal neovascularization secondary to age-related macular degeneration. *Ophthalmology* **119**, 1175–1183 (2012).
88. Zhu, M. *et al.* Intravitreal Ranibizumab for neovascular Age-related macular degeneration in clinical practice: five-year treatment outcomes. *Graefes Arch. Clin. Exp. Ophthalmol. Albrecht Von Graefes Arch. Klin. Exp. Ophthalmol.* **253**, 1217–1225 (2015).

89. Boulanger-Scemama, E. *et al.* [Ranibizumab and exudative age-related macular degeneration: 5-year multicentric functional and anatomical results in real-life practice]. *J. Fr. Ophthalmol.* **39**, 668–674 (2016).
90. Comparison of Age-related Macular Degeneration Treatments Trials (CATT) Research Group *et al.* Five-Year Outcomes with Anti-Vascular Endothelial Growth Factor Treatment of Neovascular Age-Related Macular Degeneration: The Comparison of Age-Related Macular Degeneration Treatments Trials. *Ophthalmology* **123**, 1751–1761 (2016).
91. Pedrosa, A. C. *et al.* Treatment of Neovascular Age-Related Macular Degeneration with Anti-VEGF Agents: Predictive Factors of Long-Term Visual Outcomes. *J. Ophthalmol.* **2017**, 4263017 (2017).
92. Pucci, G. C. M. F., Rech, C. R., Fermino, R. C. & Reis, R. S. Association between physical activity and quality of life in adults. *Rev. Saude Publica* **46**, 166–179 (2012).
93. Bize, R., Johnson, J. A. & Plotnikoff, R. C. Physical activity level and health-related quality of life in the general adult population: a systematic review. *Prev. Med.* **45**, 401–415 (2007).
94. Balducci, S. *et al.* Physical exercise as therapy for type 2 diabetes mellitus. *Diabetes Metab. Res. Rev.* **30 Suppl 1**, 13–23 (2014).
95. Maessen, M. F. H. *et al.* Lifelong Exercise Patterns and Cardiovascular Health. *Mayo Clin. Proc.* **91**, 745–754 (2016).

96. Lear, S. A. *et al.* The effect of physical activity on mortality and cardiovascular disease in 130 000 people from 17 high-income, middle-income, and low-income countries: the PURE study. *Lancet Lond. Engl.* **390**, 2643–2654 (2017).
97. Stillman, C. M., Cohen, J., Lehman, M. E. & Erickson, K. I. Mediators of Physical Activity on Neurocognitive Function: A Review at Multiple Levels of Analysis. *Front. Hum. Neurosci.* **10**, 626 (2016).
98. Risk factors for neovascular age-related macular degeneration. The Eye Disease Case-Control Study Group. *Arch. Ophthalmol. Chic. Ill 1960* **110**, 1701–1708 (1992).
99. Cho, B.-J., Heo, J. W., Kim, T. W., Ahn, J. & Chung, H. Prevalence and risk factors of age-related macular degeneration in Korea: the Korea National Health and Nutrition Examination Survey 2010-2011. *Invest. Ophthalmol. Vis. Sci.* **55**, 1101–1108 (2014).
100. Knudtson, M. D., Klein, R. & Klein, B. E. K. Physical activity and the 15-year cumulative incidence of age-related macular degeneration: the Beaver Dam Eye Study. *Br. J. Ophthalmol.* **90**, 1461–1463 (2006).
101. Mares, J. A. *et al.* Healthy lifestyles related to subsequent prevalence of age-related macular degeneration. *Arch. Ophthalmol. Chic. Ill 1960* **129**, 470–480 (2011).
102. Moon, B. G. *et al.* Prevalence and risk factors of early-stage age-related macular degeneration in patients examined at a health promotion center in Korea. *J. Korean Med. Sci.* **27**, 537–541 (2012).

103. Munch, I. C., Linneberg, A. & Larsen, M. Precursors of age-related macular degeneration: associations with physical activity, obesity, and serum lipids in the inter99 eye study. *Invest. Ophthalmol. Vis. Sci.* **54**, 3932–3940 (2013).
104. Nidhi, B., Mamatha, B. S., Padmaprabhu, C. A., Pallavi, P. & Vallikannan, B. Dietary and lifestyle risk factors associated with age-related macular degeneration: a hospital based study. *Indian J. Ophthalmol.* **61**, 722–727 (2013).
105. Song, S. J., Youm, D. J., Chang, Y. & Yu, H. G. Age-related macular degeneration in a screened South Korean population: prevalence, risk factors, and subtypes. *Ophthalmic Epidemiol.* **16**, 304–310 (2009).
106. Williams, P. T. Prospective study of incident age-related macular degeneration in relation to vigorous physical activity during a 7-year follow-up. *Invest. Ophthalmol. Vis. Sci.* **50**, 101–106 (2009).
107. Seddon, J. M., Cote, J., Davis, N. & Rosner, B. Progression of age-related macular degeneration: association with body mass index, waist circumference, and waist-hip ratio. *Arch. Ophthalmol. Chic. Ill 1960* **121**, 785–792 (2003).
108. Saksens, N. T. M. *et al.* Clinical characteristics of familial and sporadic age-related macular degeneration: differences and similarities. *Invest. Ophthalmol. Vis. Sci.* **55**, 7085–7092 (2014).
109. Erke, M. G. *et al.* Cardiovascular risk factors associated with age-related macular degeneration: the Tromsø Study. *Acta Ophthalmol. (Copenh.)* **92**, 662–669 (2014).

110. Nunes, S. *et al.* Adherence to a Mediterranean diet and its association with age-related macular degeneration. The Coimbra Eye Study-Report 4. *Nutr. Burbank Los Angel. Cty. Calif* **51–52**, 6–12 (2018).
111. McGuinness, M. B. *et al.* Past physical activity and age-related macular degeneration: the Melbourne Collaborative Cohort Study. *Br. J. Ophthalmol.* **100**, 1353–1358 (2016).
112. Khotcharrat, R. *et al.* Epidemiology of Age-Related Macular Degeneration among the Elderly Population in Thailand. *J. Med. Assoc. Thail. Chotmai het Thangphaet* **98**, 790–797 (2015).
113. Ristau, T. *et al.* Nongenetic risk factors for neovascular age-related macular degeneration. *Invest. Ophthalmol. Vis. Sci.* **55**, 5228–5232 (2014).
114. Heinemann, M. *et al.* Impact of visual impairment on physical activity in early and late age-related macular degeneration. *PloS One* **14**, e0222045 (2019).
115. McGuinness, M. B. *et al.* Physical Activity and Age-related Macular Degeneration: A Systematic Literature Review and Meta-analysis. *Am. J. Ophthalmol.* **180**, 29–38 (2017).
116. Akimoto, T., Ribar, T. J., Williams, R. S. & Yan, Z. Skeletal muscle adaptation in response to voluntary running in Ca²⁺/calmodulin-dependent protein kinase IV-deficient mice. *Am. J. Physiol. Cell Physiol.* **287**, C1311-1319 (2004).

117. Waters, R. E., Rotevatn, S., Li, P., Annex, B. H. & Yan, Z. Voluntary running induces fiber type-specific angiogenesis in mouse skeletal muscle. *Am. J. Physiol. Cell Physiol.* **287**, C1342-1348 (2004).
118. Akimoto, T. *et al.* Exercise stimulates Pgc-1alpha transcription in skeletal muscle through activation of the p38 MAPK pathway. *J. Biol. Chem.* **280**, 19587–19593 (2005).
119. Koves, T. R. *et al.* Peroxisome proliferator-activated receptor-gamma co-activator 1alpha-mediated metabolic remodeling of skeletal myocytes mimics exercise training and reverses lipid-induced mitochondrial inefficiency. *J. Biol. Chem.* **280**, 33588–33598 (2005).
120. Ajjjola, O. A. *et al.* Voluntary running suppresses proinflammatory cytokines and bone marrow endothelial progenitor cell levels in apolipoprotein-E-deficient mice. *Antioxid. Redox Signal.* **11**, 15–23 (2009).
121. Lira, V. A. *et al.* Autophagy is required for exercise training-induced skeletal muscle adaptation and improvement of physical performance. *FASEB J. Off. Publ. Fed. Am. Soc. Exp. Biol.* **27**, 4184–4193 (2013).
122. Laker, R. C. *et al.* Ampk phosphorylation of Ulk1 is required for targeting of mitochondria to lysosomes in exercise-induced mitophagy. *Nat. Commun.* **8**, 548 (2017).
123. Sasaki, H. *et al.* Forced rather than voluntary exercise entrains peripheral clocks via a corticosterone/noradrenaline increase in PER2::LUC mice. *Sci. Rep.* **6**, 27607 (2016).

124. Sasaki, H. *et al.* Phase shifts in circadian peripheral clocks caused by exercise are dependent on the feeding schedule in PER2::LUC mice. *Chronobiol. Int.* **33**, 849–862 (2016).
125. Castillo, C., Molyneux, P., Carlson, R. & Harrington, M. E. Restricted wheel access following a light cycle inversion slows re-entrainment without internal desynchrony as measured in Per2Luc mice. *Neuroscience* **182**, 169–176 (2011).
126. Leasure, J. L. & Jones, M. Forced and voluntary exercise differentially affect brain and behavior. *Neuroscience* **156**, 456–465 (2008).
127. Moraska, A., Deak, T., Spencer, R. L., Roth, D. & Fleshner, M. Treadmill running produces both positive and negative physiological adaptations in Sprague-Dawley rats. *Am. J. Physiol. Regul. Integr. Comp. Physiol.* **279**, R1321-1329 (2000).
128. Carmody, J. & Cooper, K. Swim stress reduces chronic pain in mice through an opioid mechanism. *Neurosci. Lett.* **74**, 358–363 (1987).
129. Sciolino, N. R. & Holmes, P. V. Exercise offers anxiolytic potential: a role for stress and brain noradrenergic-galaninergic mechanisms. *Neurosci. Biobehav. Rev.* **36**, 1965–1984 (2012).
130. Yuede, C. M. *et al.* Effects of voluntary and forced exercise on plaque deposition, hippocampal volume, and behavior in the Tg2576 mouse model of Alzheimer's disease. *Neurobiol. Dis.* **35**, 426–432 (2009).

131. Ke, Z., Yip, S. P., Li, L., Zheng, X.-X. & Tong, K.-Y. The effects of voluntary, involuntary, and forced exercises on brain-derived neurotrophic factor and motor function recovery: a rat brain ischemia model. *PloS One* **6**, e16643 (2011).
132. Ke, Z. *et al.* The effects of voluntary, involuntary, and forced exercises on motor recovery in a stroke rat model. *Annu. Int. Conf. IEEE Eng. Med. Biol. Soc. IEEE Eng. Med. Biol. Soc. Annu. Int. Conf.* **2011**, 8223–8226 (2011).
133. Mizutani, T. *et al.* Nucleoside Reverse Transcriptase Inhibitors Suppress Laser-Induced Choroidal Neovascularization in Mice. *Invest. Ophthalmol. Vis. Sci.* **56**, 7122–7129 (2015).
134. Lambert, V. *et al.* Laser-induced choroidal neovascularization model to study age-related macular degeneration in mice. *Nat. Protoc.* **8**, 2197–2211 (2013).
135. Goh, J. & Ladiges, W. Voluntary Wheel Running in Mice. *Curr. Protoc. Mouse Biol.* **5**, 283–290 (2015).
136. Espinosa-Heidmann, D. G. *et al.* Gender and estrogen supplementation increases severity of experimental choroidal neovascularization. *Exp. Eye Res.* **80**, 413–423 (2005).
137. De Bono, J. P., Adlam, D., Paterson, D. J. & Channon, K. M. Novel quantitative phenotypes of exercise training in mouse models. *Am. J. Physiol. Regul. Integr. Comp. Physiol.* **290**, R926-934 (2006).

138. Oh, H. *et al.* The potential angiogenic role of macrophages in the formation of choroidal neovascular membranes. *Invest. Ophthalmol. Vis. Sci.* **40**, 1891–1898 (1999).
139. Cherepanoff, S., McMenamin, P., Gillies, M. C., Kettle, E. & Sarks, S. H. Bruch's membrane and choroidal macrophages in early and advanced age-related macular degeneration. *Br. J. Ophthalmol.* **94**, 918–925 (2010).
140. Killingsworth, M. C., Sarks, J. P. & Sarks, S. H. Macrophages related to Bruch's membrane in age-related macular degeneration. *Eye Lond. Engl.* **4 (Pt 4)**, 613–621 (1990).
141. Lopez, P. F. *et al.* Pathologic features of surgically excised subretinal neovascular membranes in age-related macular degeneration. *Am. J. Ophthalmol.* **112**, 647–656 (1991).
142. Sakurai, E., Anand, A., Ambati, B. K., van Rooijen, N. & Ambati, J. Macrophage depletion inhibits experimental choroidal neovascularization. *Invest. Ophthalmol. Vis. Sci.* **44**, 3578–3585 (2003).
143. Nagai, N. *et al.* Spontaneous CNV in a novel mutant mouse is associated with early VEGF-A-driven angiogenesis and late-stage focal edema, neural cell loss, and dysfunction. *Invest. Ophthalmol. Vis. Sci.* **55**, 3709–3719 (2014).
144. Trott, D. W. *et al.* Age-related arterial immune cell infiltration in mice is attenuated by caloric restriction or voluntary exercise. *Exp. Gerontol.* **109**, 99–107 (2018).

145. Kawanishi, N., Yano, H., Yokogawa, Y. & Suzuki, K. Exercise training inhibits inflammation in adipose tissue via both suppression of macrophage infiltration and acceleration of phenotypic switching from M1 to M2 macrophages in high-fat-diet-induced obese mice. *Exerc. Immunol. Rev.* **16**, 105–118 (2010).
146. Kawanishi, N., Mizokami, T., Yano, H. & Suzuki, K. Exercise attenuates M1 macrophages and CD8⁺ T cells in the adipose tissue of obese mice. *Med. Sci. Sports Exerc.* **45**, 1684–1693 (2013).
147. Lewis, D. Y. & Brett, R. R. Activity-based anorexia in C57/BL6 mice: effects of the phytocannabinoid, Delta9-tetrahydrocannabinol (THC) and the anandamide analogue, OMDM-2. *Eur. Neuropsychopharmacol. J. Eur. Coll. Neuropsychopharmacol.* **20**, 622–631 (2010).
148. O’Neal, T. J., Friend, D. M., Guo, J., Hall, K. D. & Kravitz, A. V. Increases in Physical Activity Result in Diminishing Increments in Daily Energy Expenditure in Mice. *Curr. Biol. CB* **27**, 423–430 (2017).
149. Swallow, J. G., Koteja, P., Carter, P. A. & Garland, T. Food consumption and body composition in mice selected for high wheel-running activity. *J. Comp. Physiol. [B]* **171**, 651–659 (2001).
150. Bell, R. R., Spencer, M. J. & Sherriff, J. L. Voluntary exercise and monounsaturated canola oil reduce fat gain in mice fed diets high in fat. *J. Nutr.* **127**, 2006–2010 (1997).
151. Leon, A. S. *et al.* Blood lipid response to 20 weeks of supervised exercise in a large biracial population: the HERITAGE Family Study. *Metabolism.* **49**, 513–520 (2000).

152. Meissner, M., Nijstad, N., Kuipers, F. & Tietge, U. J. Voluntary exercise increases cholesterol efflux but not macrophage reverse cholesterol transport in vivo in mice. *Nutr. Metab.* **7**, 54 (2010).
153. Gehrke, N. *et al.* Voluntary exercise in mice fed an obesogenic diet alters the hepatic immune phenotype and improves metabolic parameters - an animal model of life style intervention in NAFLD. *Sci. Rep.* **9**, 4007 (2019).
154. Marchianti, A. C. N., Arimura, E., Ushikai, M. & Horiuchi, M. Voluntary exercise under a food restriction condition decreases blood branched-chain amino acid levels, in addition to improvement of glucose and lipid metabolism, in db mice, animal model of type 2 diabetes. *Environ. Health Prev. Med.* **19**, 339–347 (2014).
155. Chrysostomou, V. *et al.* Exercise reverses age-related vulnerability of the retina to injury by preventing complement-mediated synapse elimination via a BDNF-dependent pathway. *Aging Cell* **15**, 1082–1091 (2016).
156. Kim, C.-S. *et al.* Treadmill Exercise Attenuates Retinal Oxidative Stress in Naturally-Aged Mice: An Immunohistochemical Study. *Int. J. Mol. Sci.* **16**, 21008–21020 (2015).
157. Lawson, E. C. *et al.* Aerobic exercise protects retinal function and structure from light-induced retinal degeneration. *J. Neurosci. Off. J. Soc. Neurosci.* **34**, 2406–2412 (2014).

158. Zhang, X. *et al.* Wheel running exercise protects against retinal degeneration in the I307N rhodopsin mouse model of inducible autosomal dominant retinitis pigmentosa. *Mol. Vis.* **25**, 462–476 (2019).
159. Rim, T. H. *et al.* A Nationwide Cohort Study on the Association Between Past Physical Activity and Neovascular Age-Related Macular Degeneration in an East Asian Population. *JAMA Ophthalmol.* **136**, 132–139 (2018).
160. McGuinness, M. B., Simpson, J. A. & Finger, R. P. Analysis of the Association Between Physical Activity and Age-Related Macular Degeneration. *JAMA Ophthalmol.* **136**, 139–140 (2018).
161. Wang, Y. X., Wei, W. B., Xu, L. & Jonas, J. B. Physical activity and eye diseases. The Beijing Eye Study. *Acta Ophthalmol. (Copenh.)* **97**, 325–331 (2019).
162. Bowling, A. Mode of questionnaire administration can have serious effects on data quality. *J. Public Health Oxf. Engl.* **27**, 281–291 (2005).
163. Subhi, Y. & Sørensen, T. L. Physical activity patterns in patients with early and late age-related macular degeneration. *Dan. Med. J.* **63**, A5303 (2016).
164. Gelfand, B. D. & Ambati, J. A Revised Hemodynamic Theory of Age-Related Macular Degeneration. *Trends Mol. Med.* **22**, 656 (2016).
165. Mechanistic Insights into Pathological Changes in the Diabetic Retina: Implications for Targeting Diabetic Retinopathy - ScienceDirect. <https://www.sciencedirect.com/science/article/pii/S0002944016304138>.

166. Wong, W. L. *et al.* Global prevalence of age-related macular degeneration and disease burden projection for 2020 and 2040: a systematic review and meta-analysis. *Lancet Glob. Health* **2**, e106–e116 (2014).
167. Yau, J. W. Y. *et al.* Global prevalence and major risk factors of diabetic retinopathy. *Diabetes Care* **35**, 556–564 (2012).
168. Lou, D. A. & Hu, F. N. Specific antigen and organelle expression of a long-term rhesus endothelial cell line. *Vitro Cell. Dev. Biol. J. Tissue Cult. Assoc.* **23**, 75–85 (1987).
169. Zeng, S. *et al.* Molecular response of chorioretinal endothelial cells to complement injury: implications for macular degeneration. *J. Pathol.* **238**, 446–456 (2016).
170. Patro, R., Duggal, G., Love, M. I., Irizarry, R. A. & Kingsford, C. Salmon provides fast and bias-aware quantification of transcript expression. *Nat. Methods* **14**, 417–419 (2017).
171. Sonesson, C., Love, M. I. & Robinson, M. D. Differential analyses for RNA-seq: transcript-level estimates improve gene-level inferences. *F1000Research* **4**, 1521 (2016).
172. Love, M. I., Huber, W. & Anders, S. Moderated estimation of fold change and dispersion for RNA-seq data with DESeq2. *Genome Biol.* **15**, 550 (2014).

173. R Development Core Team (2010) R: A Language and Environment for Statistical Computing. R Foundation for Statistical computing, Vienna, Austria. <http://www.R-project.org>.
174. Sandler, V. M. *et al.* Reprogramming human endothelial cells to haematopoietic cells requires vascular induction. *Nature* **511**, 312–318 (2014).
175. Savage, S. R., Bretz, C. A. & Penn, J. S. RNA-Seq Reveals a Role for NFAT-Signaling in Human Retinal Microvascular Endothelial Cells Treated with TNF α . *PLoS ONE* **10**, e0116941 (2015).
176. Savage, S. R., McCollum, G. W., Yang, R. & Penn, J. S. RNA-seq identifies a role for the PPAR β/δ inverse agonist GSK0660 in the regulation of TNF α -induced cytokine signaling in retinal endothelial cells. *Mol. Vis.* **21**, 568–576 (2015).
177. Schubert, C. *et al.* Cadherin 5 is Regulated by Corticosteroids and Associated with Central Serous Chorioretinopathy. *Hum. Mutat.* **35**, 859–867 (2014).
178. PADGEM (GMP140) Is a Component of Weibel-Palade Bodies of Human Endothelial Cells - ScienceDirect. <https://www.sciencedirect.com/science/article/pii/S0006497120755291?via%3Dihub>.
179. Storage of Tissue-Type Plasminogen Activator in Weibel-Palade Bodies of Human Endothelial Cells | Arteriosclerosis, Thrombosis, and Vascular Biology. https://www.ahajournals.org/doi/10.1161/01.atv.19.7.1796?url_ver=Z39.88-2003&rfr_id=ori:rid:crossref.org&rfr_dat=cr_pub%20%20pubmed.

180. Utgaard, J. O., Jahnsen, F. L., Bakka, A., Brandtzaeg, P. & Haraldsen, G. Rapid Secretion of Prestored Interleukin 8 from Weibel-Palade Bodies of Microvascular Endothelial Cells. *J. Exp. Med.* **188**, 1751–1756 (1998).
181. Koina, M. E. *et al.* Evidence for Lymphatics in the Developing and Adult Human Choroid. *Invest. Ophthalmol. Vis. Sci.* **56**, 1310–1327 (2015).
182. Abri, A., Binder, S., Pavelka, M., Tittl, M. & Neumüller, J. Choroidal neovascularization in a child with traumatic choroidal rupture: clinical and ultrastructural findings. *Clin. Experiment. Ophthalmol.* **34**, 460–463 (2006).
183. Schraermeyer, U. & Julien, S. Effects of bevacizumab in retina and choroid after intravitreal injection into monkey eyes. *Expert Opin. Biol. Ther.* **13**, 157–167 (2013).
184. Archer, D. B. & Gardiner, T. A. Electron microscopic features of experimental choroidal neovascularization. *Am. J. Ophthalmol.* **91**, 433–457 (1981).
185. Browning, A. C., Gray, T. & Amoaku, W. M. Isolation, culture, and characterisation of human macular inner choroidal microvascular endothelial cells. *Br. J. Ophthalmol.* **89**, 1343–1347 (2005).
186. A Novel Choroidal Endothelial Cell Line Has a Decreased Affinity for the Age-Related Macular Degeneration-Associated Complement Factor H Variant 402H - PubMed. <https://pubmed.ncbi.nlm.nih.gov/29392318/>.
187. Structural organization of Weibel-Palade bodies revealed by cryo-EM of vitrified endothelial cells | PNAS. <https://www.pnas.org/doi/10.1073/pnas.0902977106>.

188. Hannah, M. J. *et al.* Weibel-Palade bodies recruit Rab27 by a content-driven, maturation-dependent mechanism that is independent of cell type. *J. Cell Sci.* **116**, 3939–3948 (2003).
189. Nightingale, T. D., Pattni, K., Hume, A. N., Seabra, M. C. & Cutler, D. F. Rab27a and MyRIP regulate the amount and multimeric state of VWF released from endothelial cells. *Blood* **113**, 5010–5018 (2009).
190. Zografou, S. *et al.* A complete Rab screening reveals novel insights in Weibel-Palade body exocytosis. *J. Cell Sci.* **125**, 4780–4790 (2012).
191. Craig, L. E., Spelman, J. P., Strandberg, J. D. & Zink, M. C. Endothelial cells from diverse tissues exhibit differences in growth and morphology. *Microvasc. Res.* **55**, 65–76 (1998).
192. Liu, S. Q. & Goldman, J. Role of blood shear stress in the regulation of vascular smooth muscle cell migration. *IEEE Trans. Biomed. Eng.* **48**, 474–483 (2001).
193. Lee, A. A., Graham, D. A., Dela Cruz, S., Ratcliffe, A. & Karlon, W. J. Fluid shear stress-induced alignment of cultured vascular smooth muscle cells. *J. Biomech. Eng.* **124**, 37–43 (2002).
194. Ng, C. P. & Swartz, M. A. Fibroblast alignment under interstitial fluid flow using a novel 3-D tissue culture model. *Am. J. Physiol. Heart Circ. Physiol.* **284**, H1771–1777 (2003).

195. Ng, C. P., Hinz, B. & Swartz, M. A. Interstitial fluid flow induces myofibroblast differentiation and collagen alignment in vitro. *J. Cell Sci.* **118**, 4731–4739 (2005).
196. Augustin, H. G. & Koh, G. Y. Organotypic vasculature: From descriptive heterogeneity to functional pathophysiology. *Science* **357**, eaal2379 (2017).
197. Starke, R. D. *et al.* Endothelial von Willebrand factor regulates angiogenesis. *Blood* **117**, 1071–1080 (2011).
198. Donovan, D., Brown, N. J., Bishop, E. T. & Lewis, C. E. Comparison of three in vitro human ‘angiogenesis’ assays with capillaries formed in vivo. *Angiogenesis* **4**, 113–121 (2001).
199. Basu, G. D. *et al.* A novel role for cyclooxygenase-2 in regulating vascular channel formation by human breast cancer cells. *Breast Cancer Res. BCR* **8**, R69 (2006).
200. Francescone, R. A., Faibish, M. & Shao, R. A Matrigel-based tube formation assay to assess the vasculogenic activity of tumor cells. *J. Vis. Exp. JoVE* 3040 (2011) doi:10.3791/3040.
201. Maniotis, A. J. *et al.* Vascular channel formation by human melanoma cells in vivo and in vitro: vasculogenic mimicry. *Am. J. Pathol.* **155**, 739–752 (1999).
202. El Hallani, S. *et al.* A new alternative mechanism in glioblastoma vascularization: tubular vasculogenic mimicry. *Brain J. Neurol.* **133**, 973–982 (2010).

203. Dirks, W. G., MacLeod, R. A. & Drexler, H. G. ECV304 (endothelial) is really T24 (bladder carcinoma): cell line cross- contamination at source. *In Vitro Cell. Dev. Biol. Anim.* **35**, 558–559 (1999).
204. Scavelli, C. *et al.* Vasculogenic mimicry by bone marrow macrophages in patients with multiple myeloma. *Oncogene* **27**, 663–674 (2008).
205. Chatterjee, R. Cell biology. Cases of mistaken identity. *Science* **315**, 928–931 (2007).
206. Stacey, G. N. Cell contamination leads to inaccurate data: we must take action now. *Nature* **403**, 356 (2000).
207. Hughes, S. E. Functional characterization of the spontaneously transformed human umbilical vein endothelial cell line ECV304: use in an in vitro model of angiogenesis. *Exp. Cell Res.* **225**, 171–185 (1996).
208. Abdelsaid, K. *et al.* Exercise improves angiogenic function of circulating exosomes in type 2 diabetes: Role of exosomal SOD3. *FASEB J. Off. Publ. Fed. Am. Soc. Exp. Biol.* **36**, e22177 (2022).

